# INAUGURAL–DISSERTATION

zur

Erlangung der Doktorwürde

der

Naturwissentschaftlich–Mathematischen

Gesamtfakultät

der

Ruprecht–Karls–Universität

Heidelberg

vorgelegt von

**Dipl.–Phys. Agnès D.F. Metanomski**
aus Paris

Tag der mündl. Prüfung: 22. April 1998

# Optical study of F, G and K stars
# in the ROSAT All-Sky Survey

Gutachter: Herr Prof. Dr. Joachim Krautter

Herr Prof. Dr. Reiner Wehrse

## Zusammenfassung

Ich untersuche eine Stichprobe von 107 Südhimmels-Sternen von Spektraltyp A bis K. Diese Sterne sind als die optischen Gegenstücke zu Röntgen-Quellen, die der ROSAT Satellit während seines All-Sky Survey (RASS) entdeckte, identifiziert wurden. Die Untersuchung wird mit Hilfe optischen Beobachtungen, sowohl photometrischer als auch spektroskopischer, durchgeführt. Verschiedene Parameter werden für die untersuchten Objekte bestimmt, wie z.B. Spektraltyp und Leuchtkraftklasse, absolute Helligkeit, Entfernung, Radialgeschwindigkeit, projezierte Rotationsgeschwindigkeit, Effektivtemperatur, Lithium Häufigkeit.

Ich vergleiche die Röntgen-Parameter meiner Stichproben-Sterne mit denen aus einer ähnlichen Stichprobe von Sternen, die vom *Einstein Observatory* während dessen Medium Sensitivity Survey (EMSS) entdeckt wurden. Ich suche auch nach Korrelationen zwischen verschiedenen Parametern, die für meine Stichproben-Sterne bestimmt wurden und vergleiche die Ergebnisse mit denen, die für die EMSS Stichprobe erhalten wurden, sowie mit den Ergebnissne anderer, früherer Studien.

## Abstract

I analyze a sample of 107 southern stars of spectral types A to K, which were identified as the optical counterparts of X-ray sources detected by ROSAT during its All-Sky Survey. The study is conducted using optical observations, photometric as well as spectroscopic (high-resolution). Various parameters are determined for the sample objects, mainly spectral types and luminosity classes, absolute magnitudes, distances, radial velocities, projected rotational velocities, effective temperatures, Lithium abundances.

I compare the X-ray parameters of my sample stars with those of a similar sample, detected by the *Einstein Observatory* during its Medium Sensitivity Survey (EMSS). I also look for correlations between the different stellar parameters determined for my sample, and compare those results to those obtained for the EMSS sample, and also to some results obtained from other, earlier studies.

# *Contents*

# *List of Figures*

# List of Tables

# 1 Introduction

## 1.1 Stellar X-ray emission

From observations of the Sun during solar eclipses, it was known that the atmosphere extends itself well beyond the normally visible solar "surface", into regions that only have a thin, but very hot plasma. Through models and observations the atmosphere was divided into three zones: the photosphere, where most absorption lines are created, the chromosphere and the corona. The chromosphere appears were the temperature inversion occurs, ie. after the point at which the temperature of the atmospheric plasma starts rising again.

The corona has a very low density but high temperatures, of the order $10^6 - 10^7$ K. At such temperatures the plasma emits the most in the higher energy bands. If the plasma can be approximated to a black body, then the maximum of the emission lies in the range around 0.1 keV, that is in the soft X-ray range.

Studies made of the solar corona have shown that its luminosity varies strongly over time. The X-ray luminosity of the Sun has a minimal value of $\sim 10^{25} erg\ s^{-1}$ and a maximum around $10^{27} erg\ s^{-1}$.

As a matter of fact, the Sun shows variations in many different features, the most visible being the variation of the number and position of solar spots. The variations extend over a period of 11 years, which is considered now as the activity cycle of the Sun. The variations of the corona could be linked to this cycle.

The Sun, being so near, is the easiest star to study, especially in the high energy ranges of the X-ray emission. But without comparisons to other, similar stars, it is impossible to determine how far the solar activity is typical for stellar activity, and the models developed for the Sun can be applied to other stars. This requires the study of stellar coronae and activity for as broad a range of spectral types as possible. This is the central goal of my work, for which I have made use of X-ray observations obtained for a relatively large sample of late-type stars.

### 1.1.1 Pre-Einstein Era

X-ray astronomy is said to have started with a successful rocket flight on June 19th 1962 (see Giaconni et al. 1962). This flight detected the first non-solar X-ray sources. It was followed by a series of rocket and satellites flights, and the launch of the first satellites dedicated to X-ray observations, the UHURU (1970) and HEAO-1 (1977-1979) satellites, in the course of the sixties and seventies. A review on these and all the following X-ray satellites has been given by Bradt et al. (1992).

These experiments allowed the detection and first study of a wide variety of X-ray sources, as well as the study of the diffuse X-ray background. Among the types of sources detected were X-ray binaries, cataclysmic variables, supernova remnants, quasars, and galaxies. But only very few "normal" stars could be detected. This was mainly due to the lack of sensitivity of the instruments used, and to the energy ranges (2-20 keV) in which the observations were carried out. In the harder X-ray energy range the emission from stellar sources drops strongly, making their detection with low-sensitivity instruments very difficult. Some stars were detected (Capella being the first, observed in 1975), but not enough to allow the conclusion that X-ray emission is a normal phenomenon for stars. The only type of stars that were observed sufficiently to allow their classification as an X-ray emitting class were the RS CVn binaries.

The results obtained during that period of time are summarized by Mewe (1979).

### *1.1.2 Einstein Era*

With the launch of the *Einstein Observatory* on November 3, 1978, stellar X-ray astronomy really started. The *Einstein Observatory* was the first satellite bearing an X-ray telescope together with an imaging device, the Imaging Proportional Counter (IPC). The IPC allowed the imaging of the sky in the X-ray, making the spatial resolution of sources, and the observation of multiple sources with one exposure. The choice of the instrument made the use of a softer X-ray energy range necessary, making the satellite particularly efficient for the detection of stellar X-ray sources.

This is the reason why among the sources detected by the Einstein Satellite during its Medium Sensitivity Survey (EMSS), a, at the time surprisingly, high number of stellar sources were present. About 26% of the total sample of serendipitously discovered sources studied by Stocke et al. (1991) were stellar sources. Various studies of the stellar sources discovered in the EMSS were carried out. A sample of stars (including 129 objects of spectral type A to K) was studied in detail by Fleming (Fleming, 1988, Fleming et al. 1989). Other, more or less specialized, subsets were studied by various groups (for example Golub et al. 1983, Maggio et al. 1987, Pallavicini et al. 1981, Schmitt et al. 1990). A list of specialized studies is given in Linsky (1990).

## *1.2 Results from the Einstein Observatory*

One of the major results obtained by the *Einstein Observatory* was the detection of X-ray emission from nearly all types of stars, as can be recognized from Fig. 1.1. The shaded areas in the Hertzsprung-Russell diagram of Fig. 1.1 show the location of detection of X-ray emission in stars.

The main exceptions, for which no X-ray emission could be detected, are A-stars (B9-A7, to be precise), and giants/supergiants beyond the so-called Coronal Dividing Line, more precisely all giants later than K2 and all supergiants later than G0.

The mechanisms responsible for the X-ray emission have not been positively

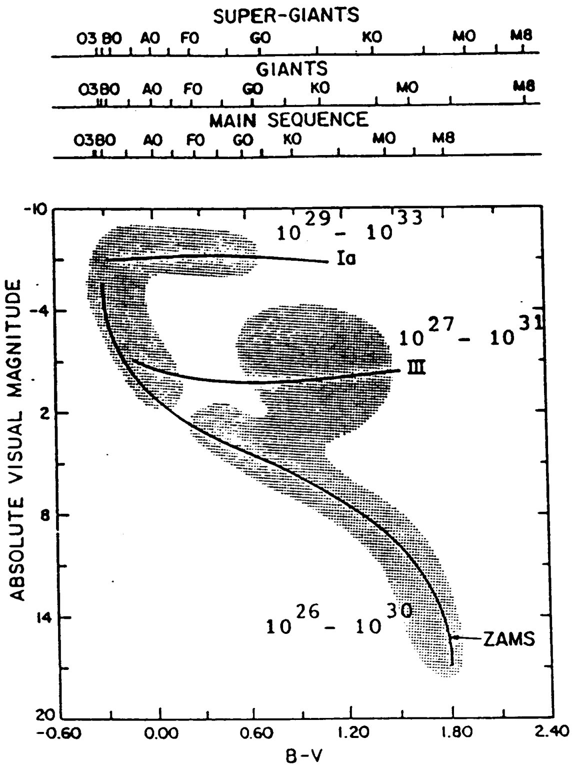


Figure 1.1: Representation of X-ray activity on the Hertzsprung-Russell diagram. The shaded areas indicate the classes of stars detected as X-ray emitters, as well as the X-ray luminosity ranges found for them. Figure taken from Rosner, Golub and Vaiana (1985).

identified. The assumption is that different mechanisms are at the source of the emission for different types of stars.

For early-type stars of spectral types O and B, the X-ray luminosity has been found to correlate with the bolometric luminosity (Pallavicini, 1989). Among all the models proposed to explain the X-ray emission in such stars the most successfull so far has been the model of shocks. This model assumes instabilities in the stellar winds, which lead to the formation of shock fronts in the outflow, which produce the X-ray emission.

Figure 1.2 shows a best fit model to the observed spectrum of $\epsilon$ Ori (a B0Iae star). The model reproduces the observations very well, if strong and infrequent shocks are assumed.

Still, the model awaits complete confirmation.

Late-type stars, including main-sequence F to M stars, giants earlier than K2 and supergiants earlier than G0, show a clear correlation between rotation and X-ray luminosity. Noteworthy is the fact that the sample studied by Pallavicini et al. (1981) displays a different correlation to the one found by Fleming for his EMSS sample (Fleming 1988, Fleming et al. 1989). Pallavicini et al. (1981) find

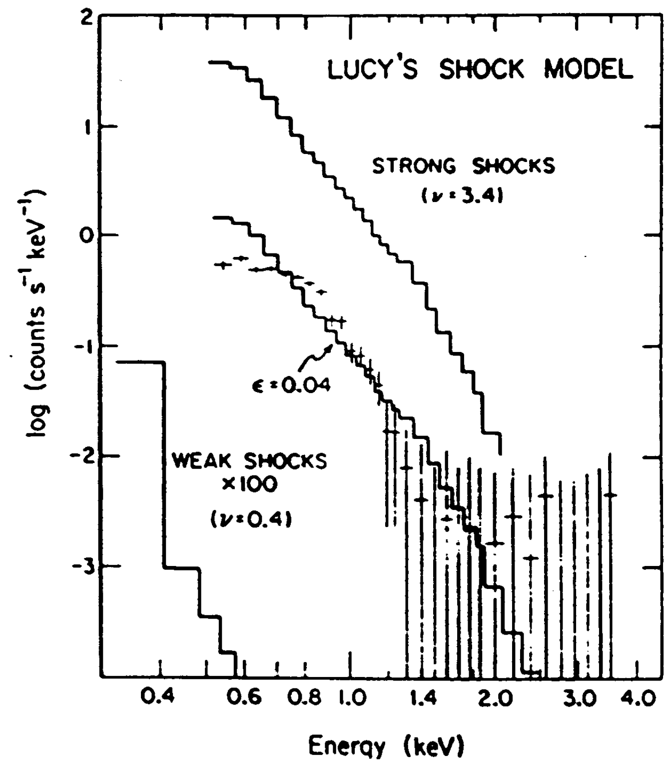


Figure 1.2: Comparison of the Einstein spectrum of $\epsilon$ Ori with the shock model of Lucy (1982). The best fit to the observations requires strong, but infrequent shocks (image taken from Cassinelli and Swank 1983).

a correlation of the X-ray luminosity with the square of the projected rotation rate: $L_X \propto (v \sin i)^2$, as can be seen on Fig. 1.3, while Fleming finds a correlation with the projected rotation rate: $L_X \propto v \sin i$. The observed continuum for late-type stars suggests thermal bremsstrahlung emission from hot ($T \sim 7-20 \cdot 10^6$K) plasma.

The most commonly used model to explain the X-ray emission as well as the correlation of the X-ray luminosity with rotation is a model based on magnetic heating of the corona, and a magnetic (**B**) field generated by a dynamo mechanism (Parker 1979). Differential rotation at the base of the convection zone leads to the generation of toroidal **B** fields from the primordial poloidal **B** field (the so-called $\Omega$ effect). These new fields rise through the convection zone due to magnetic buoyancy. The turbulent motions in the convection zone lead to the production of new poloidal **B** fields from the toroidal field (the $\alpha$ effect), which in their turn produce new toroidal fields, "feeding" the dynamo. The toroidal field, when reaching the stellar surface, is still embedded in the stellar material, and thus affected by the turbulent surface motions. This causes the plasma enclosed in the field lines to be heated. The corona formed that way is highly inhomogeneous, and

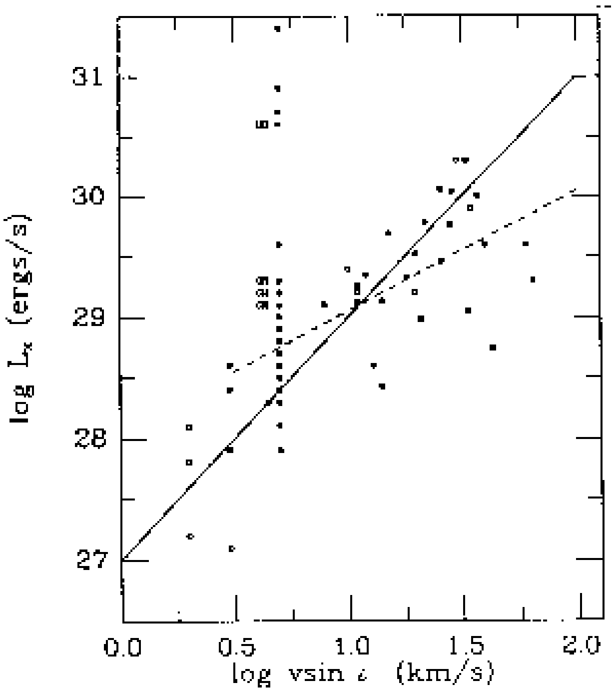


Figure 1.3: The relation between X-ray luminosity and projected rotation rate for the EMSS sample (filled squares) of Fleming (1988) and the sample studied by Pallavicini et al. (1981). The lines show the correlations found by Pallavicini et al. (1981, continuous line) and Fleming (1988, broken line). Image taken from Fleming (1988).

has a strength dependent on the stellar rotation and the depth of the convection zone.

Active binaries of the RS CVn, W UMa or Algol types, which are situated in the same area of the Hertzsprung-Russell Diagram as single late-type stars are believed to have the same basic mechanism for X-ray emission as the single stars, but enhanced through the interaction between the binary system components.

## *1.3 Dissertation project*

Our knowledge of stellar X-ray emission has grown with the study of the stars detected serendipitously by the *Einstein Observatory* and EXOSAT, that allowed the construction of the first X-ray selected star samples.

The amount of knowledge that could be gained to date was limited by the relatively small spatial coverage and the therefore limited number of sources detected (Einstein: about 10% of the sky observed, and 129 stellar sources of spectral types

A to K, see Stocke et al. 1991; EXOSAT: $\sim$ 100 stellar sources, see Giommi et al. 1991).

The ROSAT satellite, with its All-Sky Survey (RASS), has changed this situation. Larger X-ray selected samples can be now constructed. But since the energy range used in the RASS (0.2-2.4 keV) is different to the energy ranges used in the observations of the *Einstein Observatory* (0.1-3.5 keV) and *EXOSAT* (1-50 keV), it is important first to compare the samples obtained, to see if the samples can be considered representative of the stellar X-ray population in the solar neighborhood. This is important in view of the potential of the RASS, which can contain in the order of 15.000 stars, should the percentage of stellar sources be similar to the one obtained in the EMSS. With such a large number of sources, many of the models and assumptions made to explain previous observations can be checked.

I have limited my thesis work to the study of a sample of 107 stars in the southern hemisphere, though a similar sample of 193 stars in the northern hemisphere was also available. Both samples are X-ray selected and composed of all the stars of spectral type A to K located in high-galactic latitude fields. The samples are described in more detail in Chapter 2. The reasons for the limitation to one of the samples is the amount of work involved in getting complete sets of observations for a sample of more than 100 stars. Managing two samples in the course of one thesis work would be quite impossible.

I also concentrated on a certain number of observations, to allow a determination of the most important stellar parameters. With the results from these observations, described in Chapters 3 and 4, the sample can be compared to the EMSS (Fleming 1988, Fleming et al. 1995) and EXOSAT (Tagliaferri et al 1994, Cutispoto et al. 1996) samples. Also, correlations between different parameters can be looked for, in particular the correlation between projected rotation rate $v \sin i$ and X-ray luminosity $L_X$, to verify the assumptions of current models. The properties of my sample, compared to those of the EMSS and EXOSAT samples, as well as the results of the correlation search, will be discussed in Chapter 5.

# 2 The ROSAT All-Sky Survey

The major drawback of the Einstein Survey was its spatial limitation. The observations carried out were only pointed ones, and the total area covered only made up $\sim$ 10% of the sky. Thus the construction of very large samples of stellar X-ray sources was strongly restricted. The total number of available stars in the EMSS is of $\sim$ 215, all spectral types included (Stocke et al. 1991).

This problem was addressed with the construction and launch of a new X-ray satellite, the ROSAT satellite.

## 2.1 The survey

The ROSAT satellite was successfully launched on June 1st, 1990. It was placed on a circular orbit, with an inclination of 53°, at an altitude of 580 km.

During the following six months, from July 1990 to January 1991 it surveyed the entire sky both in the soft X-ray and in the UV. Some additional observations were carried out in the course of February and August 1991.

The X-ray observations were made in range 0.1 to 2.4 keV. The instrument used was the X-ray Telescope (XRT) and a Position Sensitive Proportional Counter (PSPC) placed in the focal plane of the telescope. The mean sensitivity limit for the survey was at an observed flux of $f_X \sim 2 \cdot 10^{-13} erg\ s^{-1}\ cm^{-2}$. At the ecliptic poles, the sensitivity was higher, with a limiting flux of down to $2 \cdot 10^{-14} erg\ s^{-1}\ cm^{-2}$ and total exposure times of up to 50.000s. At the ecliptic equator, the mean exposure time lay around 400s, and the limiting flux was of $5 \cdot 10^{-13} erg\ s^{-1}\ cm^{-2}$. The survey contains ∼60.000 X-ray sources (Voges 1993).

The survey and instruments are described with more detail for example by Trümper at al. (1991). Figure 2.1 shows a sketch of the satellite.

The sources were detected in the images by using a maximum-likelihood algorithm that is described by Cruddace, Hasinger and Schmitt (1988).

## 2.2 The sample

In order to study the characteristics of X-ray sources detected by ROSAT during its All-Sky Survey, various projects were started. Among these programs were two that consisted of the complete identification of all the X-ray sources within a number of high-galactic latitude fields with optical counterparts.

One of the programs consisted of the study of four fields in the southern hemisphere. This project was granted time at the European Southern Observatory at La Silla as an ESO Key Project (Danziger et al. 1990). The fields comprised a total area of $\sim$ 575 square degrees, and $\sim$ 600 X-ray sources.

The other program, carried out as a collaboration between the Landessternwarte Heidelberg, the INAOE in Mexico and the MPIE in Garching, studied the

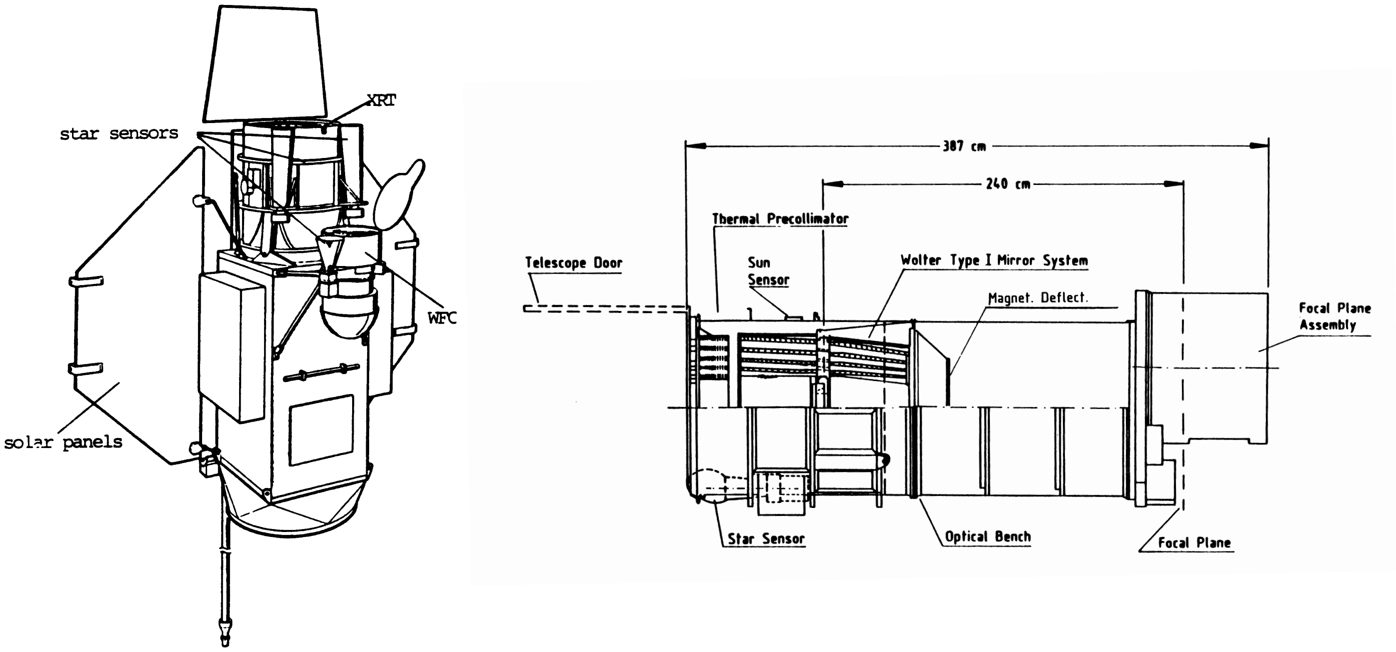


Figure 2.1: Schematic view of the ROSAT satellite and X-ray telescope.

X-ray sources (down to a limiting countrate of 0.03 counts/s, or 0.01 counts/s in one field) of six fields in the northern hemisphere, covering $\sim 684$ square degrees and some 674 X-ray sources (Appenzeller et al. 1997, Zickgraf et al. 1997).

The position of these ten fields is shown in image 2.2.

In order to identify the X-ray sources with optical counterparts, low-resolution spectra of all sources within the error circle of the ROSAT position ($\sim 30''$) were taken.

For the southern hemisphere sample, the optical candidates were observed with the Boller & Chivens spectrograph at the 1.52 m ESO telescope, and with the EFOSC1 spectrograph at the 3.6 m telescope at the La Silla. The resolutions used were of 7Å and 16Å. In addition to that, intermediate resolution (2Å) spectra of the H$\alpha$ line were obtained for some of the late-type stars. This was done to confirm whether these objects could be coronal sources, by checking out the presence of enhanced chromospheric activity showed through partial/complete filling-in or emission in the H$\alpha$ line.

The northern hemisphere sample was studied using mainly the 2.15 m telescope equipped with the *Landessternwarte Faint Object Spectrograph* (LFOSC) at the Guillermo Haro Observatory in Mexico. But some observations were done using the 72 cm Waltz telescope and a Boller & Chivens spectrograph at the Landessternwarte Heidelberg (Ziegler, 1993), and the 2.2 m telescope with EFOSC2 at La Silla. The resolution used was of 13Å and 18 Åfor LFOSC, 2 Å for the Boller & Chivens, and 24 Å for EFOSC2. For more details on the identification methods and a list of identifications for the northern sample, see Zickgraf et al. (1997), Appenzeller et al. (1997).

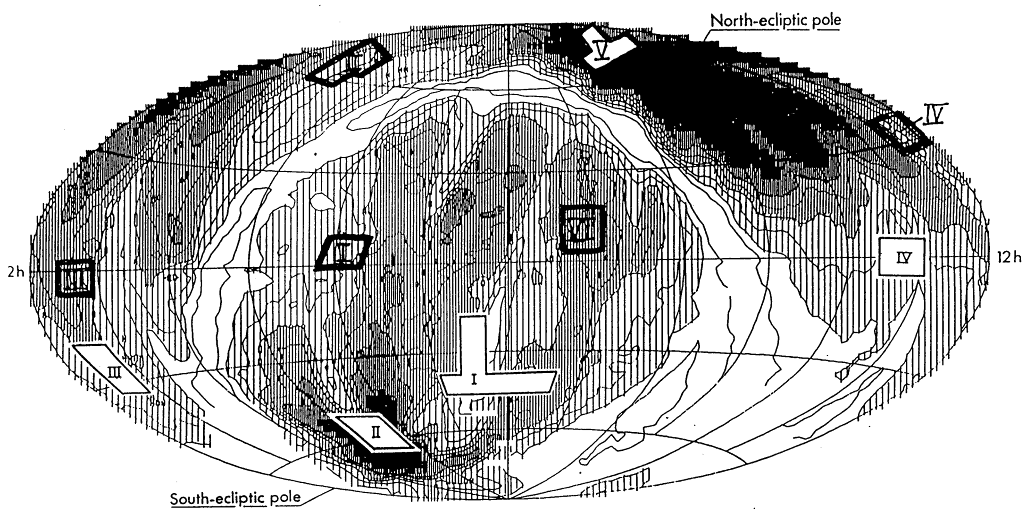


Figure 2.2: Location of the fields studied in the southern and northern identification programs.

The low-resolution spectra obtained were used for a first spectral classification of the stellar sources. In cases of bright stars, the classification from the SIMBAD database was used. The optical identifications are listed in Table B.1, Appendix B for the southern sample and E.1, Appendix E, for the northern one.

Of these two samples, only the southern one could be studied in some detail due to time restrictions. The study of three out of the six northern fields could only be started, and will therefore not be included in most of this work.

# 3 Observations

To study the properties of the stars in the sample, two types of observations were used: photometric and high-resolution spectroscopic observations. The spectroscopic observations were done mostly in two wavelength ranges, the first around the Li I 6708 Å doublet, and the second around the Ca II H and K lines. For the early F stars, for which very weak Ca II lines could be expected, the observation of the H and K lines were replaced by observations of the He I $D_3$ 5876 Å triplet.

For the southern hemisphere sample, the observations were carried out mostly at the European Southern Observatory, with some stars also observed at the Mount Stromlo Observatory. Some data was gathered, for a limited number of stars in the northern sample, spectroscopic observations at the Observatoire de Haute Provence and Calar Alto Observatory, and photometric observations at the Skinakas and Wise Observatories. For more details on the observing runs, see Tables 3.1 and 3.4.

## 3.1 Photometry

The photometric observations carried out for the southern sample were all done at the ESO 50 cm telescope, using a photon-counting photomultiplier tube.

Two different tubes were used, a red sensitive dry-ice cooled EMI 9658R and a Peltier cooled Hamamatsu GaAs. The red EMI tube was preferred in the first runs, as it is less sensitive than the Hamamatsu, and allowed therefore the photometry of the brighter stars in the sample, up to V=5.5. For the fainter stars (V$\leq$12) the more sensitive Hamamatsu tube was preferred. The ESO standard $UBV(RI)_C$ filters were used (see Table 3.2).

Four objects had magnitudes above V=5.5 and could therefore not be observed. For these objects data from the literature was gathered. The objects in question are listed in Table 3.3 with the literature references used.

Each measurement consisted normally of three 10s integrations in each filter, except for the $U$ filter, which needed for all but the brightest stars longer integration times (15s-30s). For the faintest stars, longer integration times of 20s-30s were used also in the $BV(RI)_C$ filters. To obtain the transformation coefficients, standard stars from the Cousin's E-regions were observed, and the atmospheric extinction coefficients were obtained by observing two E-region standards of very different spectral types. These standards are listed in the Table D.1 in Appendix D.

The intention was to obtain also light curves for as many sources as possible, to determine the periods of binaries and rotation period of active stars, but the weather condition at La Silla (only 50% photometric weather), the number of sources and the reduced knowledge about binarity available in the early phases

| Southern Sample | | | | |
|---|---|---|---|---|
| Dates | Observatory | Telescope | Detector | Prog. ID |
| 22 Apr. ÷ 02 May 1994 | La Silla | 50cm ESO | EMI 9658R | 53.7-0132 |
| 01 Oct. ÷ 10 Oct. 1994 | La Silla | 50cm ESO | EMI 9658R | 54.E-0382 |
| 02 Nov. ÷ 12 Nov. 1995 | La Silla | 50cm ESO | Hamamatsu | 56.E-0117 |
| 06 May ÷ 16 May 1996 | La Silla | 50cm ESO | Hamamatsu | 57.E-0382 |
| Northern Sample | | | | |
| Dates | Observatory | Telescope | Detector | Prog. ID |
| 17 Nov. ÷ 27 Nov. 1995 | Skinakas | 1.3m | CCD camera | |
| 30 Nov. ÷ 11 Dec. 1995 | Wise | 1m | CCD camera | |

Table 3.1: Observing periods, for photometry.

| Filter | central $\lambda$ | $\Delta\lambda$ | Transmission |
|---|---|---|---|
| U | 3703 | 485 | 55.8 |
| B | 4424 | 980 | 54.8 |
| V | 5227 | 1040 | 78.4 |
| R | 5965 | 1212 | 71.1 |
| I | 7519 | 3002 | 94.0 |

Table 3.2: The ESO Cousins filters.

of the thesis unfortunately did not allow a successful execution of this part of the observing plan.

The data reduction was done using the PEPSYS package in MIDAS. The error resulting is of the order of 0.01 mag for the stars with V≤10 in all filters, for stars with V≥10 the error is of the order 0.02 mag in the *U* filter, and 0.01 mag in the other filters, for stars with V≥12, the error is of the order 0.05 mag in the U filter, 0.04 mag in the B filter and 0.03 mag in the remaining filters.

| Source | $m_v$ | References |
|---|---|---|
| RXJ 0505.6-5728 | 4.70 | Bessel, 1990 |
| RXJ 1132.9-3151 | 3.54 | Eggen, 1977 |
| RXJ 1428.2-0213 | 4.89 | Bessel, 1990 |
| RXJ 1446.3+0153 | 3.72 | Cousins, 1964<br>Andrillat et al., 1995 |

Table 3.3: The references used for the brightest sources in the sample.

| Southern Sample | | | | |
|---|---|---|---|---|
| Dates | Observatory | Telescope | Instrument | Prog. ID |
| 22 Apr. ÷ 02 May 1994 | La Silla | 1.4m CAT | CES | 53.E-0132 |
| 11 Oct. ÷ 21 Oct. 1994 | La Silla | 1.4m CAT | CES | 54.E-0382 |
| 14 July ÷ 17 July 1995 | La Silla | 3.6m | CASPEC | 55.E-0437 |
| 13 Mar. ÷ 18 Mar. 1996 | Mount Stromlo | 74' | Echelle Spectr. | |
| 23 Sep. ÷ 29 Sep. 1996 | La Silla | 1.4m CAT | CES | 00.0-0000 |
| 11 Oct. ÷ 16 Oct. 1996 | La Silla | 1.4m CAT | CES | 58.E-0615 |
| 18 Feb. ÷ 21 Feb. 1997 | La Silla | 3.6m | CASPEC | 58.E-0615 |
| 12 Mar. ÷ 14 Mar. 1997 | La Silla | 1.4m CAT | CES | 58.E-0615 |
| 27 June ÷ 29 June 1997 | La Silla | 3.6m | CASPEC | 59.E-0128 |
| Northern Sample | | | | |
| Dates | Observatory | Telescope | Detector | Prog. ID |
| 06 Dec. ÷ 17 Dec. 1994 | OHP | 1.53m | AURELIE | |
| 20 Dec. ÷ 27 Dec. 1994 | Calar Alto | 2.2m | Coude Spectr. | |

Table 3.4: Observing periods, for spectroscopy. The observing period between Sept. 23d abd 29th corresponds to reserved time for the 1.4 m CAT and CES.

Some of the stars from the northern sample could be observed during the runs at the Skinakas and Wise Observatories. The observations there were done using a CCD camera and the available sets of $UBV(RI)_C$ filters, although at the Skinakas Observatory, the $U$ filter could not be used, due to damage. To obtain the transformation coefficients as well as the atmospheric extinction coefficients, a set of open clusters with well studied photometry were also observed. The used clusters are listed in Table D.2 in the Appendix D.

These observations have not been fully reduced yet.

## *3.2 High-resolution spectroscopy*

The spectroscopy for the southern sample was carried out at the ESO Osbervatory at two different telescopes: the 1.4 m Coudé Auxiliary Telescope (CAT) with the Coudé Echelle Spectrograph (CES) for the brighter stars ($m_V \leq 11$ in the red, and $m_V \leq 10$ in the blue), and the 3.6 m telescope with the Cassegrain Echelle Spectrograph (CASPEC) for all the other fainter sources.

The resolution used in the spectroscopic observations was dependent on the instrument used. With the CES, a resolving power of 80.000 was used in the first two runs, during which the older CCD # 34 was employed. The new CCD # 38 was used in the last two runs due to its higher sensitivity especially in the blue. Because of a diffusion effect, the resolving power was degraded and only 70.000 could be obtained.

The observations at the 3.6m telescope with CASPEC have a resolving power of 40.000, the maximum obtainable with the spectrograph, for a slit-width of 1". The Echelle Spectrograph at Mount Stromlo Observatory reached a resolution of 50.000. But the spectra obtained there were very faint, the light path of the telescope being inadequate for the spectrograph, strongly reducing its efficiency.

For the observations around the Li I 6708Å line, radial and rotational standards were also observed, to allow the determination of $v_{\rm rad}$ and $v \sin i$ for the sample stars. The standards used are listed in Tables D.3 and D.4, together with the references from which they were obtained. A spectrum of the Sun was taken at twilight to serve as template for the radial and rotational velocity determination.

In addition to the observations around the Ca II H & K lines, B stars were observed. The B star spectra are more adequate for the correction of the instrumental slope than flatfields, so that the corrected spectra can then be flux calibrated (Pasquini et al. 1988). The observations of the He I $D_3$ line were accompanied by the observation of A-type stars, to remove the atmospheric lines present in that spectral range.

The spectra were extracted using the noao.imred.echelle package in IRAF, after being bias subtracted and flatfield corrected. The wavelength calibration was done using ThAr spectra.

A few of the northern stars could also be observed, with the 1.53 m Telescope and AURELIE, at the Observatoire de Haute Provence, and with the 2.2 m and Coudé Spectrograph at the Calar Alto Observatory. All the Lithium spectra obtained were taken at the Observatoire de Haute Provence, with a resolution of 35.000, the Helium line was observed at the Calar Alto Observatory, and Calcium line spectra were obtained from both observatories.

In total 26% of the stars of the northern sample were observed in the Lithium range and 29% in the Ca II/He I range. The observations were reduced using the Long Slit package in MIDAS, after being bias subtracted and flatfield corrected. The wavelength calibration was done using ThAr spectra.

# 4 Analysis

## 4.1 Photometry

### 4.1.1 Spectral classification

From the magnitudes in the the $UBV(RI)_C$ filters obtained from the photometric observations the colour indices $(U-B)$, $(B-V)$, $(V-R)_C$ and $(V-I)_C$ were defined for all the sample stars. For the four bright stars mentioned in Sect. 3.1, the indices obtained from the literature were used. These indices were then used to verify and precise the spectral classification that had been obtained in the course of the identification program either from the low-resolution spectra or from the SIMBAD database.

For this purpose, tables containing mean values of the colour indices for stars of spectral types A to K and luminosity classes V, IV, and III were used. These tables have been compiled by Cutispoto et al. (1996).

For each star, the observed colour indices were compared with the values in the tables. The combination of spectral type and luminosity class that best matched the observed values was then selected for the star's spectral classification. In some cases, no matching set could be found. The star was then assumed to be a binary, and the combination of two stars that matched the observed data best was selected as classification. The single-star/binary assumption was checked using the high-resolution spectra around the Li I 6708 Å line. In most cases, the spectra confirmed the assumption. In a few cases, though, the classification had to be revised after such a check. Those were mostly cases in which the colour indices matched a single star but the spectrum clearly showed two line systems, or the very few cases (2) in which the object revealed itself to be a triple system.

This method is based on the assumption that the stars in the sample are normal, unreddened stars. Considering the detection limits of X-ray observatories, and the relatively low level of the X-ray emission of stars (normally $10^{25} - 10^{32} erg\ s^{-1}$), this assumption is not unreasonable. Most observed stars will be near to the Sun, and therefore have a negligible reddening through the Interstellar Medium (ISM). Nonetheless, it is not a perfect way of classifying the stars, since no tables exist for highly active or Pre-Main-Sequence (PMS) stars, for which the colour indices strongly differ from those for "normal" Main-Sequence and older stars.

### 4.1.2 The $(U-B)$ colour index

In the course of the classification process, it was noted that, for most stars, the observed $(U-B)$ colour index was systematically bluer than expected for the spectral types best matching the other three colour indices. Figure 4.1 shows this tendency clearly.

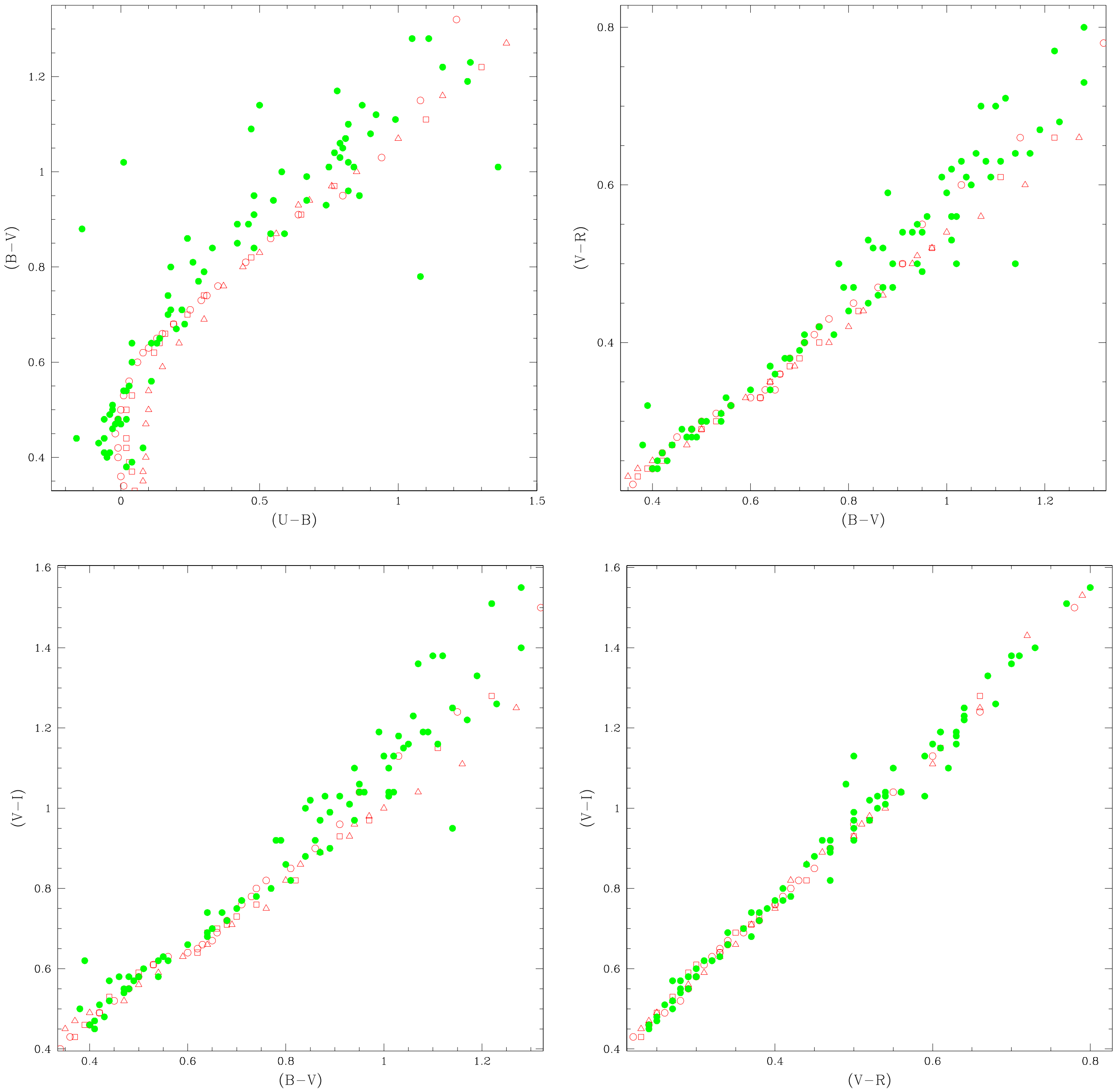


Figure 4.1: Color-Color plots. The filled green circles represent the data observed with the ESO 50 cm for the southern sample. The empty red symbols represent the mean values from the tables of Cutispoto et al. (1996), circles being the data for main-sequence stars, squares for subgiants and triangles for giants.

The reason for this trend is not fully understood yet. Some of the problem surely comes from the large errors in the U filter, and also in the B filter for the fainter stars. This at least is indicated by the spread observed in the three first plots of Fig. 4.1, which all include at least the $(B-V)$ colour index. The spread is rather large towards the K stars, where the fainter stars are mostly to be found, and nearly inexistent at the bluer end, where the brighter F stars are located. This is further confirmed by the lack of such a spread in the last, $(V-I)$ vs $(V_R)$ plot, where the observations had a small error bar for all stars.

But the error in the U-filter cannot be the only explanation for the nearly always bluer value of the $(U-B)$ colour, since this is the only index for which a shift as well as a spread is observed. More data is necessary to determine the cause of the problem.

### *4.1.3 Effective temperature*

The effective temperature $T_{\rm eff}$, necessary among others to get the synthetic spectra for the lithium abundance determination of fast rotators and multiple systems, can be calculated from the $(B-V)$ index. For this I used the work of Alonso et al. (1996), in which the data from a huge sample of stars with known effective temperature and colour indices was used to derive relations between a colour index and $T_{\rm eff}$.

Among the different equations derived in the work of Alonso et al. (1996), the appropriate one for my sample stars is:

$$\begin{aligned} \theta_{\rm eff} &= 0.541 + 0.533(B-V) + 0.007(B-V)^2 \\ &\quad -0.019(B-V)[\mathrm{Fe/H}] - 0.047[\mathrm{Fe/H}] - 0.011[\mathrm{Fe/H}]^2 \qquad (4.1) \\ \sigma(\theta_{\rm eff}) &= 0.023 \end{aligned}$$

with $\theta_{\rm eff}$ defined as $\theta_{\rm eff} = 5040/T_{\rm eff}$.

For the single stars, I used directly the observed $(B-V)$ index. For the binaries and multiple systems, on the other hand, the tables of Cutispoto et al. (1996) were used to get an estimate of the $(B-V)$ colour of each component, and this index was then used to get the effective temperature.

For the metallicity, I assumed solar metallicity for all the stars. This is a reasonable assumption, since the stars are near to the Sun. It turned out to be correct, in first approximation, for most of the objects. A few, though, displayed a metallicity that was clearly not solar. For these stars, the metallicity will have to be determined using spectroscopic observations in appropriate wavelength ranges.

The error in the $(B-V)$ index is, for the single stars, of the order of 0.02 mag to 0.05 mag. For the binaries, with a possible error of one spectral type for each component, the error lies in the range of 0.02 mag to 0.10 mag. This, together with the error of the equation itself, leads to an error in the effective temperature of up to 10%.

The results are listed in Table B.1, in Appendix B.

### 4.1.4 Absolute magnitude, distance and X-ray luminosity

The $(B-V)$ index was also used to get the absolute magnitude and the distance from the Sun of the sample objects. For this, as for the effective temperature, the $(B-V)$ colour from the colour tables of Cutispoto et al. (1996) was taken for the binaries and multiple systems, and the observed $(B-V)$ index was used for the single stars. The absolute magnitude was obtained from the $(B-V)$ vs. $M_V$ tables in Gliese (1982) for the later main-sequence stars ($(B-V) \geq 0.5$). For the earlier stars, as well as the giants and subgiants, the $M_V$ values listed in the tables of Cutispoto et al. (1996) were taken.

The error in $(B-V)$, given in the previous section, leads to an error in the absolute magnitude of 0.1 to 0.5 mag for the single stars, and 0.2 to 0.7 mag for the binaries. The corresponding error in the distance is of 5% to 23% for the single stars, and up to 30% for the binaries.

To calculate the observed X-ray flux $f_X$ from the ROSAT countrates, a conversion factor is needed. In most cases, a constant conversion factor is used. But there is an alternative conversion factor for coronal sources, that is a function of the first hardness ratio. This conversion factor was determined by Fleming et al. (1995) and is given by the following equation:

$$CF = (8.31 + (5.30 \cdot HR1)) \cdot 10^{-12} erg\ cm^{-2}\ count^{-1} \tag{4.2}$$

with the hardness ratio HR1, defined as:

$$\mathrm{HR1} = \frac{CR[ch52-201] - CR[ch11-41]}{CR[ch11-240]} \tag{4.3}$$

$CR[chA-B]$ is the countrate in the channels "A" to "B" of the PSPC.

Since most of the sample stars are within a circle of 200pc radius, extinction could be considered negligible. The remaining stars are still reasonably near to the Sun for the extinction to be neglected too. This allowed the use of this conversion factor, which takes the slope of the X-ray continuum at least partly into account, to determine the X-ray flux.

The error in the observed flux depends thus both on the error for the countrate and the one for the hardness ratio. Since the total number of counts is small in most cases, these two errors are quite large, adding up to a large error in the flux and in the X-ray luminosity derived from it. The error for the X-ray luminosity is of up to a factor 2.

The X-ray data obtained from the ROSAT observations is listed in Table A.1 in Appendix A, the data obtained from the photometric observations, as well as

| Name | Hipparcos data | | | Data from spectr. class. | | | Revised Spectral |
|---|---|---|---|---|---|---|---|
| | $\pi$ (m") | Dist. | $M_V$ | Spectral type | Dist. | $M_V$ | classif. |
| 2331.4−4209 | 10.16 | 98.4 | 3.28 | F9V+G1V | 77 | 3.83 | F8/9V+F9V+G1V |
| 2356.2−3903 | 45.28 | 22.0 | 6.51 | K3V | 21 | 6.60 | |
| 0005.9−4145 | 24.85 | 40.0 | 4.49 | G1V | 37 | 4.70 | |
| 0038.6−2335 | 16.01 | 62.5 | 3.12 | F3/4V | 58 | 3.30 | |
| 0053.0−3021 | 71.01 | 14.0 | 6.50 | K2/3V | 14 | 6.50 | |
| 0055.5−3731 | 12.22 | 81.8 | 4.10 | G6V | 46 | 5.35 | G6V/IV |
| 0105.4−4016 | 18.20 | 54.9 | 3.47 | F3V | 62 | 3.20 | |
| 0121.5−4058 | 11.16 | 89.6 | 3.82 | F6V | 90 | 3.80 | |
| 0135.8−3956 | 26.54 | 37.7 | 3.53 | F4V | 40 | 3.40 | |
| 0141.4−3808 | 23.87 | 41.9 | 3.07 | F3V | 39 | 3.20 | |
| 0440.3−5856 | 32.30 | 31.0 | 4.08 | G5V | 19 | 5.17 | G5V/IV |
| 0454.9−5832 | 32.38 | 30.9 | 3.66 | F5V | 32 | 3.60 | |
| 0505.5−5728 | 85.83 | 11.6 | 4.38 | F7/8V | 13 | 4.15 | |
| 0507.6−5459 | 15.05 | 66.4 | 3.23 | F5/6V | 50 | 3.80 | F5/6V/IV |
| 0527.6−6024 | 51.10 | 19.6 | 5.55 | G9V | 18 | 5.60 | |
| 0534.4−6006 | 12.48 | 80.1 | 3.88 | F7V | 76 | 4.00 | |
| 0535.0−6110 | 9.37 | 106.7 | 1.19 | G8/9IV | 44 | 3.10 | G4/5III |
| 0541.1−6151 | 4.90 | 204.1 | 3.07 | F3/4V | 192 | 3.20 | |
| 0545.3−5543 | 11.21 | 89.2 | 3.47 | F5V+G6V | 92 | 3.40 | |
| 0549.7−5950 | 7.07 | 141.4 | 3.11 | F7/8V(3x) | 148 | 2.91 | |
| 1121.5−3131 | 16.82 | 59.4 | 3.87 | F7/8V | 54 | 4.10 | |
| 1121.8−2411 | 20.82 | 48.0 | 4.71 | G3V | 43 | 4.93 | |
| 1122.0−2446 | 21.43 | 46.7 | 5.59 | K4/5V+K7V+.. | 28 | 6.74 | PMS system |
| 1123.3−2342 | 5.85 | 170.9 | 1.00 | G8III | 187 | 0.80 | |
| 1132.9−3151 | 25.23 | 39.6 | 0.55 | G8III | 35 | 0.80 | |
| 1354.2−0157 | 14.03 | 71.3 | 4.05 | F8V | 64 | 4.30 | |
| 1354.9−0222 | 8.40 | 119.0 | 3.51 | F9V+G5V | 97 | 3.97 | |
| 1358.4−0139 | 7.94 | 125.9 | 4.11 | G0V+G5V | 123 | 4.16 | |
| 1401.9+0025 | 15.60 | 64.1 | 4.26 | F8V | 63 | 4.30 | |
| 1404.0−0021 | 4.31 | 232.0 | 1.67 | F9V+G5V | 79 | 3.97 | F8 IV+G3IV+G3IV |
| 1411.5+0121 | 21.78 | 45.9 | 3.10 | F6V | 33 | 3.80 | |
| 1413.7−0050 | 17.94 | 55.7 | 2.17 | F6V | 50 | 2.41 | |
| 1428.2−0213 | 24.15 | 41.4 | 1.73 | G6IV+K5V | 22 | 3.08 | G2 III/IV+K0:V |
| 1446.3+0153 | 25.35 | 39.4 | 0.74 | A0V | 41 | 0.83 | |
| 1451.9+0201 | 25.68 | 38.9 | 5.39 | G5/6V | 41 | 5.30 | |

Table 4.1: The sources of the southern sample for which Hipparcos data was found.

X-ray flux, distance and X-ray luminosity are listed in the Table B.1, in Appendix B.

### 4.1.5 Hipparcos data

For some of the stars in the southern sample, Hipparcos data was available, most particularly the trigonometric parallaxes determined by Hipparcos, which allowed a determination of the distance independent of the photometric "parallaxe".

The objects, 35 in total, are listed in Table 4.1. For most the distances derived from the Hipparcos parallax fell well within the error of the distances determined using the spectral classification. But for a few stars, this was not the case. For these objects, the spectral classification was revised. The results of this new classification are summarised in Table 4.1.

## 4.2 Spectroscopy

### 4.2.1 Radial and rotational velocity

The high-resolution spectra taken around the lithium I 6708 Å line could be used to determine the radial velocities and projected rotational velocities for my stars. For this, the cross-correlation method, described by Tonry & Davis (1979),

$$f(\lambda) * g(\lambda) = \int_{-\infty}^{+\infty} f(\alpha)g(\alpha - \lambda)d\alpha \tag{4.4}$$

was chosen. $f(\lambda)$ and $g(\lambda)$ represent two here mathematical functions of a variable $\lambda$.

For this a template star with low rotation was observed, usually the Sun. The shift of the peak resulting from the cross-correlation of a star with the template represents the shift in $\lambda$ and the width of the peak the relative broadening between the two sets of lines.

To allow the translation of the shifts and widths of the cross-correlation peaks to radial and rotational velocities, a set of standards for both parameters was observed during each run as well. The standards used are listed in Tables D.3 and D.4 in Appendix D.

To derive the radial velocities, the radial velocity standards were first cross-correlated with the solar template, and the shift of the peak registered. The radial velocities of the standards were corrected to include the Earth movement, and the resulting line fitted. Then the actual sample stars were cross-correlated with the template, to get the shift, and their radial velocities, uncorrected for the Earth motion, calculated using the fit obtained for the standards. The heliocentric radial velocities were then determined through the substraction of the corresponding barycentrique velocity of the Earth.

For the rotational velocities, the method was similar. First the rotation standards were cross-correlated to the solar template. The width of the peak was

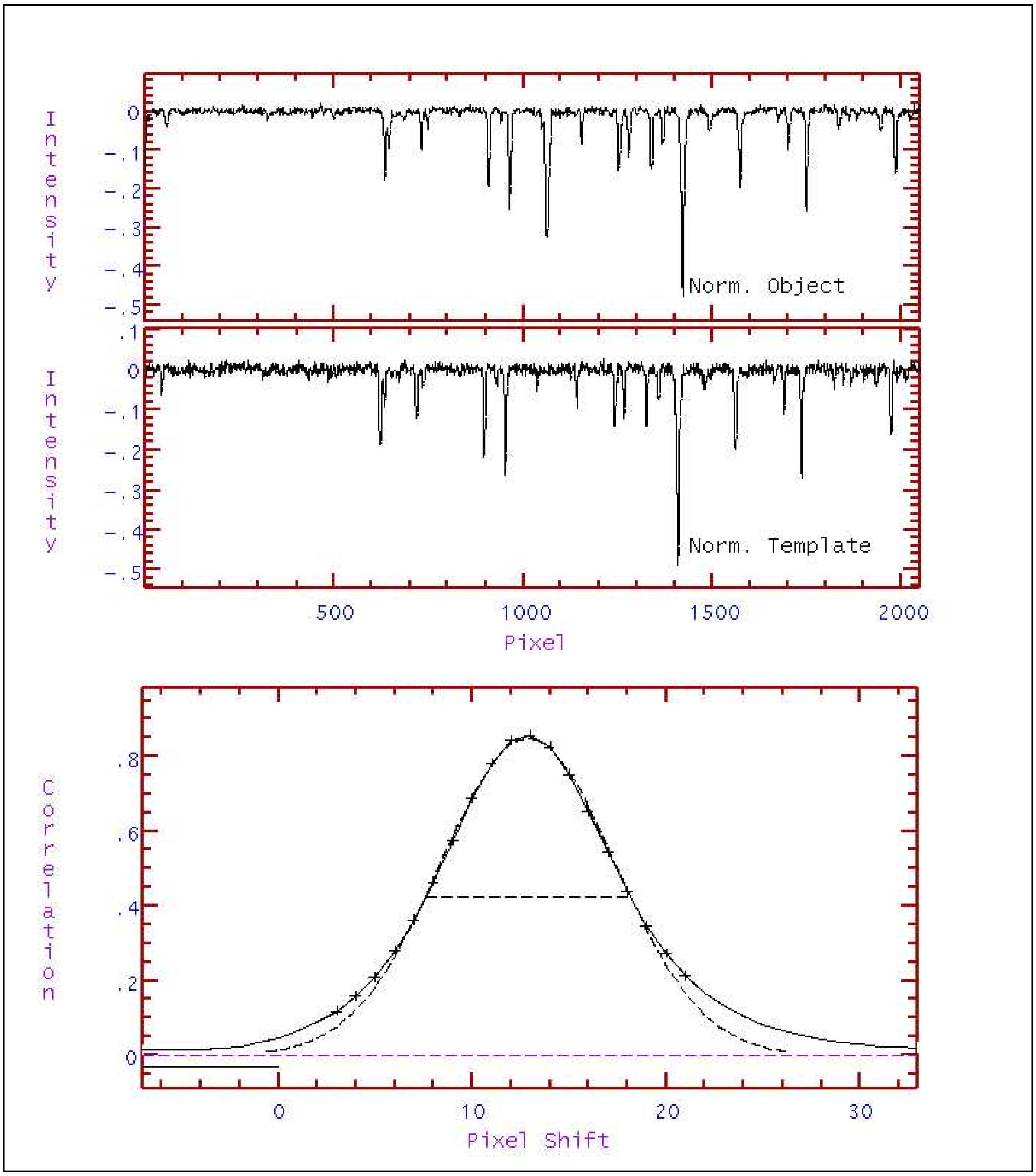


Figure 4.2: Spectrum, solar template and cross-correlation function with fit, for a slow rotating single star, RXJ 1121.8-2411, $v \sin i = 5$ km/s. .

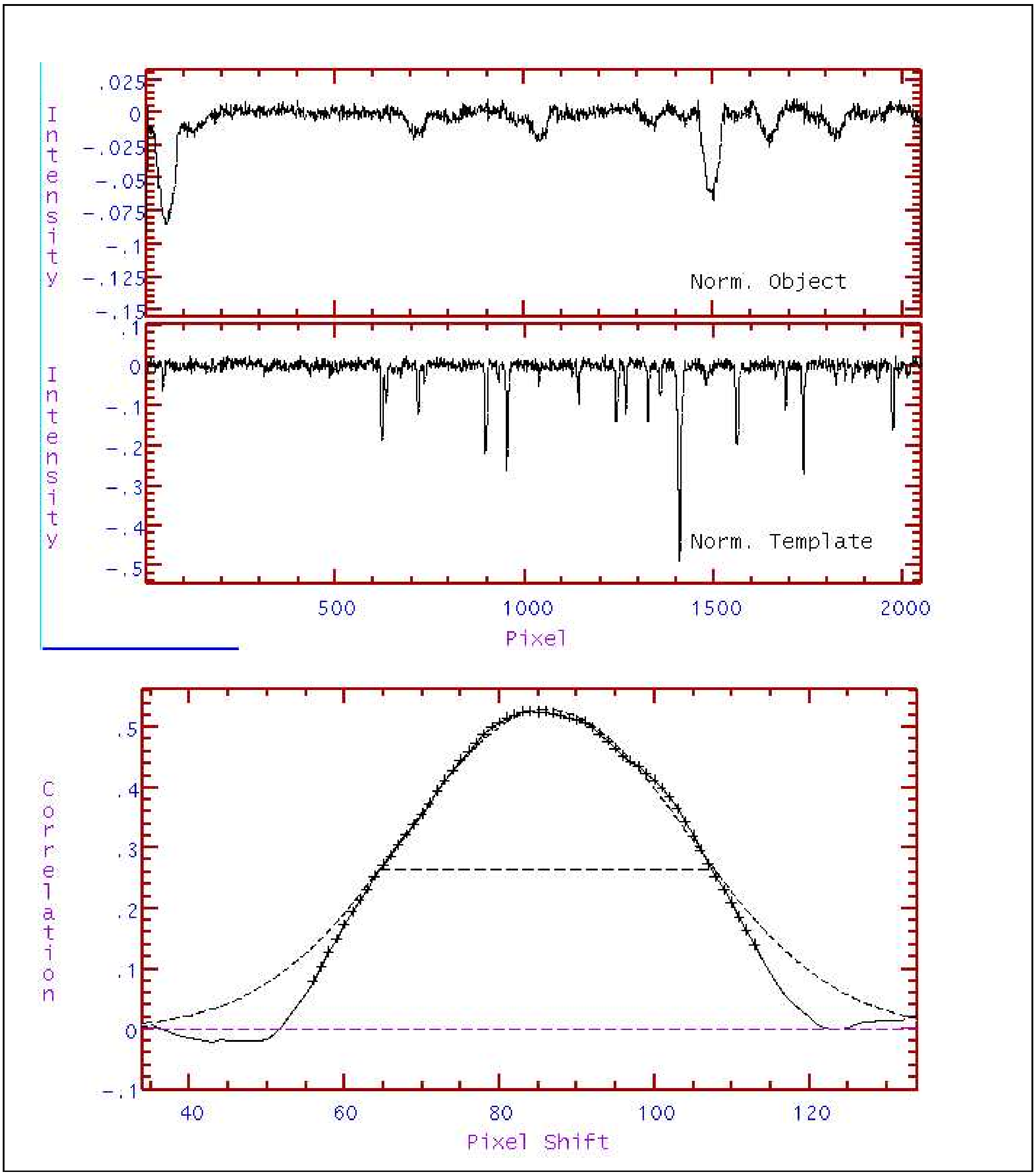


Figure 4.3: Spectrum, solar template and cross-correlation function with fit, for a single fast rotator, RXJ 0135.8-3956, $v \sin i = 33$ km/s. .

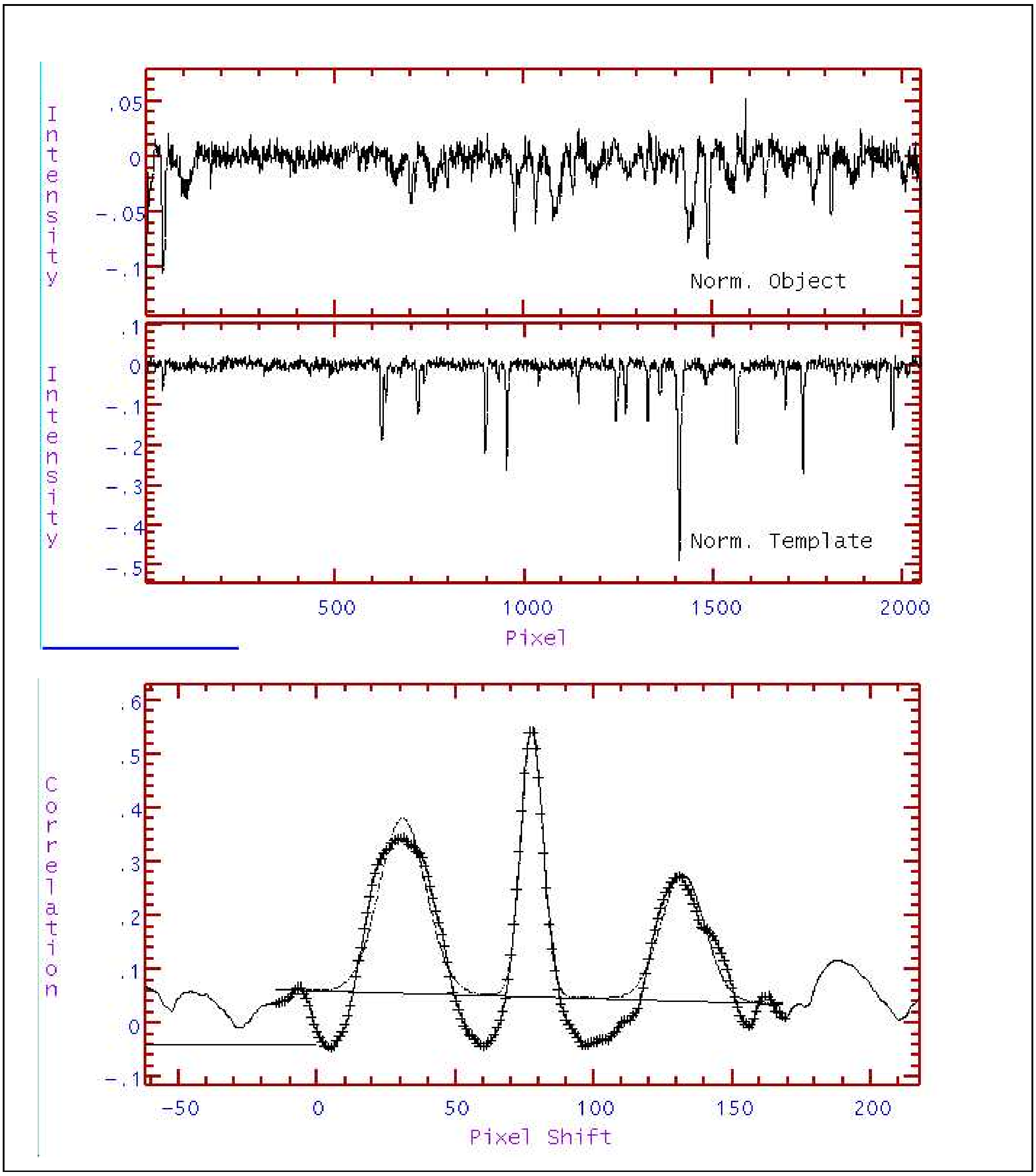


Figure 4.4: Spectrum, solar template and cross-correlation function with fit, for one of the triple systems in the sample, RXJ 2331.4-4209.

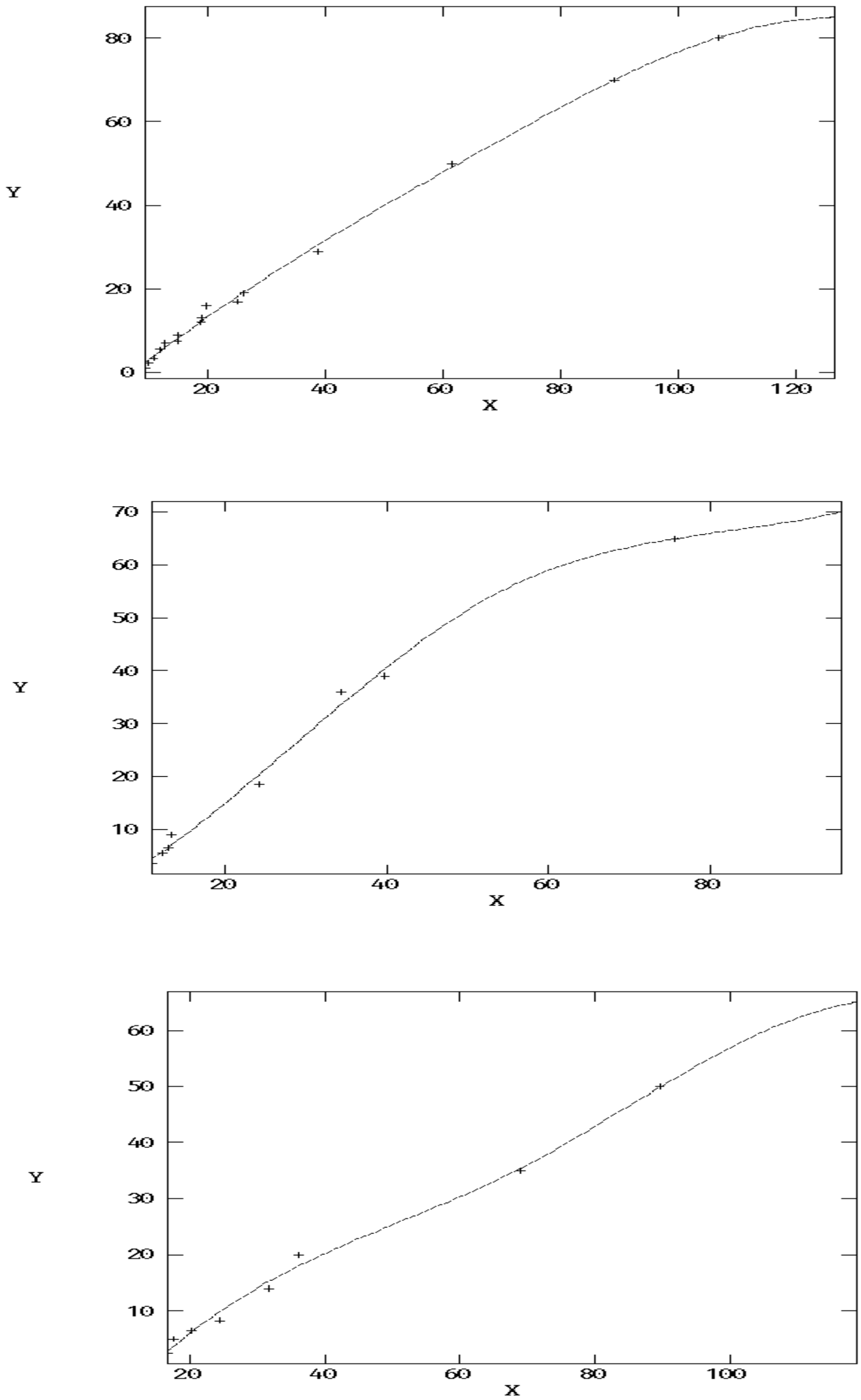


Figure 4.5: The fits obtained from the rotational velocity standards, for the determination of the projected rotational velocity of the sample stars. Top picture: the fit for the observations at the 1.4 m CAT, with the CES and CCD #34. Middle plot: the fit for the observations at the 1.4 m CAT with the CES and CCD #38. Last plot: the fit for the observations at the 3.6 m telescope with CASPEC. The width of the correlation peak (in pixels) is represented on the X axis, the vsini values in the Y axis.

determined, and the resulting $v \sin i$ vs width points were fitted with a polynomial. The cross-correlation peak width for the sample stars was then obtained, and the rotational velocity calculated using the fitted polynomial.

The cross-correlation was done using the **fxcor** routine in IRAF, the fitting with the **curfit** program. Some examples of cross-correlation peaks and gaussian curves fitted to the peaks to obtain the peak shift and width, are shown in Figures 4.2 to 4.4. The fits for the rotational velocity are shown in Fig. 4.5.

The uncertainty for $v \sin i$ depends to a large extent on the the fit. For the spectra taken with the CES, the resolution limit is of 3.5 km/s, for the CASPEC spectra the resolution limit is 7.5 km/s. I assume an error of $\sim$ 2 km/s for the fits for the low velocity end. For the higher velocities ($v/sini/ge50$), the determination of the width of the peak was more difficult, and so the error is larger, of up to 5 km/s.

For fast rotating binaries for which the lines overlap strongly, the error in $v \sin i$ is larger, due to the fact that an exact measurement of the width of the correlation peaks was not possible. The error here can be as large as 5 km/s.

### *4.2.2 Lithium abundance*

The high-resolution spectra were also used to determine the lithium abundance of the sample stars. The lithium dublett at 6708 Å is mostly used for this, and that was the primary motivation for the choice of the wavelength range for the observations.

For the slow-rotating single stars, for which the lithium line could be easily identified and measured, the abundance was determined directly using the equivalent width (EW) of the line. The major problem for this method is the blend of the lithium line with the neighbouring Fe I 6707.44 Å line. For the contribution to the total equivalent width of this iron line, the relation given by Soderblom et al. (1993)

$$W_\lambda(6707.44) = 20(B - V) - 3 \text{ mÅ} \tag{4.5}$$

was used. The EW obtained for the lithium line, after removal of the contribution of the iron line, was then transformed into an abundance using the curves of growth listed in Soderblom et al. (1993).

For the single stars with high rotational rate and for the binaries, the lithium abundance was determined using synthetic spectra. The synthetic spectra were calculated using the program SYNTH (Piskunov 1992) and model atmospheres from Kurucz (1993). To avoid the problems coming from errors in the excitation potential and log(gf) factor for the lines in the wavelength range considered, I used an atomic line list provided by Randich (1997). I first checked out the result by calculating a solar spectrum and comparing it to the solar spectra I had observed. To verify the validity of the result obtained with the synthetic spectra, a few low-rotating single stars were also fitted. The results from the EW method and of the synthetic fit were identical, within an error of 0.01 dex. Fig. 4.6 shows some examples of fitted spectra.

The synthetic spectra were wavelength-shifted, to fit the radial velocity shift of the observed spectra, and broadened to the rotational velocity of the corresponding stars, then superposed on the observations. For many of the binaries, only approximate values for the lithium abundance could be determined. This was due to the noise present in the spectrum.

The lithium abundances obtained are listed in Table C.1 in Appendix C. Errors lie in the range of 0.01 dex for the slow rotating single stars to 0.05 dex for the binaries with strong blends.

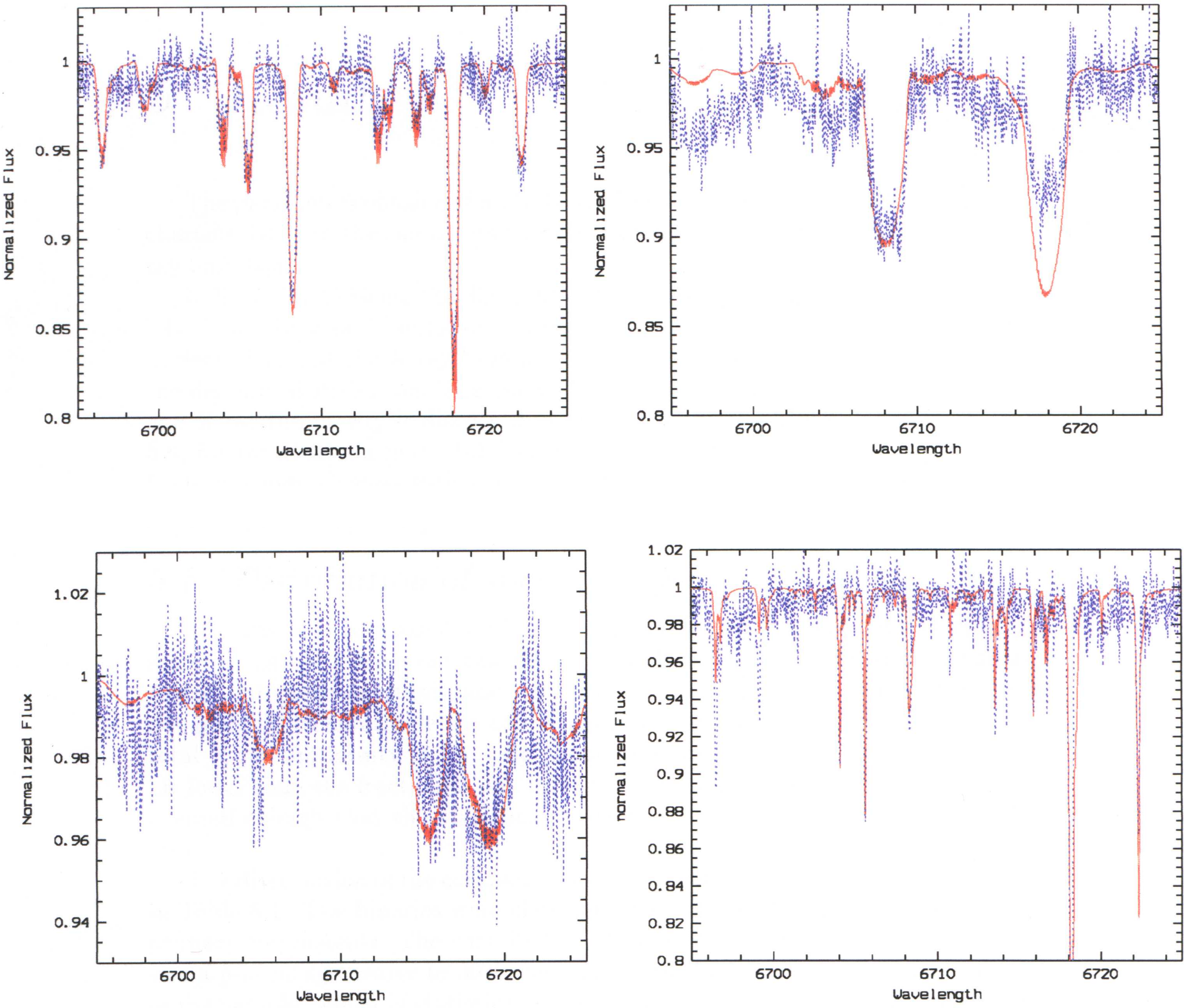


Figure 4.6: Some examples for the synthetic spectra used to determine lithium abundance in rapidly rotating stars and binaries/multiple systems. The stars shown are, from left to right and top to bottom: RXJ 0547.3-5450, RXJ 0505.6-5755, RXJ 1358.4-0139 and RXJ 2331.4-4209. RXJ 0505.6-5755 seems to have a non-solar metallicity.

# 5 Results

The parameters obtained for all the studied stars can now be used to determine characteristics of the sample and correlations between stellar parameters and X-ray emission.

In Sect. 5.1 I discuss the distribution of the stars among spectral type classes. The X-ray to visual luminosity ratios as function of spectral types are studied in Sect. 5.2, and the X-ray luminosity functions in Sect. 5.3. Sect. 5.4 handles the distance distribution. The search for correlations between stellar parameters and X-ray luminosity is discussed in Sects. 5.5, for the lithium abundance, and 5.6, for rotation. In Sect. 5.5 I also compare the lithium abundances to those from two open clusters with known age (the Hyades and Pleiades), to get a first estimate for the age or evolutionary status of my sample stars.

## 5.1 Distribution of spectral types

My sample is composed of 81 single stars (76%) and 26 binaries and multiple systems (24%). I have not taken into account which of the binaries are short-period, interactive systems, and which are wide systems at this stage, since it is not possible to determine the contribution of the individual components to the total X-ray luminosity in the long-period systems. The fraction of binaries is a bit lower than the fraction of one third of the sample expected. Still, the sample is small enough that the statistical errors can account for a large part for this also.

The distribution of the complete sample between spectral type groups is shown in Table 5.1. The binaries were classified according to the spectral type of their primary components. The contribution of the G stars seems a bit low, expected was a percentage nearer to 30%, comparable to the fraction of F stars. The size of the sample, which is statistically still rather small, is probably responsible for this effect, as is confirmed by the statistical errors.

| Spectral type | my sample | | EMSS sample | | EXOSAT sample | |
|---|---|---|---|---|---|---|
| A stars | 1±1 | 1±1% | 5±2 | 3±1% | 2±1 | 7±3% |
| F stars | 34±6 | 32±6% | 51±7 | 30±4% | 5±2 | 17±7% |
| G stars | 24±5 | 22±5% | 45±7 | 27±4% | 14±4 | 48±14% |
| K stars | 48±7 | 45±6% | 68±8 | 40±5% | 8±3 | 28±10% |

Table 5.1: Distribution of the X-ray sources among the spectral types studied, for my sample, the EMSS sample (Stocke et al. 1991) and the EXOSAT sample (Cutispoto et al. 1996)

Table 5.1 also lists the distributions for two other samples, the *Einstein Observatory* Medium Sensitivity Survey (EMSS) sample (Stocke et al. 1991) and the EXOSAT sample (Cutispoto et al. 1996).

My sample and the EMSS sample show a very similar distribution between spectral types. Since the samples are of similar size, and both X-ray selected, this result was expected. Clearly, this seems to indicate that both samples are composed of stars from similar populations. When taking into account statistical errors, the small differences become completely negligible.

The EXOSAT sample, on the other hand, differs from both my sample and the EMSS one. Here the greatest contribution to the sample comes from the G stars, the K stars being a poor second. But since the sample is a very small one, being composed only of 29 stars, it is doubtful whether this is more than a selection effect. The statistical errors are large enough that, when considered, the distribution of the EXOSAT sample can be neared to that of the other two. To confirm the possibility of the EXOSAT distribution being similar, down to statistical errors, to mine, I applied a Wilcoxon test (Zeidler, 1996) to both distributions.

Given two binned distributions X and Y, with respectively $n_1$ and $n_2$ bins. $x_i$ is the number of events in bin $i$ of the first distribution, $y_j$ the number of events in bin $j$ of the second distribution.

The Wilcoxon test consists of verifying for every pair ($x_i$,$y_j$) whether $y_j < x_i$. Every positive result of this verification is called an inversion. $U$ is defined as the total number of inversions present, $U_\alpha$ is a parameter dependent on the error probability $\alpha$ chosen.

Two distributions are said to have a significant difference, with an error probability $\alpha$, if the following condition is valid:

$$\left| U - \frac{n_1 n_2}{2} \right| > U_\alpha \tag{5.1}$$

The result for the distributions in spectral type bins for my sample and the EXOSAT sample, $|U - n_1 n_2/2| = 4 < U_\alpha = 8$ for $\alpha = 0.05$ clearly indicates that the distributions can be considered similar. The differences noted must come from statistical errors.

## 5.2 X-ray luminosity as a function of spectral type

From the X-ray luminosity and the visual magnitude, the ratio of the X-ray luminosity to the visual luminosity for each sample star can be obtained. The result is shown in Fig. 5.1. All the sources, single stars as well as multiple systems, are considered for this.

Also included in Fig. 5.1 are saturation levels found or calculated from previous studies. These saturation levels correspond, according to current models, to the level of activity for which the whole surface of a star is covered with active

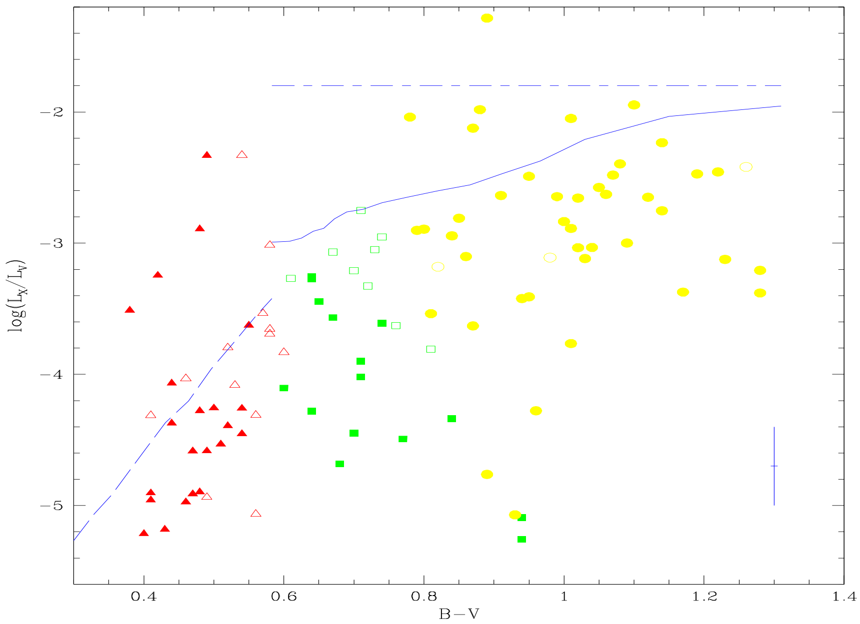


Figure 5.1: $\log(L_X/L_V)$ vs. the $(B-V)$ color index for the studied RASS sample. The red triangles represent the F stars, blue squares the G stars and green circles the K stars. Filled symbols stand for single stars, empty ones for the binaries and multiple systems. The continuous line represents the saturation level of $F_X \sim 7 \cdot 10^7 erg\ s^{-1}\ cm^{-2}$ detected by Fleming in his sample (Fleming, 1988). The dashed line is the upper limit for $L_X$ as calculated by Vilhu and Walter (1987). The dash-dot line is a constant $\log(L_X/L_V)$ of -1.8

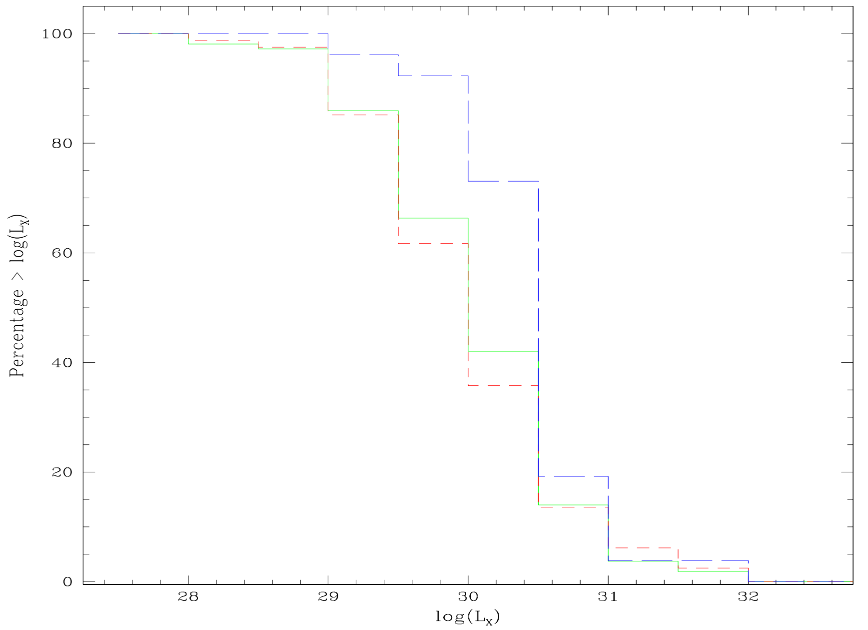


Figure 5.2: Luminosity distribution for the studied sample. Continous green line: the complete sample; red short-dashed line: the single stars; blue long-dashed line: the binaries and multiple systems.

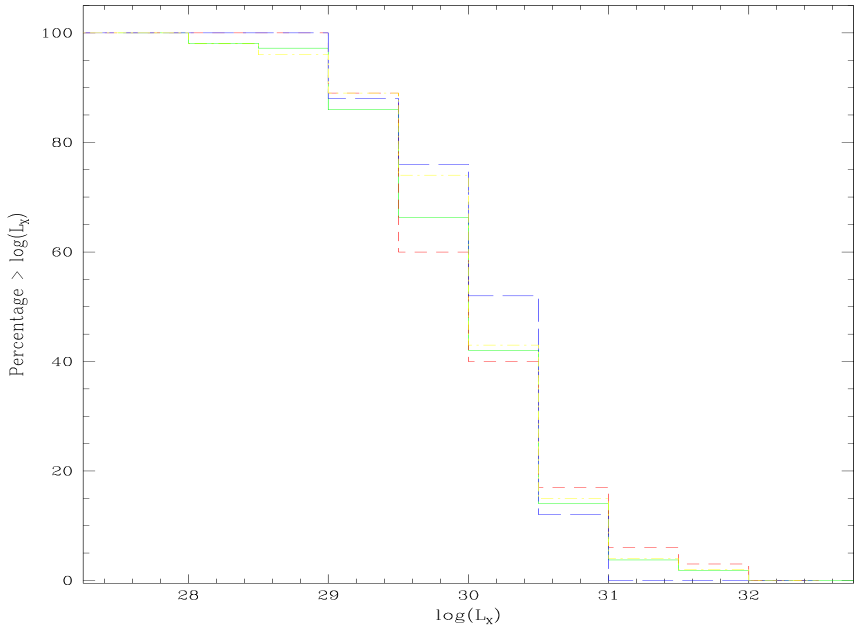


Figure 5.3: Luminosity distribution for the studied sample. Continous green line: the complete sample; red short-dashed line: the F stars; blue long-dashed line: the G stars; yellow dot-dashed line: the K stars.

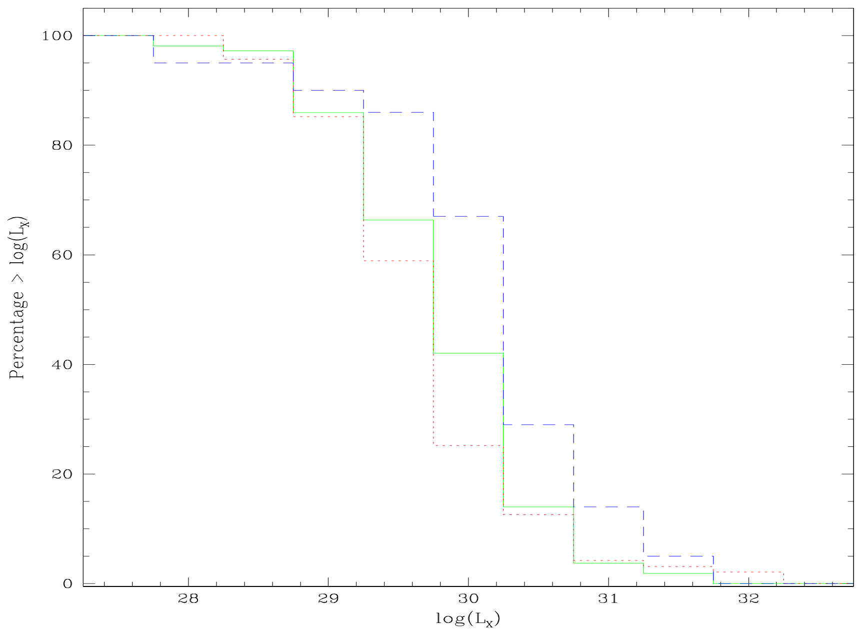


Figure 5.4: Luminosity distribution for the studied sample (continous green line), compared to the luminosity function for the EMSS sample (Fleming 1988, doted red line line) and the EXOSAT sample (Cutispoto et al. 1996, dashed blue line).

regions. For the earlier type stars ($(B-V) \leq 0.64$) I have included the saturation level calculated by Vilhu and Walter (1987), for the later spectral types the possible saturation surface flux found by Fleming (1988) for the EMSS sample he studied.

The first thing that can be noted in Fig. 5.1 is the large spread present for each spectral type. The spread is larger than can be accounted for by the large error from the X-ray luminosity, and is therefore real. It is an indication for the large spread in activity levels present among the stars in my sample.

Most of the stars in my sample stay bellow the upper limits obtained from previous works. The bluer stars, with $(B-V) \leq 0.64$, follow well the saturation level calculated by Vilhu and Walter (1987), while the redder stars with $(B-V) \geq 0.64$ follow the curve corresponding to the limiting surface flux of $F_X \sim 7 \cdot 10^7\ erg\ s^{-1}\ cm^{-2}$ found by Fleming (1988) for his EMSS sample. A few stars, though, do not follow this behavior, but have instead values for the ratio well above the saturation levels. If these stars were binaries, the excessive levels of X-ray emission could be understood, but for the most part, the over-bright objects are single stars. This is a surprising result, and still badly understood, since more data about the stars would be necessary to fully analyze it. One possible explanation would be that these objects are up to now unrecognized multiple systems.

Another notable feature in Fig. 5.1 is the lack of low X-ray luminosity objects for $(B-V)$ values above 1.0, or spectral type K4. For all earlier spectral types, the spread goes from an $\log(L_X/L_V)$ of $\sim$ -5.6 up to, and even above, the corresponding saturation limit. But for the later K stars, the lowest detected star has an X-ray to visual luminosity ratio of $10^{-3.5}$.

For those late K stars, the levels of activity $\log(L_X/L_V)$ between -4 and -5 correspond to X-ray luminosities between 28.5 and 27.5. According to the flux limit of the RASS, this means that such stars can only be detected if they lie within a radius of 36pc for the higher activity level, and 10pc for the lower one. Schmitt et al. (1995) have made a study of a complete, volume-limited sample of K stars. The sample was limited to the K stars within 7pc of the Sun. This study has shown that the X-ray luminosities corresponding to the absent activity levels are quite rare among the nearby K stars. Only 27% of the K stars in the volume-limited sample of Schmitt et al. (1995) have an X-ray luminosity of $\log(L_X) \geq 27.5$, which would make them detectable at distances of $\sim$ 10pc. My sample contains only 15 K stars of spectral type later than K4 and belonging to the Gliese catalogue. Among those stars, only 2 are within 10-11pc from the Sun, and another two lie at a distance of 12pc. According to the statistics from the sample of Schmitt et al. (1995), at the most one of these objects should have an X-ray luminosity of $\log(L_X) \sim 27.5$, making it detectable at this distance. This causes the gap observed in Fig. 5.1.

| First sample | Second sample | $\chi^2$ | $\nu$ | $P_{\chi^2}$ |
|---|---|---|---|---|
| RASS complete sample | RASS single stars | 0.997 | 8 | 0.998 |
| RASS complete sample | RASS binaries | 14.674 | 8 | 6.579e-2 |
| RASS single stars | RASS binaries | 20.947 | 8 | 7.289e-3 |
| RASS complete sample | RASS F stars | 1.342 | 8 | 0.995 |
| RASS complete sample | RASS G stars | 21.857 | 8 | 5.188e-3 |
| RASS complete sample | RASS K stars | 0.560 | 8 | 0.9998 |
| RASS complete sample | EMSS sample | 6.974 | 9 | 0.640 |
| RASS complete sample | EXOSAT sample | 20.598 | 8 | 8.296e-3 |

Table 5.2: Results of the $\chi^2$ tests for the X-ray luminosity distributions.

## *5.3 Luminosity function*

A useful characteristic of the sample is the X-ray luminosity function. The luminosity function for the whole sample can be obtained, as well as the functions for the different spectral types, since the X-ray luminosity has been determined for every star in the sample.

First, I shall consider the distribution of the X-ray luminosity for the whole sample. Fig. 5.2 shows the corresponding histogram, for the percentage of stars with $\log(L_X) \geq \log(L_X)_{\rm min}$. It is clear that the largest part of the sample has a luminosity between 29.0 and 30.5, with only very few stars at lower or higher luminosities. 75% of the stars lie in this mid-luminosity range. The small number of low-luminosity stars can be explained by the flux-limit of the ROSAT All-Sky Survey. Stars with X-ray luminosities below 28.5 could only be detected if they were within a distance of 36pc. For the high-luminosity stars, on the other hand, the small number of detections leads to the assumption that such sources are rare, at least within the detection sphere of the RASS.

Also shown in Fig. 5.2 are the distributions for the single stars and the multiple systems. In those cases the percentage is calculated relative to the corresponding subsample. It is clear that the detected multiple systems tend towards the higher X-ray luminosities. I applied $\chi^2$ tests to the three distributions, whole sample, single star subsample and binary subsample.

If $R_i$ is the number of events in bin $i$ for the first sample, and $S_i$ the number of events in the same bin for the second sample. Then $\chi^2$ is defined as

$$\chi^2 = \sum_i \frac{(R_i - S_i)^2}{R_i + S_i} \tag{5.2}$$

The probability $P_{\chi^2}$ to find, in random distributions, a value of $\chi^2$ that is larger or equal the one found (i.e. the significance of $\chi^2$) is given by the incomplete gamma function

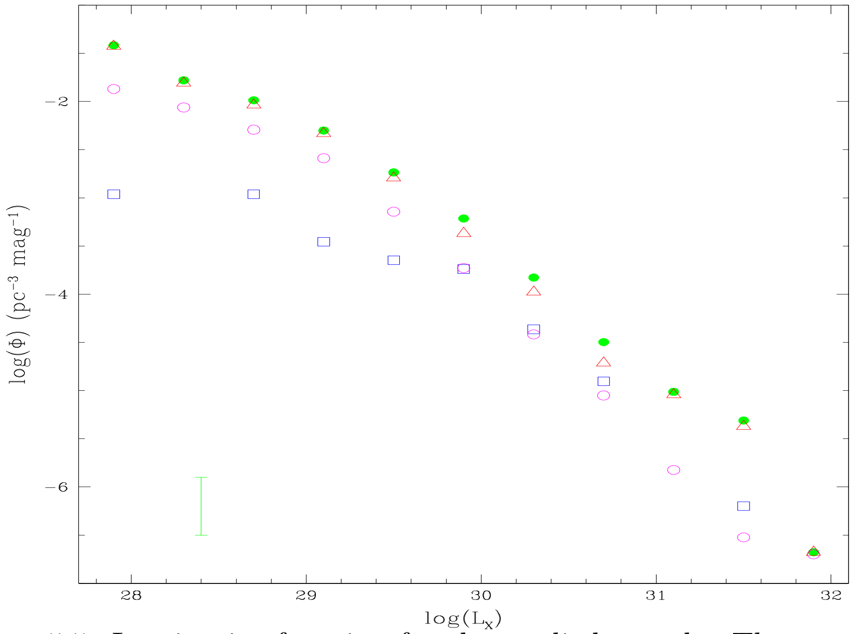

Figure 5.5: Luminosity function for the studied sample. The green filled points represent the whole sample, the red triangles the luminosity function for the single stars alone and the blue squares the luminosity function for the binaries. The empty circles represent the luminosity function for the EMSS subsample, for which ROSAT X-ray luminosites were available.

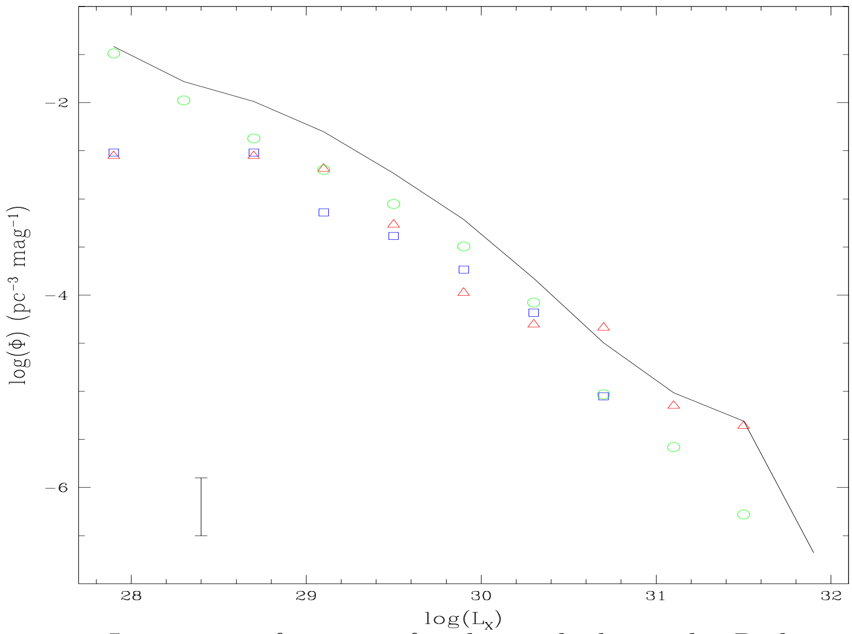

Figure 5.6: Luminosity functions for the studied sample. Red triangles: F stars; blue squares: G stars; green points: K stars. Both single stars and binaries are taken into account. The black line represents the luminosity function for the complete sample.

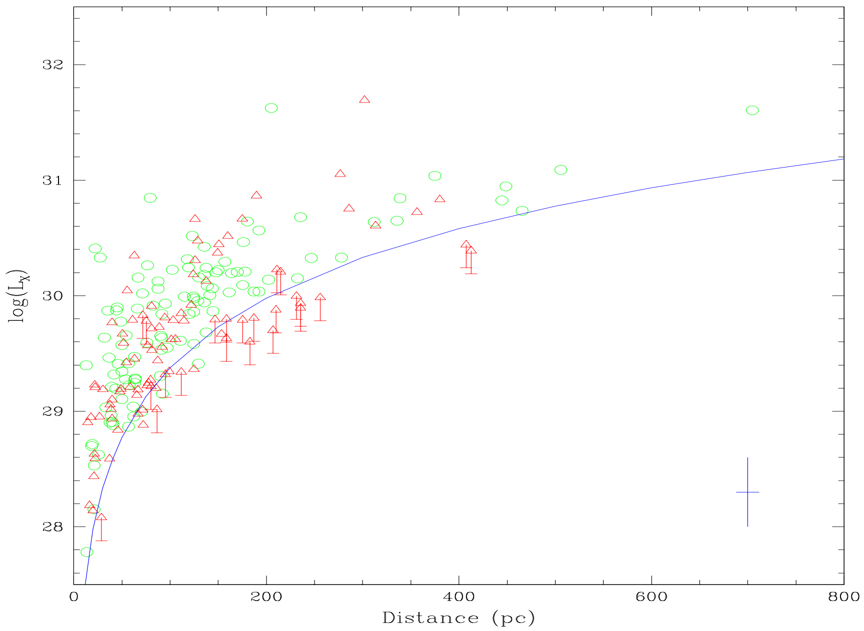


Figure 5.7: X-ray luminosity as a function of distance for the studied RASS sample (open circles) and for the EMSS sample (open triangles). Triangles with downward pointing lines represent upper limits for the X-ray luminosity of EMSS objects. The continous line represents the detection limit of ROSAT.

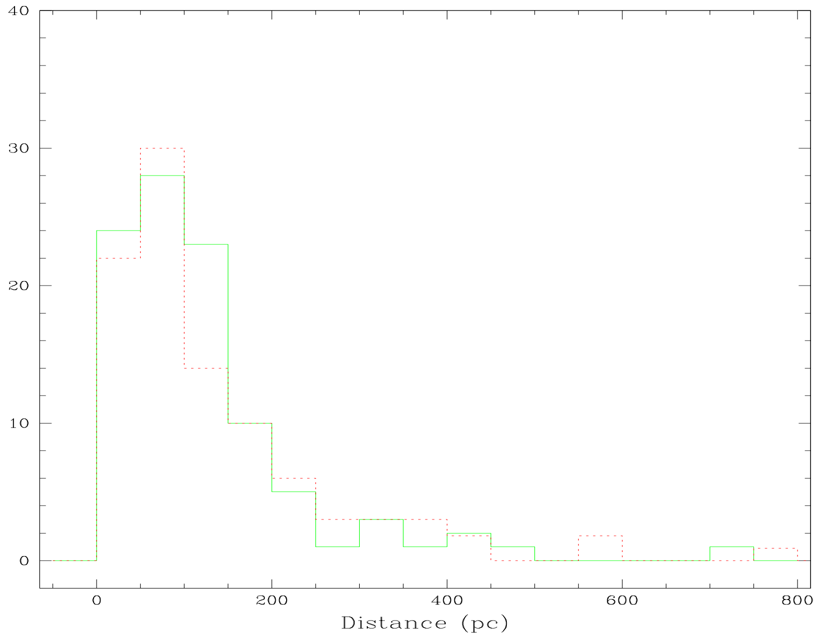


Figure 5.8: Histrogram of the distance distribution. Continuous green line: my RASS sample; red pointed line: the EMSS sample. Values are percentage of the whole sample.

$$Q(\frac{\chi^2}{2}, \frac{\nu}{2}) \equiv \frac{1}{\Gamma(\frac{\nu}{2})} \int_{\chi^2/2}^{\infty} e^{-t} t^{(\nu/2)-1} dt \tag{5.3}$$

were $\nu$ represents the degrees of freedom and $\Gamma(x)$ is the Gamma Function. The test was taken from Press et al. (1992).

The smaller $Q(\frac{\chi^2}{2}, \frac{\nu}{2})$, the less probable it is that the two distributions compared are similar. A small value of $Q(\frac{\chi^2}{2}, \frac{\nu}{2})$ (of the order 0.05) means that the two samples compared are significantly different.

The results, listed in Table 5.2, show that the single stars have an X-ray luminosity distribution similar to the one of the complete sample, while the distribution for the binaries shows significant differences to both other distributions. The similarity between the distribution for the complete sample and the single star subsample can be explained by the fact that the single stars constitute the largest part of the complete sample. As for the binaries and multiple systems, most of the detected ones can be expected to be short-period interacting ones, where the interaction should enhance stellar activity. So their luminosity distribution should tend towards the higher luminosities.

The breakdown of the distribution among the three spectral type classes studied is shown in Fig. 5.3. The percentages are calculated again relative to the respective subsamples. From this plot, it is recognizable that the F stars tend to contribute more to both extremes of the luminosity distribution rather than to the mid-luminosity range of $\log(L_X)$ between 29.0 and 30.5. The G stars, on the other hand, have X-ray luminosities lying only in the mid-luminosity range, up to a $\log(L_X)$ of 31.0. The K stars are more evenly distributed over the whole range. $\chi^2$ tests (Table 5.2) show that only the distribution for the G star subsample can be considered significantly different from the distribution for the complete sample. Since a large fraction of the G star subsample is composed of binaries, this is not surprising.

In order to compare the distribution of X-ray luminosities of my sample with those from the EMSS and EXOSAT samples, I plotted the three distributions in Fig. 5.4. The X-ray luminosities used for the EMSS sample are ROSAT luminosities taken from Fleming et al (1995). In this paper the results of a re-detection of the EMSS sources in the RASS are listed. Only 95 sources out of the 109 late-type sources studied by Fleming (1988) were re-detected with ROSAT. These sources were used to determine the X-ray luminosity distribution, to facilitate the comparison with my sample. The luminosities given for the EXOSAT sample, on the other hand, are the EXOSAT luminosities. A direct comparison between this sample and my RASS sample is more difficult, since the energy range of both surveys are very different (ROSAT: 0.1-2.4 keV, EXOSAT: 1-50 keV). The sample was added for completeness. The large difference in the distributions is hard to interpret. It would be useful to get ROSAT luminosities for the EXOSAT objects, to allow a better comparison of this sample, which appears to be very different from both the EMSS and my RASS samples.

Figure 5.4 shows again a strong similarity between my sample and the EMSS sample, as is confirmed by the $\chi^2$ test performed (see Table 5.2). Both have the strongest concentration of stars between $\log(L_X)$ of 29.0 and 30.5. The mean values of both samples are near to identical, $< \log(L_X) > = 29.77$ for my sample, and 29.68 for the EMSS sample. On the other hand, the median values are very different: 29.78 for my sample, and 29.62 for the EMSS sample. The difference in the median value is due to the uneven distribution of the sources between luminosity bins. The distribution is not even near Gaussian, having two bins with very large concentration of sources. Therefore I consider the difference of nearly 0.2 dex between the median values of the two samples as a negligible difference, caused by the errors inherent to such statistically small samples, and tend to consider both samples as coming from the same stellar X-ray population.

The one major difference between the two samples is the presence of very high X-ray luminosity ($\log(L_X) \geq 32$) stars in the EMSS. Four such stars are contained in the sample studied by Fleming (1988), of which one has been re-detected with ROSAT, and a second has an upper limit for its ROSAT luminosity. Such extremely luminous stars are not present in my sample. This is most probably due to the fact that such sources are extremely rare. But this difference could also be partly due to the identification criteria used in the identification programs as well as the spectral classification. The spectral classification is in so far critical, as it is sometimes difficult to distinguish luminosity classes (for instance dwarfs and subgiants), and a misclassification in the luminosity class would lead to a very large error in the distance and the X-ray luminosity.

To check out the validity of the assumption that both X-ray luminosity distributions, my sample's and the EMSS's, are significantly similar, I have applied to the distributions two statistical tests: the Wilcoxon test mentioned in Sect. 5.1, and the $\chi^2$ test.

The results of both tests (Wilcoxon:$|U - n_1 n_2/2| = 9 < U_\alpha = 27$; $P_{\chi^2}$=0.640, see Table 5.2) indicate that the null hypothesis, that the two X-ray luminosity distributions are similar, cannot be disproved. Both samples can be considered to have similar X-ray luminosity distributions. A similar $\chi^2$ test applied to my RASS sample and the EXOSAT one confirms, on the other hand, the differences between the X-ray luminosity distributions to be significant.

Since all the stars of my sample have known X-ray luminosities, I can also construct luminosity functions for various subsamples. I can do this, since my sample can be considered complete within the studied fields.

To obtain the luminosity function, I use a method described by Schmidt (1968). For each star, the maximal radius and volume $V_a$ at which it could still be detected by ROSAT is calculated. To take into account the spatial distribution of the stars in a disk, a new volume $V'_a$ is defined:

$$dV'_a = e^{-z/z_0} dV_a \tag{5.4}$$

where $z$ is the height above the galactic plane, and $z_0$ is the stellar scale height (Upgren 1963). The values for the stellar scale height used were 115pc for the A star, 190pc for the F dwarfs, 340pc for the G dwarfs and 400pc for the giants, and 350pc for the K dwarfs. These are the same values as those used by Fleming (1988) to determine the X-ray luminosity function for the EMSS sample. The contribution of each star to the total luminosity function is then given by $1/V_a'$. The X-ray luminosities are binned in 0.4dex intervals, which roughly correspond to one optical magnitude.

The resulting luminosity functions for the available range of $\log(L_X)$ between 27.5 and 32.0 are shown in the Fig. 5.5 and 5.6.

Fig. 5.5 shows the luminosity function of the whole sample as well as those for the single stars and the multiple systems. The trends already visible in the corresponding X-ray distributions are even more marked here.

The luminosity function for the whole sample has the strongest slope between $\log(L_X)$ 29.0 and 31.5. The contribution of the binaries to the total luminosity function is small, with the largest contribution at the high-luminosity end. The single stars have nearly the same luminosity function as the complete sample. Unfortunately, the number of binaries in the sample is small, so their luminosity function is rather uncertain.

Also plotted in Fig. 5.5 is the luminosity function for the EMSS sample. The similarity between both this sample and my RASS one are again visible. Only toward the high-luminosity end do both samples differ from one another.

The luminosity functions for the F-, G- and K-stars subsamples are given in Fig. 5.6. In these cases also, the trends recognizable in the X-ray distribution are more notable. The luminosity function for the F stars rises strongly at the low-luminosity end, while the function for the G stars starts around $\log(L_X)$=30.5 and rises until $\log(L_X)$=29.0, where it flattens. The luminosity function that best reproduces the one for the whole sample is that of the K stars.

## 5.4 *Distribution with distance*

More information about the general properties of the sample is given by the distribution of the X-ray luminosity with distance. Fig. 5.7 shows a plot of $L_X$ as a function of the distance for my sample as well as the EMSS sample. In this case also, the available ROSAT X-ray luminosities were used for the EMSS sample, to facilitate a comparison between the two samples.

Figure 5.7 is a plot of the X-ray luminosity as a function of distance for both samples. Here, as well as with the X-ray luminosity distribution, both samples display a similar behavior. A few of the EMSS stars have upper limits for their ROSAT luminosity that lie bellow the detection limit of the RASS. Apart from this, and the already mentioned, in the plot not visible, high-luminosity tail at $\log(L_X) \geq 32$, the distribution of the X-ray luminosity with distance is very similar for the two samples. This was at least partly substantiated by a 2

| First sample | Second sample | $\chi^2$ | $\nu$ | $P_{\chi^2}$ |
|---|---|---|---|---|
| RASS complete sample | EMSS sample | 9.436 | 12 | 0.665 |
| RASS single stars | RASS binaries | 46.588 | 11 | 2.544e-6 |

Table 5.3: Results of the $\chi^2$ tests for the distance distributions.

dimensional Kolmogorov-Smirnov test applied to the two sets of (distance,$L_X$) data points.

The Kolmogorov-Smirnov test for two samples, as described by Fasano & Franceschini (1987), consists of determining the maximal difference $D$ between the data points of both samples. The procedure was taken from Press et al. (1992).

The significance of this maximal difference is then given by:

$$P_{KS}(D > observed) = Q_{KS}\left(\frac{\sqrt{N}D}{1+\sqrt{1-r^2\left(0.25-0.75/\sqrt{N}\right)}}\right) \quad (5.5)$$

where $Q_{KS}$ is defined as:

$$Q_{KS}(x) = 2\sum_{J=1}^{\infty}(-)^{j-1}e^{-2j^2x^2} \quad (5.6)$$

The number of data points $N$ for two samples is $N = \frac{N_1 N_2}{N_1+N_2}$, and $r$ is a combination of Pearson's $r$ for each sample, $r = \sqrt{1-0.5(r_1^2 r_2^2)}$. The smaller $P_{KS}$, the less probable it is that both samples have the same distribution. A small value, of the order of 0.05, means that both samples have to be considered significantly different.

The results of this test, $D = 0.197$ and $P_{KS} = 0.101$, confirm the similarity of the distribution of X-ray luminosity with distance for both samples.

Figure 5.7 also shows a higher density of X-ray sources for distances of $\leq$ 200pc. To verify this, I have plotted the distance histograms for both the EMSS and my sample, only with percentages of the total sample instead of the number of objects for every bin. The histograms, in Fig. 5.8, confirm the higher concentration of stars at distances $\leq$ 200pc. Indeed, for my sample $\sim$ 85% lie within the sphere of radius 200pc, while for the EMSS sample, it is 76%. A $\chi^2$ test for the two distributions shows again that both samples display strong similarities (see Table 5.3).

This result confirms the assumption made for the reddening of the stars. Most of them lie within distances that make a correction for reddening negligible.

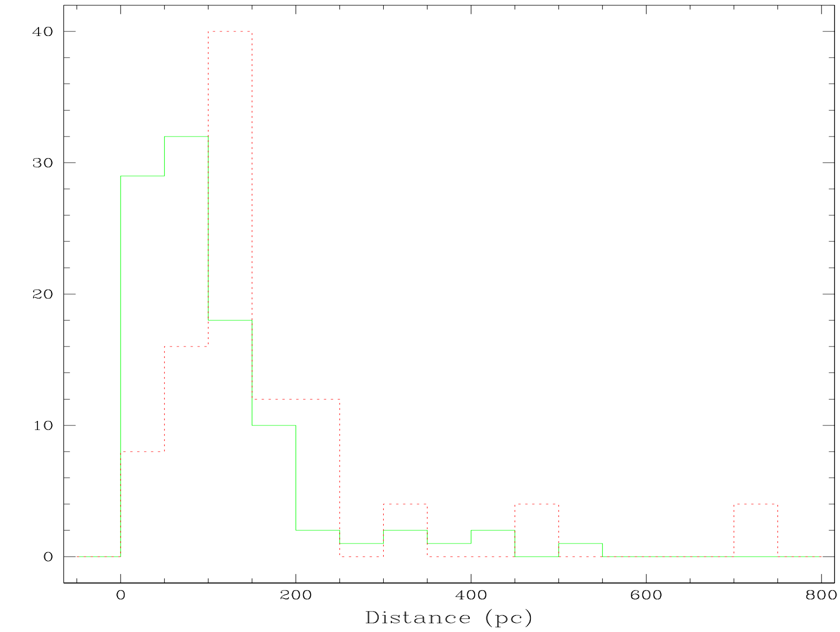


Figure 5.9: Histogram of the distance distribution. Green continuous line: the single stars in my sample; red dotted line: the binaries and multiple systems.

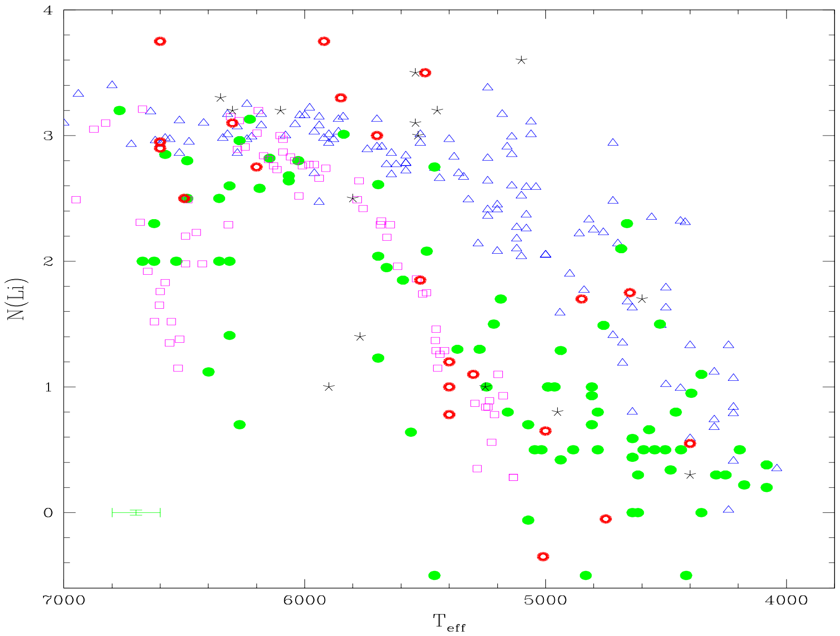


Figure 5.10: Lithium abundances for single stars as a function of effective temperature. Blue triangles: Pleiades data (Soderblom et al. 1993); purple squares: Hyades data (Balachandran 1995); green filled circles: my RASS sample; red empty circles: the EMSS sample (Fleming et al. 1995, Favata et al 1995); black stars: the EXOSAT sample (Tagliaferri et al. 1994).

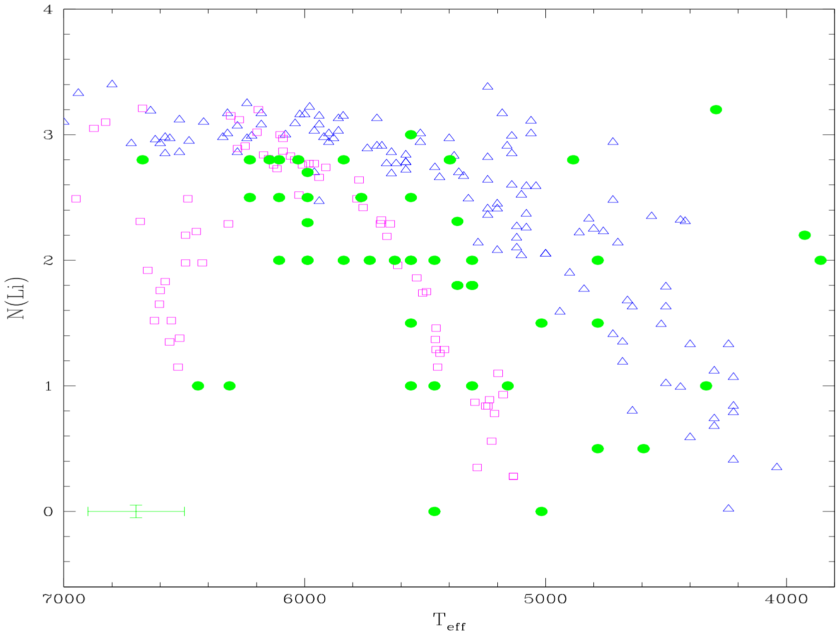


Figure 5.11: Lithium abundances for the binaries and multiple systems as a function of effective temperature. Blue triangles: Pleiades data (Soderblom et al. 1993); purple squares: Hyades data (Balachandran 1995); green filled circles: my RASS sample.

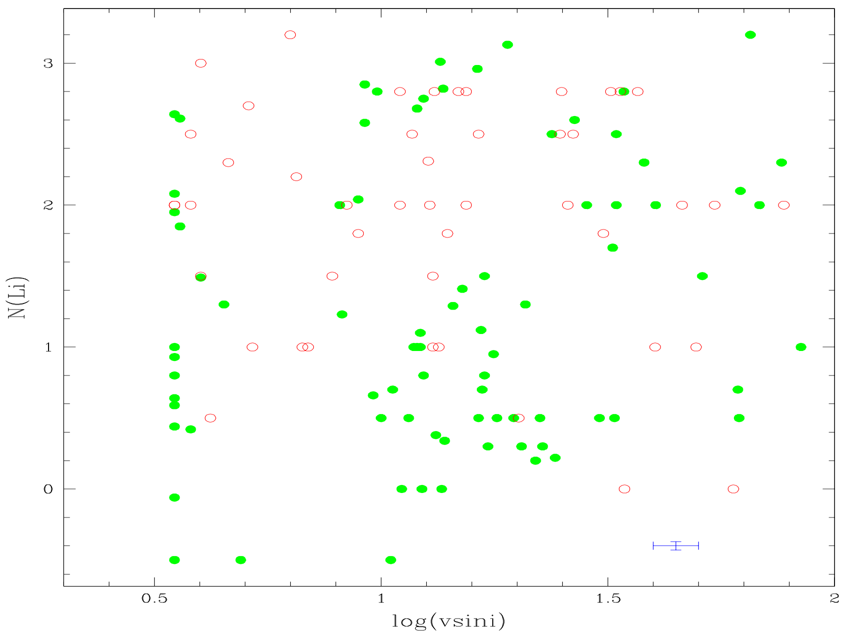


Figure 5.12: Lithium abundance vs rotational velocity for the single stars (filled circles) and multiple systems (empty circles) of the studied sample.

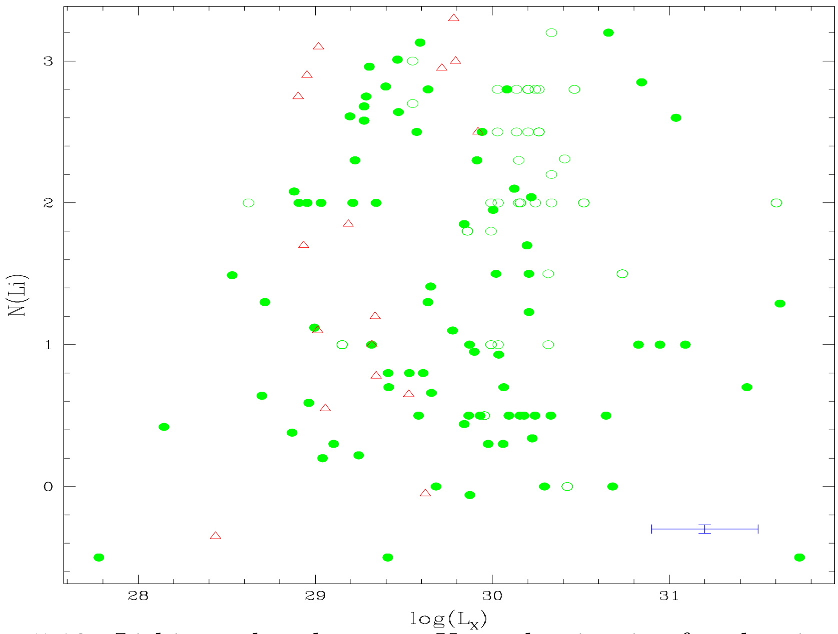


Figure 5.13: Lithium abundance vs X-ray luminosity for the single stars (filled circles) and the multiple systems (open circles) of the studied sample, as well as the stars from the EMSS with available lithium abundances (red open triangles).

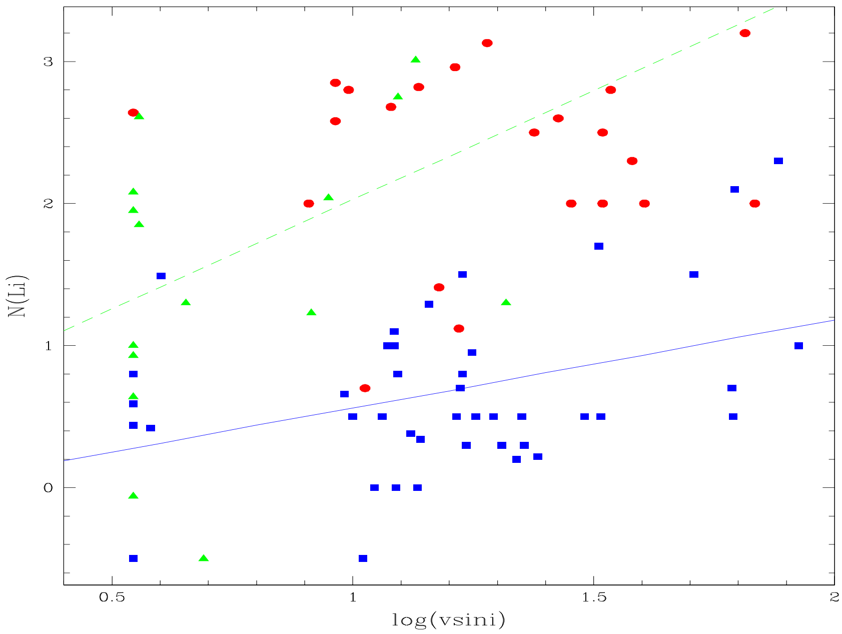


Figure 5.14: Lithium abundance vs. rotational velocity for the single stars of my sample. The red circles represent the early F stars, the green triangles the late F and G stars and the blue squares the K stars. The linear regression fits found for the F7 to G9 stars (dashed green line) and the K stars (continous blue line) are also plotted.

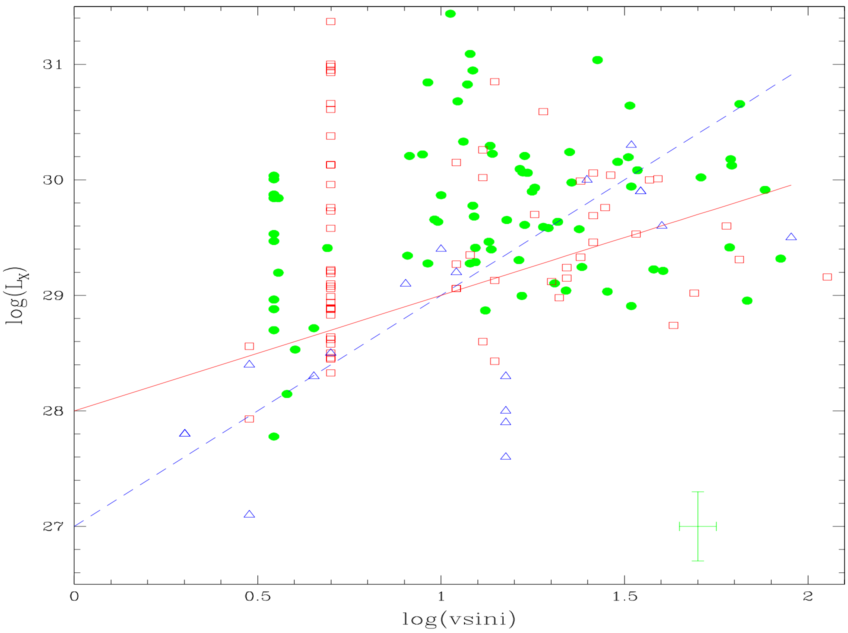

Figure 5.15: X-ray luminosity vs. rotational velocity for the single stars of my sample (green filled circles), the EMSS sample (empty red squares) and the opticaly selected sample of Pallavicini et al. (1981) (empty blue triangles). The correlations found by Pallavicini et al. (1981) (dashed blue line) and Fleming (1988)(continous red line) are also plotted.

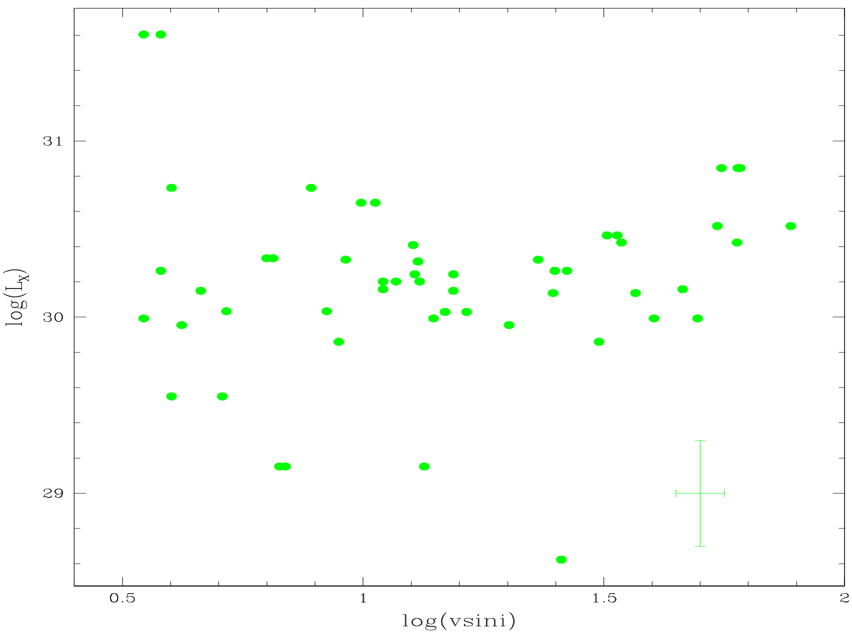

Figure 5.16: X-ray luminosity vs. rotational velocity for the multiple systems in my RASS sample.

Since both samples display such similarities in their general properties, as seen already in Sects. 5.1 and 5.3, and now with the distance distribution, I tend to assume that indeed both are representative of the late-type stellar X-ray population in the solar neighborhood.

Since my single stars and multiple systems subsamples had displayed previously differences, I also compare the distribution of distance for those two subsamples. This is done in Fig. 5.9. The percentage values are calculated relative to the number of sources in the corresponding subsample. The two subsamples display also in this case differences which are significant, as the $\chi^2$ test shows (Table 5.3). Although the largest part of both subsamples is still contained within the first 200pc from the Sun, it is easy to recognize that the multiple systems tend towards larger distances. The peak of the distribution for the multiple systems lies in the 100-150pc bin, instead of the 50-100pc bin where the distribution of the single stars peaks. 79% of the single stars lie between 0pc and 200pc. A comparative percentage of the binaries, 80%, lie 50pc further, between 50pc and 250pc. Only 8% of the binaries are within 50pc from the Sun, compared to the 20% of the single stars. This is consistent with the X-ray luminosity distribution for the binaries, which tends towards the higher luminosities.

## 5.5 *Lithium abundances*

The lithium abundance determined for each star in my sample can be used to get a first idea of the star's age. Since the lithium in late-type stars is destroyed pretty fast once the stars reach the main-sequence, the lithium abundance was thought to be a good age indicator. But it has been noted in recent years that this simple model is not adequate. Many evolved late-type stars with high lithium abundances have been detected, stars which, according to the simple model should show no, or only very little lithium in the spectrum (see for example Favata et al. 1997 and 1996, Pasquini et al. 1994, Randich & Pallavicini 1991). So lithium abundances cannot be used as an age indicator, but can still give an idea of the evolutionary phase the star is currently passing through.

For this, the lithium abundances can be compared, for instance, to those of stars of similar spectral types belonging to open clusters of known age. The most popular, and among the best studied open clusters are the Zero-Age Main-Sequence (ZAMS) Pleiades cluster, with an age of $\sim 10^8$ years, and the older ($\sim 10^9$ years) Hyades cluster. The lithium data for the Pleiades was taken from Soderblom et al. (1993), the data for the Hyades was obtained from Balachandran (1995). Stars that show a lithium abundance well above the abundance of the Pleiades stars can be considered as Pre-Main-Sequence (PMS) stars. All other stars are either Main Sequence or older.

The distribution of lithium abundances for the single stars in my sample, compared to the abundances found for the Pleiades and Hyades clusters as well as some data from the EMSS and EXOSAT samples, is shown in Fig. 5.10, while Fig. 5.11 shows a similar plot, but for the components of the binaries and multiple systems. The lithium abundance is given as N(Li)$\equiv \log \epsilon$(Li) relative to the hydrogen abundance N(H)=12.

The first thing that can be recognized from Fig. 5.10 is that among the single stars no PMS candidates are present. The youngest stars in my sample can only be ZAMS stars, with an age similar to that of the Pleiades stars. In this again, my sample differs from the EMSS sample, which does contain PMS candidates, as can be seen in Fig. 5.10.

Previous works, using the EMSS sample, have shown that about a third of the sample is composed of young stars, at least stars younger than the Hyades stars (Favata et al. 1993). A comparison of the lithium abundances for the single stars in my sample with those for the Hyades stars shows that about 32% (34 stars) of my sample has indeed lithium abundances high enough to be considered young, in accordance with the results of Favata et al. (1993).

For the binaries, the problem of age determination is even more complex than that for the single stars. It has been found that short-period interacting binaries often show a lithium overabundance. A proposed explanation for this is that the high rotation rate induced by the interaction between the binary components inhibits the transport of lithium to the deeper layers where it is destroyed. Only for one system is the case clear enough: it is the quadruple system RXJ 1122.0-2446, better known as HD 98800. The distance information from Hipparcos, as well as the lithium abundances (taken from Soderblom et al. 1997) show clearly that this system must be composed of PMS stars.

According to different studies of the lithium abundance in late-type stars, a correlation between stellar activity, or the related rotation, and the lithium abundance can be detected (Soderblom et al. 1993, Favata et al. 1997), although some samples do not display such a correlation (Favata et al. 1995). The dynamo model for the activity of late-type stars also predicts a slowing down of the rotation rate of a star through magnetic breaking. The older a star, therefore, the slower it should rotate, and the less active it should be. Since the lithium abundance is related to age, and also to rotation insofar as high rotation rates inhibit the destruction of lithium, a correlation between lithium abundance and rotation or X-ray luminosity would be a simple consequence of the models.

Since the stars in my sample show a wide range of lithium abundances, I decided to check whether a correlation between lithium and rotation or X-ray emission exists. Figures 5.12 and 5.13 show the lithium abundance as a function of either rotational velocity or X-ray luminosity.

Both the single stars and the binaries are represented. It is clearly recognizable that no correlation can be detected for the lithium abundance of the complete single star subsample with either parameter. To confirm the lack of correlation, I applied two statistical tests to my single star subsample, Pearson's $r$ and Spearman's Rank Order Coefficient $r_s$.

Both are correlation tests, but differ in that Pearson's $r$ compares the actual data points while Spearman's Coefficient compares the ranks of the data point values within the whole sample.

For a sample composed of $N$ data points $(x_i, y_i)$, Pearson's $r$ is defined as:

$$r = \frac{\sum_i (x_i - \bar{x})(y_i - \bar{y})}{\sqrt{\sum_i (x_i - \bar{x})^2}\sqrt{\sum_i (y_i - \bar{y})^2}} \tag{5.7}$$

with $\bar{x}$ being the mean value of all $x_i$'s, and $\bar{y}$ the mean value of all $y_i$'s.

The significance of Pearson's $r$ is given by the error function, a special case of the incomplete Gamma function:

$$P_r \equiv 1 - \frac{2}{\sqrt{\pi}} \int_x^\infty e^{-t^2} dt \tag{5.8}$$

Spearman's Rank Order Coefficient considers the ranks of the $x_i$ and $y_i$. If $R_i$ is defined as the rank of $x_i$ among all the other $x$ values, and $S_i$ the rank of $y_i$ among all the $y$ values, then Spearman's $r_s$ is given by:

$$r_s = \frac{\sum_i (R_i - \bar{R})(S_i - \bar{S})}{\sqrt{\sum_i (R_i - \bar{R})^2}\sqrt{\sum_i (S_i - \bar{S})^2}} \tag{5.9}$$

The significance of $r_s$ is given by computing

$$P_{r_s} \equiv t = r_s \sqrt{\frac{N-2}{1-r_s^2}} \tag{5.10}$$

which is distributed like Student's distribution with $n - 2$ degrees of freedom.

Pearson's $r$ and Spearman's $r_s$ have values lying between -1 and 1. The closer the result is to $|1|$, the more significant is the correlation between the two variables being compared is. On the other hand, the smaller the value for $P_r$ and $P_{r_s}$ are, the more significant the correlation between the two variables. These tests, as the $\chi^2$ test before, have been taken from Press et al. (1992).

The results of both tests, listed in Table 5.4, for between the lithium abundances and the X-ray luminosity or the rotational velocity confirm the lack of correlation of N(Li) with either of the other parameters, when the complete sample is taken.

Many factors could cause the lack of correlation observed between lithium abundance and either X-ray luminosity or rotational velocity. One of the most obvious factors is the lithium dip in the early F stars. To verify whether the lithium dip could indeed be one of the causes for the absence of any notable correlation, I checked out possible correlations for the K single star as well as the late F/G single star subsample separately. The results are also listed in Table 5.4.

For the lithium abundance as a function of X-ray luminosity, the result remained, for both subsamples, the same as for the complete single star subsample.

| Subsample tested | Variable correlated to N(Li) | $r$ | $P_r$ | $r_s$ | $P_{r_s}$ |
|---|---|---|---|---|---|
| all single stars | $v \sin i$ | 0.181 | 0.108 | 0.146 | 0.197 |
| all single stars | $\log L_X$ | -6.173e-2 | 0.586 | -9.865e-2 | 0.384 |
| all binary stars | $v \sin i$ | -0.102 | 0.490 | -3.990e-2 | 0.788 |
| all binary stars | $\log L_X$ | 0.101 | 0.496 | 0.148 | 0.315 |
| single F7 to G9 stars | $v \sin i$ | 0.469 | 2.759e-2 | 0.540 | 9.534e-3 |
| single F7 to G9 stars | $\log L_X$ | -0.207 | 0.356 | -0.210 | 0.348 |
| all F7 to G9 stars | $v \sin i$ | 0.233 | 0.153 | 0.367 | 2.166e-2 |
| single K stars | $v \sin i$ | 0.380 | 1.195e-2 | 0.226 | 0.144 |
| single K stars | $\log L_X$ | 0.133 | 0.395 | 0.133 | 0.396 |
| all K stars | $v \sin i$ | 0.233 | 0.118 | 0.193 | 0.198 |

Table 5.4: Results of the correlation tests Pearson's $r$ and Spearman's $r_s$ tests for the lithium abundance.

There is no detectable correlation between these two stellar parameters for my sample. One reason for this could be that I do not have any very young stars, and so have only a limited range in N(Li) over which to look for correlations. But with the information available this cannot be verified.

For the lithium abundance vs. rotational velocity, on the other hand, the result changed drastically as soon as the single star subsample was divided into spectral types. Both for the K single stars and the G ones, there appears a clear correlation between N(Li) and $v \sin i$. I calculated the corresponding correlation functions using the least square fit method.

For the K stars subsample the best fit was

$$N(Li) \propto (0.620 \pm 0.236) \cdot v \sin i + (-6.060e - 2 \pm 0.295)$$

while for the late F and G stars, it was

$$N(Li) \propto (1.541 \pm 0.649) \cdot v \sin i + (0.485 \pm 0.586)$$

Both relations are drawn in Fig. 5.14. Statistical errors could be partly cause for this difference, since both subsamples are quite small, especially the late-F/G stars subsample (22 stars). The early F stars show no correlation, which is due to a large part to the strong dip in lithium abundance for main-sequence or older stars in that temperature range. No correlation could be found between lithium abundance and X-ray luminosity for any of the subsamples.

The binaries do not display any correlation, no matter how the sample is divided. But since for the binaries the errors in determining both rotational velocity and lithium abundance are larger, and the total number of objects small, a correlation could still exist, without being detected.

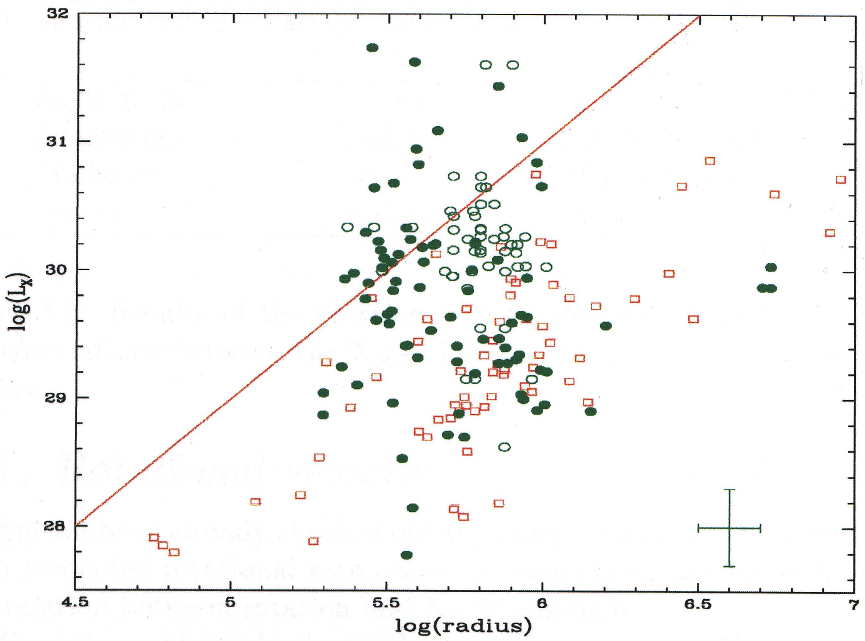


Figure 5.17: X-ray luminosity vs. radius for the single stars (filled circles) and multiple systems (empty circles) in my RASS sample, as well as the EMSS stars (empty red squares). The correlation and at the same time upper limit found by Fleming for his sample is given by the continous line. The error bars represent typical errors for my sample.

| Subsample tested | Variable correlated to $L_X$ | $r$ | $P_r$ | $r_s$ | $P_{r_s}$ |
|---|---|---|---|---|---|
| single stars | $v \sin i$ | 0.132 | 0.241 | 9.957e-2 | 0.376 |
| single stars | radius | -5.293e-2 | 0.639 | -0.151 | 0.179 |
| binaries | $v \sin i$ | 2.957e-2 | 0.833 | 0.104 | 0.458 |
| binaries | radius | -0.107 | 0.460 | -0.128 | 0.376 |

Table 5.5: Results of the correlation tests Pearson's $r$ and Spearman's $r_s$ tests for correlations between the X-ray luminosity and the rotational velocity or the radius.

## 5.6 *Rotational velocity*

Since I have already checked out the possible correlation of lithium abundance with projected rotational rate $v \sin i$, it seems adequate to continue by studying the relation between rotation and X-ray emission.

First, I consider only the single stars of my sample. Older studies have shown that a clear correlation between the projected rotational velocity and the X-ray luminosity exists. This was detected first for an optically selected sample (Pallavicini et al. 1981), then also for the EMSS sample (Fleming 1988). But the correlation itself differs for both samples. Pallavicini et al. found a correlation between the X-ray luminosity and the square of the rotational velocity $L_X \propto (v \sin i)^2$, while Fleming gets a linear correlation between X-ray luminosity and rotation $L_X \propto v \sin i$.

Since the sample studied by Pallavicini et al. (1981) is optically selected, it seems reasonable to assume that the differences between the two correlations are a result of the strong bias present in this sample, and that the correlation found by Fleming corresponds more to the true correlation between X-ray luminosity and rotation. To check this assumption, I have plotted the X-ray luminosity as a function of rotational velocity for the single stars in Fig. 5.15. I have added both the EMSS sample and the sample of Pallavicini et al., as well as the correlations found for each sample.

The surprising result was a total lack of detectable correlation between projected rotational velocity and X-ray emission for my single star subsample. This is unexpected, since the model for the origin of the X-ray emission in late-type stars (see Chapter 1) clearly requires a correlation between the X-ray luminosity and rotation.

To make sure that the appearances really correspond to the "truth", I have calculated the linear correlation coefficient, Pearson's r, and the Spearman Rank Order Coefficient $r_s$,as described in the previous section, for my single star subsample. The results, listed in Table 5.5, confirm the lack of correlation between

$v \sin i$ and $L_X$.

The reason for this lack of correlation is hard to determine with the available data. One assumption would be that the lack of correlation comes from the use of the *projected* instead of the true rotational velocity. This would be easy to verify, but for this, the true rotational velocity has first to be determined, which will require more observations.

Another possibility would be the fact that my sample is composed mainly of high-activity stars, near the saturation limit. In this case, the lack of correlation would be even easier to explain, and would be even expected. Unfortunately, the global properties of my sample, first of all the spread present in the X-ray to visual luminosity ratio for every spectral type, imply that my sample is composed of stars with very different levels of activity, not only near-saturated ones.

One possible check of this hypothesis is by determining the radius for each single star, and looking for a correlation with the X-ray luminosity. Since saturation means that a star has its complete surface covered by active zones, the X-ray luminosity for saturated and near-saturated stars should correlate with the surface, and therefore also with the radius.

To estimate the radius, I used the information given by Popper (1980) as well as the $(B - V)$ index and the absolute magnitude derived from it. The radii obtained are listed in Table C.1. The result is plotted in Fig. 5.17.

Not so surprisingly no correlation can be detected in this case either. The calculated correlation coefficients confirm again the lack of correlation. Also noteworthy is the fact that quite a few stars have values of $\log(L_X)$ above the limit detected by Fleming (1988).

Clearly, my single stars subsample displays an unexpected behavior that is hard to explain with the available data. The lack of correlation between X-ray emission and rotation clearly doesn't come from a bias toward near-saturated stars in my X-ray selected sample. More data will be necessary to understand this behavior.

The binaries don't show any correlation either, neither between X-ray luminosity and rotation nor radius. But in this case, the behavior corresponds to the one shown by the stars in the EMSS sample, and can be due at least in part to the errors for $v \sin i$.

For the fast rotators among the binaries, determining with precision the rotational velocity is difficult, all the more so when the lines of the two line systems blend heavily. And the orbital motion of the system also contributes to the broadening of the lines, enlarging the error for the rotational velocity. More data will be necessary, spread over a few orbital periods, to try and get rotational velocities with less error. Only then will a conclusion about the correlation, or rather lack thereof, between rotation and X-ray luminosity be possible for the binaries.

# 6 Discussion

I presented optical observations of an X-ray selected sample of stars of spectral types F to K detected during the ROSAT All-Sky Survey. These stars are located in four high-galactic latitude fields of the southern hemisphere.

The observations were used to determine different stellar parameters. A spectral classification was done for each sample object, from which the distance and X-ray luminosity could be determined. Binary and multiple systems were identified. For each single star and multiple system component the effective temperature, radial and projected rotational velocities and lithium abundances were determined.

The distribution of the sample between the spectral types studied is as expected, within the statistical error limits. The largest part of the sample is by far composed of K stars, with about a third being F stars, and less than a fourth G stars. The G stars fraction is a bit lower than the one third of the sample expected, but this is certainly just a statistical effect.

The fraction of binaries is also near to the expected fraction of about a third of the sample. Although this estimate was done without differentiating between the short-period (1 to 15 days) active binaries, and the longer period ones. Most of the binaries detected are expected to be short-period ones, so the fraction of binaries to single stars would not be much modified by reclassifying the long period binaries into the single star subsample.

A study of the X-ray to visual luminosity ratio as a function of the color index $(B-V)$ showed that the activity levels for the sample stars cover 3 orders of magnitude. Most of the stars have X-ray luminosities well within the saturation limits found in previous works (Vilhu and Walter 1987 for the bluer stars, and Fleming 1988 for the later spectral types), with only a few stars being outside of those limits. This stands already in some contradiction to the results obtained by Fleming (1988). The study of the EMSS sample seemed to indicate that the stars in an X-ray selected sample tend rather towards saturation, instead of spanning such a broad range of activity levels.

The X-ray luminosity distribution as well as the distance distribution of my sample reproduces well the expected trends. Most stars have X-ray luminosities in the mid- to high-level range, from $10^{29}$ to $10^{31} erg\ s^{-1}$. Since the RASS was a flux-limited survey, it is expected that the sample should be biased towards higher levels of X-ray luminosities. Most of the stars detected are concentrated in a sphere of 200pc radius from the Sun. Considering the flux limitation of the RASS, of $\sim 2 \cdot 10^{-13} erg\ cm^{-2}\ s^{-1}$, this is very near to the limiting distance for the detection of stars with an X-ray luminosity of $10^{30} erg\ s^{-1}$. Since most of my stars have luminosities between $\log(L_X)$ of 29.0 and 31.0, a concentration of stars within such a relatively small radius is normal.

The X-ray luminosity and distance distributions of the single stars are very similar to the distributions obtained for the complete sample. Since the largest part of the sample is composed of single stars, this is a logical result. But the multiple system distributions show significant differences to the distributions of the complete sample. The multiple systems tend towards the higher X-ray luminosities and larger distances. The distribution over distance is shifted by 50pc compared to the distribution for the complete sample or for the single stars. Since most multiple systems are expected to be short-period binaries, the tendency toward higher X-ray luminosities is easy to understand. In the short-period interactive binaries, the components are tidally locked, and strongly influence one another. The tidal lock tends to synchronize the rotational velocities of the component stars with the binary period (Giuricin et al., 1984), which means that the stars have high rotational velocities and enhanced chromospheric and coronal activity. In some of the systems (Algol, W UMa), there is also mass transfer between the components, which means the existence of an accretion disk and hot spot (where the accreted matter falls upon the stellar surface) on one of the stars. The accretion disk and hot spot can contribute to the X-ray luminosity of the system.

The tendency towards larger distances is not so easily understandable. It can only mean that at high-galactic latitudes, active binaries are rare in the immediate ($\leq$50pc) solar neighborhood.

A comparison of my RASS sample with the EMSS sample of Fleming (1988) has shown that both samples display very similar characteristics. The comparison between those two samples is insofar meaningful and interesting, because the EMSS sample was, until the launch of ROSAT, the largest X-ray selected sample studied, and has many similarities to my RASS sample. It has been observed in the soft X-ray range, is composed of stars detected during flux-limited "mini-surveys" (pointed observations with a large field of view) and is composed of a similar number of stars. And to make a comparison easier, most of the sample was re-detected in the RASS, so that the X-ray luminosities can be directly compared, since they were obtained with the same instrument.

For both samples, the distribution between the studied spectral types is identical within the statistical errors. The distance and X-ray luminosity distributions are also similar. Statistical tests have confirmed, or at least not disproved, this result. This is of importance, since the results obtained with such X-ray selected samples as the RASS and EMSS ones can be relevant to the study of X-ray emission in late-type stars only if the samples can be considered representative of the corresponding stellar X-ray population. Since both samples display such similarities despite their difference in spatial distribution, the assumption that indeed both samples are representative of the stellar X-ray population in the solar neighborhood is reasonable.

The lithium abundances obtained for the sample were used to estimate the evolutionary stages the stars have reached. Works using the EMSS observations have revealed that X-ray selected samples contain a large fraction of young, or even very young stars (Favata et al. 1993, 1995). About a third of the studied sample was composed of stars that can be considered to be either still in a Pre-Main-Sequence phase, or as having just reached the Main-Sequence. A comparison of the lithium abundance obtained for my sample has shown that in this aspect too, the results corresponded to the expectations. 32% of my stars, particularly in the late-G and K spectral type range, have a lithium abundance significantly higher than the abundances found in the Hyades. Since in those stars the lithium is burned very rapidly once the Main-Sequence is reached, this leads to the conclusion that the stars must be young. But since their lithium abundance was not higher, for most even lower than the Pleiades abundances for the corresponding effective temperatures, the stars have most probably already reached the Main-Sequence. No Pre-Main-Sequence candidates could be detected among the single stars, and only one, already well known in the literature, was found among the multiple systems. It is the quadruple system HD98800 (Soderblom et al. 1997). This is a result differing from the ones obtained with the EMSS sample, since that sample contains clear PMS candidates. But it is easily understandable, if one considers that, in the regions studied, the PMS stars detected would have to be isolated PMS stars. Not many such stars are known, and their presence far from any larger star forming region is not yet understood (De la Reza et al. 1989, Rucinski 1992). It can be assumed that such sources are rare in the immediate solar neighborhood.

The activity level of a star has been found to be linked with its age. The magnetic fields necessary to heat up the corona are also responsible for slowing down the rotation of the star, leading to a reduction of the activity. Since the lithium abundance N(Li) is also dependent on age, a correlation between N(Li) and $\log L_X$ or $v \sin i$ can be expected. Such correlations were found for different samples (Soderblom et al. 1993, Favata et al. 1997). A correlation between lithium abundance and rotation could be found for two spectral type single star subsamples, the K stars and the late-F/G stars, but not for the complete single star subsample. The fact that no correlation could be found for the complete single star subsample can be ascribed to two reasons, firstly to the fact that lithium depletion is temperature dependent, and also to the inclusion of the early F stars, which lie in the range of the lithium dip. More factors can play a part in the absence of detectable correlation over the whole range of temperatures considered, but these seem to be the main factors, since a splitting of the single stars in spectral type groups reveals the existence of a correlation, as expected, between rotation and lithium abundance.

On the other hand, no splitting of the sample changed the fact that no correlation can be found between lithium abundance and X-ray luminosity. The reason for this is not understood, but could be linked to the results obtained when studying the correlation between rotational velocity and X-ray emission.

The models developed to explain the X-ray emission in late-type stars, as mentioned in Chapter 1, link the X-ray emission to a dynamo mechanism. Magnetic fields existing in the convection zone of the stars are pushed to the surface, and the plasma enclosed in the field lines is heated to the temperatures observed in coronae and necessary for X-ray emission. The higher the rotation rate of a star, the stronger the dynamo mechanism is, and the more luminous the corona can be. A correlation between X-ray luminosity and rotational velocity (mostly the projected velocity $v \sin i$) has been observed in the previous studies, though a different correlation depending on the selection method used to create the sample.

The X-ray selected EMSS sample (Fleming 1988) shows a linear correlation $L_X \propto v \sin i$ for the single stars, while the optically selected sample studied by Pallavicini et al. (1981) has a different correlation, $L_X \propto (v \sin i)^2$. The difference can be explained by the assumption that the X-ray selected sample of Fleming is composed mainly of saturated or nearly saturated stars, for which the complete available surface is covered with active regions, while the sample of Pallavicini et al., being optically selected, includes stars of different activity levels, even low-activity ones. Since Fleming found also a correlation between $L_X$ and the radii of his sample stars, but no correlation of $L_X$ with the angular rotation rate, this assumption seems reasonable.

As my sample has been created using a similar selection method than the one used for the EMSS sample, it is reasonable to assume that the projected rotational velocities and X-ray luminosities of my single star subsample will show similar correlations to the ones found by Fleming (1988) rather than the correlation found by Pallavicini et al. (1981). All the more so since the EMSS sample and mine show strong similarities in their general X-ray properties. It is therefore strange that no correlation at all could be found between $L_X$ and $v \sin i$ for the single stars of my sample. Nor could a correlation between the radii of the stars and the X-ray luminosity be found. This last result, together with the large spread in X-ray to visual luminosity ratio for any given spectral type, clearly indicates that my single star subsample is not composed only of saturated and near-saturated stars, but includes a whole range of activity levels. This makes the absence of any correlation between $v \sin i$ and $L_X$ all the stranger and more difficult to explain, since in the case of a wide range of activity, a correlation closer to the one found by Pallavicini et al. (1981) should be detected. The simplest way of explaining the result, without contradicting model predictions, is that the statistical distribution of the projection factor $\sin i$ is such that it hides the correlation. But to verify this, it would be necessary to determine the true, unprojected rotational velocities of all the single stars, and see if those velocities correlate with the X-ray luminosity.

It is clear that the data available currently for the sample stars doesn't allow a further study of this last result, and the possible explanations for it. More observations are necessary in order to be able to verify whether the X-ray luminosity really does not correlate as expected with the rotation rate for my single stars, or whether this is just an effect due to the fact that the projected velocities were used.

One way of checking this out would be by determining the true rotational velocity for as many single stars as possible. This can be done by using photometric light curves, at least for the faster rotators. Variations due to the transition of stellar spots can allow the determination of the rotation period. This method would be limited to stars for which such variations can be observed, meaning sufficiently "spotted" stars, which do not have their rotation axis parallel to the line of sight.

Another way of verifying predictions would be by looking directly for a correlation between the X-ray luminosity and the activity level of the stars. For this, spectral lines that are strongly influenced by the chromospheric activity can be used. Since models consider the X-ray emission to be linked with the chromospheric activity, an assumption that is based on observations and has been confirmed by various studies so far, this would be a much more direct check for the models than the correlation with rotation. Some of the best studied lines for chromospheric activity are the Ca II H & K lines. These lines have already been used in studies of the correlation between X-ray emission and activity (for example Eggen 1989, Piters et al. 1997). Part of the sample has already observations of those lines, and a full set of observations would allow the direct verification of the models.

The results obtained for my sample so far could also be checked against results of a similar study of the available northern sample, which contains 193 stars of spectral types A to K. With this sample added to mine, the statistical errors could be reduced, and the absence of any detectable correlation between rotation and X-ray emission revised.

# *Bibliography*


Alonso, A., Arribas, S., Martinez-Roger, C., 1996, A&A 313, 873

Andrillat, Y., Jaschek, C., Jaschek, M., 1995, A&A 112, 475

Appenzeller, I., Thiering, I., Zickgraf, F.-J., Krautter, J., Voges, W., Chavarria, C., Kneer, R., Mujica, R., Pakull, M., Rosso, C., Ruzicka, F., Serrano, A., Ziegler, B. 1997, A&A, submited

Balachandran, S. 1995, ApJ 446, 203

Bessel, M.S. 1990, A&AS 83, 357

Bradt, H.V.D., Ohashi, T., Pounds, K.A. 1992, Ann. Rev Astr. Ap. 30, 391

Cassinelli, J.P., Swank, J.H. 1983, ApJ 271, 681

Christian, C.A., Adams, M., Barnes, J.V., Butcher, H., Hayes, D.S., Mould, J.R., Siegel, M. 1985, PASP 97, 363

Cousins, A.W.J. 1964, Mon. Notes Astron. Soc. South Africa 23, 175

Cutispoto, G., Tagliferri, G., Pallavicini, R., Pasquini, L., Rodono, M. 1996, A&A Suppl. 115, 41

Cruddace, R.G., Hasinger, G.R., Schmitt, J.H., 1988, *ESO Conference on Large Databases*, F. Murtagh, A. Heck (Eds)

Danziger, I.J., et al. 1990, ESO Messenger 62, 4

De La Reza, R., Torres, C.A.O., Quast, G., Castilho, B.V., Vieira, G.L. 1989, ApJ 343, L61

Downie, N.M., Heath, R.W. 1965, *Basic Statistical Methods*, 2nd ed., New York: Harper and Row

Duquennoy, A., Mayor, M. 1991, A&A 248, 485

Eggen, O.J. 1977, ApJ 215, 812

Eggen, O.J. 1989, AJ 98, 184

Fasano, G., Franceschini, A. 1987, MNRAS 225, 155

Favata, F., Barbera, M., Micela, G., Sciortino, S. 1993, A&A 277, 428

Favata, F., Barbera, M., Micela, G., Sciortino, S. 1995, A&A 295, 147

Favata, F., Micela, G., Sciortino, S. 1996, A&A 311, 951

Favata, F., Micela, G., Sciortino, S. 1997, A&A 322, 131

Fleming, T.A. 1988, Ph.D. dissertation, University of Arizona

Fleming, T.A., Gioia, I.M., Maccacaro, T. 1989, ApJ 340, 1011

Fleming, T.A., Molendi, S., Maccararo, T., Wolter, A. 1995, ApJ Sup., 99, 701

Giacconi, R., Gursky, H., Paolini, F., Rossi, B. 1962, Phys. Rev. Lett. 9, 439

Giommi, P., Tagliaferri, G., Beuermann, K., Branduardi-Raymont, G., Brissenden, R., Graser, U., Mason, K.O., Mittaz, J.D.P., Murdin, P., Pooley, G., Thomas, H.-C., Tuohy, I. 1991, ApJ 378, 77

Giuricin, G., Mardirossian, F., Mezzetti, M. 1984, A&A 141, 227

Gliese, W. 1982, A&A Suppl. 47, 471

Golub, L., Harnden, F.R. Jr., Maxson, C.W., Rosner, R., Vaiana, G.S, Cash, W. Jr., Snow, T.P. Jr. 1983, ApJ 271, 264

Kurucz, R.L. 1993, CD-ROM No 18

Linsky, J.L. 1990, in *Imaging X-ray Astronomy*, M. Elvis (Ed.), Cambridge University Press

Lucy, L.B. 1982, ApJ 255, 286

Maggio, A., Sciortino, S., Vaiana, G.S., Majer, P., Bookbinder, J., Golub, L., Harnden, F.R. Jr., Rosner, R. 1987, ApJ 315, 687

Mewe, R. 1979, Sp. Sc. Rev. 24, 101

Odewahn, S.C., Bryja, C., Humphreys, R.M 1992, PASP 104, 553

Pallavicini, R., Golub, L, Rosner, R., Vaiana, G.S., Ayres, T., Linsky, J.L. 1981, ApJ 248, 279

Pallavicini, R. 1989, Astron. and Astroph. Rev. 1, 177

Parker, E.N. 1979, *Cosmical Magntic Fields*, Clarendon Press

Pasquini, L., Pallavicini, R., Pakull, M. 1988, A&A 191, 253

Pasquini, L., Liu, Q:, Pallavicini, R. 1994, A&A 287, 191

Perryman, M.A.C., Lindegren, L., Kovalevsky, J., Hog, E., Bastian, U., Bernecca, P.L., Greze, M., Donati, F. et al. 1997 A&A 323, L49

Piskunov, N.E. 1992, in Proceedings of *Stellar Magnetism*, Glagolevskij, Yu.V., Romanuk, I.I. (Eds), Nauka, St. Petersburg

Piters, A.J.M., Schrijver, C.J., Schmitt, J.H.M.M., Rosso, C., Baliunas, S.L., Van Paradijs, J., Zwaan, C. 1997, A&A 325, 1115

Popper, D.M. 1980, Ann. Rev. Astr. Astrop. 19, 115

Press, W.H., Teukolsky, S.A., Vetterling, W.T., Flannery, B.P. 1992, *NUmerical recipes in Fortran*, 2nd Ed., Cambridge University Press

Randich, S., Pallavicini, R. 1991, Mem. Soc. Astron. Italia vol 62, 75

Randich, S., Gratton, R., Pallavicini, R. 1993, A&A 273, 194

Randich, S. 1997, private communication

Rosner, R., Golub, L., Vaiana, G.S. 1985, Ann. Rev. Astr. Ap. 23, 415

Rucinski, S.M. 1992, PASP 104, 311

Schmidt, M. 1968, ApJ 151, 393

Schmitt, J.H.M.M., Collura, A., Sciortino, S., Vaiana, G.S., Harnden, F.R. Jr., Rosner, R. 1990, ApJ 365, 704

Schmitt, J.H.M.M., Fleming, T.A., Giampapa, M.S. 1995, ApJ 450, 392

Soderblom, D.R. 1982, Ap.J 263, 239

Soderblom, D.R., Pendelton, J., Pallavicini, R. 1989, AJ 97, 539

Soderblom, D.R:, Jones, B.F., Balachandran, S., Stauffer, J.R., Duncan, D.K., Fedele, S.B:, Hudon, J.D. 1993, AJ 106, 1059

Soderblom, D.R., Henry, T.J., Shetrone, M.D., Jones, B.F., Saar, S.H. 1997, ApJ 460, 984

Sletteback, A., Collins II, G.W, Boyce, P.B., White, N.M. 1975, Ap.J. Suppl. 281, 137

Stocke, J.T., Morris, S.L., Gioia, I.M., Maccacaro, T., Schild, R.E., Wolter, A., Fleming, T.A., Henry, J.P. 1991, ApJ Suppl. 76, 813

Tagliaferri, G., Cutispoto, G., Pallavicini, R., Randich, S., Pasquini, L. 1994, A&A 285, 272

Tonry, J., Davis, M. 1979, AJ 84, 1511

Trümper et al. 1991, Nature 349, 579

Upgren, A.R. 1963, AJ 68, 194

Vilhu, O., Walter, F.M. 1987, ApJ 321, 958

Voges, W. 1993, Adv. Space Res. Vol. 13, No. 12, 391

Vogt, N., Geisse, H.S., Rojas, S. 1981, A&A Suppl. 46, 7

Zeidler, E. (Ed.) 1996, *Teubner-Taschenbuch der Mathematik*, Teubner Verlagsgesellschaft

Zickgraf, F.-J., Thiering, I., Krautter, J., Appenzeller, I., Kneer, R., Voges, W.H., Ziegler, B., Chavarria, C., Serrano, A., Mujica, R., Pakull, M., Heidt, J. 1997, A&A Suppl. 123, 103

Ziegler, B. 1993, Diploma thesis, University of Heidelberg

# A X-ray data of the sample

Here we list the data coming from the ROSAT observations of the sample objects. The columns of the table have following meaning:

Column 1: the ROSAT name of the object, composed of the prefix RXJ and a short form of the coordinates.

Column 2: the coordinates of the X-ray source, as determined from the ROSAT plates (equinox 2000.0). The error for these positions is typically 30".

Column 3: the countrates for the X-ray sources, in counts per second.

Column 4: the total exposure time for each source.

Column 5: the hardness ratio 1 of each source.

Table A.1: ROSAT X-ray data for the sources in the studied southern sample.

| ROSAT Name RXJ | X-ray source coord. (2000.0) | Countrate (3) | $t_{exp}$ (4) | HR 1 (5) |
|---|---|---|---|---|
| 2246.6−3928 | 22 46 33.4 −39 28 44 | $0.172 \pm 0.024$ | 301.9 | $+0.06 \pm 0.16$ |
| 2258.3−4149 | 22 58 15.7 −41 49 47 | $0.107 \pm 0.030$ | 121.3 | $+0.57 \pm 0.48$ |
| 2305.1−3823 | 23 05 03.4 −38 23 37 | $0.066 \pm 0.019$ | 186.1 | $-0.23 \pm 0.67$ |
| 2306.5−3855 | 23 06 32.5 −38 55 47 | $0.124 \pm 0.026$ | 188.7 | $-0.03 \pm 0.71$ |
| 2323.3−3730 | 23 23 15.4 −37 30 53 | $0.131 \pm 0.032$ | 90.0 | $-0.12 \pm 0.53$ |
| 2331.4−4209 | 23 31 26.0 −42 09 43 | $0.153 \pm 0.032$ | 147.1 | $+0.38 \pm 0.45$ |
| 2356.2−3903 | 23 56 10.1 −39 03 20 | $0.089 \pm 0.028$ | 115.0 | $-0.30 \pm 0.64$ |
| 0005.9−4145 | 00 05 52.2 −41 45 28 | $0.170 \pm 0.031$ | 175.2 | $+0.09 \pm 0.22$ |
| 0015.0−4036 | 00 14 59.8 −40 36 07 | $0.058 \pm 0.015$ | 248.8 | $-0.18 \pm 0.69$ |
| 0022.2−3943 | 00 22 10.2 −39 43 25 | $0.037 \pm 0.010$ | 332.0 | $+0.13 \pm 0.69$ |
| 0027.7−4126 | 00 27 42.4 −41 26 07 | $0.215 \pm 0.027$ | 297.4 | $+0.28 \pm 0.13$ |
| 0028.8−3930 | 00 28 50.4 −39 30 55 | $0.061 \pm 0.021$ | 141.9 | $+0.58 \pm 0.36$ |
| 0032.1−3827 | 00 32 08.9 −38 27 17 | $0.049 \pm 0.016$ | 363.4 | $+0.42 \pm 0.43$ |
| 0035.7−2513 | 00 35 43.7 −25 13 59 | $0.111 \pm 0.019$ | 321.3 | $+0.20 \pm 0.23$ |
| 0038.6−2335 | 00 38 35.4 −23 35 46 | $0.042 \pm 0.011$ | 331.7 | $+0.03 \pm 0.71$ |
| 0041.2−2649 | 00 41 10.8 −26 49 58 | $0.075 \pm 0.015$ | 323.4 | $-0.22 \pm 0.50$ |
| 0042.7−2956 | 00 42 40.2 −29 56 49 | $0.037 \pm 0.010$ | 342.3 | $+0.60 \pm 0.45$ |
| 0045.0−4014 | 00 45 01.4 −40 14 31 | $0.033 \pm 0.009$ | 369.9 | $-0.38 \pm 0.61$ |
| 0045.2−2455 | 00 45 09.1 −24 55 03 | $0.040 \pm 0.011$ | 336.3 | $-0.40 \pm 0.59$ |
| 0047.3−2245 | 00 47 17.7 −22 45 02 | $0.196 \pm 0.023$ | 355.2 | $+0.09 \pm 0.14$ |
| 0050.6−4221 | 00 50 34.5 −42 21 20 | $0.030 \pm 0.009$ | 374.2 | $+0.18 \pm 0.68$ |
| 0052.8−2728 | 00 52 45.4 −27 28 30 | $0.162 \pm 0.026$ | 236.4 | $-0.25 \pm 0.20$ |
| 0053.0−3021 | 00 52 59.1 −30 21 33 | $0.051 \pm 0.012$ | 331.7 | $-0.56 \pm 0.36$ |
| 0055.5−3731 | 00 55 28.8 −37 31 40 | $0.044 \pm 0.011$ | 360.7 | $-0.22 \pm 0.67$ |
| 0100.2−3818 | 01 00 13.3 −38 18 36 | $0.128 \pm 0.018$ | 389.4 | $+0.37 \pm 0.16$ |
| 0105.4−4016 | 01 05 21.9 −40 16 09 | $0.032 \pm 0.009$ | 427.3 | $-0.11 \pm 0.70$ |
| 0116.8−3932 | 01 16 49.4 −39 32 10 | $0.024 \pm 0.007$ | 404.8 | $+0.51 \pm 0.52$ |
| 0121.2−3729 | 01 21 10.0 −37 29 28 | $0.386 \pm 0.032$ | 370.8 | $+0.03 \pm 0.09$ |
| 0121.5−4058 | 01 21 29.6 −40 58 17 | $0.058 \pm 0.012$ | 420.8 | $-0.03 \pm 0.26$ |

Table A.1 − continued.

| ROSAT Name RXJ | X-ray source coord. (2000.0) | Countrate (3) | $t_{exp}$ (4) | HR 1 (5) |
|---|---|---|---|---|
| 0125.6−4148 | 01 25 33.7 −41 48 35 | $0.076 \pm 0.014$ | 406.4 | $+0.20 \pm 0.24$ |
| 0126.4−4127 | 01 26 25.3 −41 27 54 | $0.037 \pm 0.009$ | 427.0 | $+0.66 \pm 0.40$ |
| 0135.8−3956 | 01 35 48.5 −39 56 44 | $0.057 \pm 0.012$ | 363.0 | $+0.03 \pm 0.71$ |
| 0136.8−3811 | 01 36 47.6 −38 11 19 | $0.072 \pm 0.019$ | 193.7 | $+0.46 \pm 0.56$ |
| 0141.4−3808 | 01 41 25.5 −38 08 06 | $0.096 \pm 0.015$ | 424.8 | $-0.04 \pm 0.20$ |
| 0155.4−3846 | 01 55 21.5 −38 46 22 | $0.470 \pm 0.042$ | 260.5 | $-0.48 \pm 0.12$ |
| 0440.3−5856 | 04 40 17.2 −58 56 31 | $0.160 \pm 0.044$ | 81.9 | $-1.05 \pm 0.50$ |
| 0450.1−5856 | 04 50 07.4 −58 56 52 | $0.933 \pm 0.252$ | 14.7 | |
| 0454.9−5832 | 04 54 53.0 −58 32 54 | $0.470 \pm 0.071$ | 93.7 | $-0.04 \pm 0.50$ |
| 0501.5−5930 | 05 01 31.8 −59 30 51 | $0.024 \pm 0.007$ | 546.0 | |
| 0505.5−5728 | 05 05 30.8 −57 28 15 | $2.024 \pm 0.015$ | 131.2 | $-0.02 \pm 0.08$ |
| 0505.6−5755 | 05 05 33.9 −57 55 28 | $0.158 \pm 0.020$ | 405.2 | $+0.17 \pm 0.16$ |
| 0505.8−6210 | 05 05 47.5 −62 10 10 | $0.063 \pm 0.013$ | 367.8 | $+0.43 \pm 0.50$ |
| 0507.6−5459 | 05 07 33.3 −54 59 04 | $0.047 \pm 0.013$ | 269.8 | |
| 0508.1−5316 | 05 08 04.2 −53 16 20 | $0.072 \pm 0.023$ | 137.1 | $+0.05 \pm 0.55$ |
| 0510.4−5732 | 05 10 26.2 −57 32 30 | $0.047 \pm 0.009$ | 577.8 | $-0.40 \pm 0.50$ |
| 0513.2−5507 | 05 13 11.5 −55 07 44 | $0.074 \pm 0.022$ | 158.4 | $+0.44 \pm 0.57$ |
| 0516.1−6006 | 05 16 07.2 −60 06 14 | $0.136 \pm 0.032$ | 130.2 | $+0.29 \pm 0.49$ |
| 0518.7−5803 | 05 18 43.3 −58 03 11 | $0.053 \pm 0.020$ | 129.2 | $+1.00 \pm 0.50$ |
| 0519.2−5756 | 05 19 14.3 −57 56 59 | $0.023 \pm 0.006$ | 567.7 | |
| 0523.2−5751 | 05 23 15.4 −57 51 14 | $0.088 \pm 0.020$ | 227.9 | $-0.09 \pm 0.22$ |
| 0523.7−6041 | 05 23 41.4 −60 41 31 | $0.050 \pm 0.011$ | 388.9 | $+0.37 \pm 0.50$ |
| 0525.8−5451 | 05 25 47.5 −54 51 11 | $0.019 \pm 0.005$ | 830.3 | $-0.31 \pm 0.50$ |
| 0527.6−6024 | 05 27 39.1 −60 24 53 | $0.172 \pm 0.034$ | 147.2 | $-0.32 \pm 0.21$ |
| 0528.3−6052 | 05 28 20.2 −60 52 03 | $0.045 \pm 0.010$ | 463.2 | |
| 0531.8−5239 | 05 31 50.3 −52 39 52 | $0.034 \pm 0.013$ | 212.9 | $-0.40 \pm 0.59$ |
| 0534.4−6006 | 05 34 24.6 −60 06 24 | $0.082 \pm 0.026$ | 123.2 | $-0.39 \pm 0.45$ |
| 0535.0−6110 | 05 34 57.5 −61 10 36 | $0.050 \pm 0.016$ | 181.4 | $+0.51 \pm 0.39$ |
| 0538.2−5555 | 05 38 13.2 −55 55 55 | $0.020 \pm 0.009$ | 231.2 | $+0.66 \pm 0.40$ |

Table A.1 − continued.

| ROSAT Name RXJ | X-ray source coord. (2000.0) | Countrate (3) | $t_{exp}$ (4) | HR 1 (5) |
|---|---|---|---|---|
| 0538.4−5718 | 05 38 24.5 −57 18 57 | $0.072 \pm 0.021$ | 214.9 | $-0.19 \pm 0.53$ |
| 0539.1−5657 | 05 39 05.4 −56 57 54 | $0.032 \pm 0.012$ | 211.5 | $+0.09 \pm 0.55$ |
| 0540.0−5343 | 05 40 01.4 −53 43 42 | $0.046 \pm 0.015$ | 216.4 | $+0.44 \pm 0.57$ |
| 0541.1−6151 | 05 41 04.4 −61 51 23 | $0.077 \pm 0.026$ | 116.2 | $+0.24 \pm 0.51$ |
| 0543.9−6005 | 05 43 51.7 −60 05 56 | $0.110 \pm 0.026$ | 166.2 | $-0.22 \pm 0.51$ |
| 0544.4−5523 | 05 44 21.1 −55 23 36 | $0.033 \pm 0.012$ | 246.2 | $+0.55 \pm 0.37$ |
| 0545.3−5543 | 05 45 15.2 −55 43 22 | $0.020 \pm 0.004$ | 1328.5 | $-0.18 \pm 0.50$ |
| 0545.4−5411 | 05 45 26.9 −54 11 48 | $0.060 \pm 0.015$ | 273.9 | $-0.14 \pm 0.52$ |
| 0547.3−5450 | 05 47 17.8 −54 50 35 | $0.029 \pm 0.009$ | 377.4 | $-0.20 \pm 0.68$ |
| 0548.0−6241 | 05 48 01.0 −62 41 14 | $0.042 \pm 0.014$ | 205.8 | $+0.53 \pm 0.51$ |
| 0549.7−5950 | 05 49 42.1 −59 50 10 | $0.073 \pm 0.015$ | 334.3 | $+0.17 \pm 0.50$ |
| 1053.9−2423 | 10 53 51.1 −24 23 25 | $0.031 \pm 0.041$ | 365.5 | $+0.46 \pm 0.56$ |
| 1056.1−2653 | 10 56 04.7 −26 53 13 | $0.049 \pm 0.010$ | 376.7 | $+0.00 \pm 0.71$ |
| 1058.2−2926 | 10 58 11.6 −29 26 29 | $0.075 \pm 0.015$ | 314.5 | $+0.01 \pm 0.52$ |
| 1101.1−3132 | 11 01 10.1 −31 32 48 | $0.083 \pm 0.015$ | 374.2 | $-0.02 \pm 0.21$ |
| 1102.1−2252 | 11 02 07.2 −22 52 37 | $0.030 \pm 0.009$ | 379.5 | $-0.37 \pm 0.61$ |
| 1108.5−3007 | 11 08 35.0 −30 07 41 | $0.015 \pm 0.006$ | 368.8 | $+0.55 \pm 0.49$ |
| 1110.5−3027 | 11 10 35.7 −30 27 20 | $0.030 \pm 0.009$ | 352.2 | $+0.61 \pm 0.33$ |
| 1110.6−2853 | 11 10 39.8 −28 53 34 | $0.049 \pm 0.012$ | 356.8 | $+0.39 \pm 0.60$ |
| 1115.9−2750 | 11 15 54.8 −27 50 19 | $0.040 \pm 0.015$ | 176.4 | $+0.47 \pm 0.43$ |
| 1118.3−3234 | 11 18 23.8 −32 34 48 | $0.031 \pm 0.016$ | 345.0 | $+0.68 \pm 0.38$ |
| 1119.5−2351 | 11 19 29.4 −23 51 49 | $0.026 \pm 0.009$ | 333.3 | $+0.60 \pm 0.46$ |
| 1121.5−3131 | 11 21 34.6 −31 31 40 | $0.051 \pm 0.012$ | 339.3 | $+0.09 \pm 0.70$ |
| 1121.8−2411 | 11 21 49.1 −24 11 16 | $0.060 \pm 0.013$ | 349.4 | $+0.23 \pm 0.50$ |
| 1122.0−2446 | 11 22 04.6 −24 46 34 | $0.973 \pm 0.071$ | 190.9 | $+0.02 \pm 0.07$ |
| 1122.9−2545 | 11 22 55.9 −25 45 39 | $0.056 \pm 0.013$ | 329.4 | $-0.22 \pm 0.51$ |
| 1123.3−2342 | 11 23 18.1 −23 42 27 | $0.036 \pm 0.010$ | 354.6 | $+0.09 \pm 0.70$ |
| 1124.0−2404 | 11 24 02.5 −24 04 34 | $0.067 \pm 0.020$ | 170.7 | $+0.35 \pm 0.46$ |

Table A.1 − continued.

| ROSAT Name RXJ | X-ray source coord. (2000.0) | Countrate (3) | $t_{exp}$ (4) | HR 1 (5) |
|---|---|---|---|---|
| 1132.9−3151 | 11 32 58.0 −31 51 42 | $0.424 \pm 0.055$ | 140.1 | $+0.20 \pm 0.15$ |
| 1345.2−0043 | 13 45 10.3 −00 43 39 | $0.040 \pm 0.010$ | 412.9 | $+0.21 \pm 0.68$ |
| 1354.2−0157 | 13 54 09.0 −01 57 03 | $0.039 \pm 0.010$ | 386.4 | $-0.08 \pm 0.70$ |
| 1354.9−0222 | 13 54 51.8 −02 22 53 | $0.026 \pm 0.008$ | 395.9 | $-0.06 \pm 0.70$ |
| 1355.5+0015 | 13 55 27.5 +00 15 26 | $0.025 \pm 0.008$ | 378.2 | $+0.23 \pm 0.67$ |
| 1358.4−0139 | 13 58 24.9 −01 39 45 | $0.160 \pm 0.020$ | 415.6 | $+0.48 \pm 0.14$ |
| 1358.9+0058 | 13 58 52.1 +00 58 00 | $0.038 \pm 0.009$ | 412.9 | $+0.39 \pm 0.60$ |
| 1401.9+0025 | 14 01 53.4 +00 25 14 | $0.066 \pm 0.012$ | 424.2 | $+0.15 \pm 0.51$ |
| 1404.0−0021 | 14 04 02.4 −00 21 41 | $0.090 \pm 0.014$ | 434.0 | $+0.71 \pm 0.25$ |
| 1411.5+0121 | 14 11 31.7 +01 21 59 | $0.071 \pm 0.012$ | 460.0 | $-0.41 \pm 0.43$ |
| 1413.7−0050 | 14 13 40.5 −00 50 45 | $0.115 \pm 0.017$ | 407.6 | $+0.08 \pm 0.21$ |
| 1428.2−0213 | 14 28 12.3 −02 13 40 | $1.341 \pm 0.062$ | 348.0 | $+0.16 \pm 0.05$ |
| 1429.4−0049 | 14 29 26.1 −00 49 34 | $0.120 \pm 0.018$ | 356.7 | $+0.41 \pm 0.20$ |
| 1432.1−0114 | 14 32 07.5 −01 14 42 | $0.040 \pm 0.011$ | 338.4 | $+0.05 \pm 0.71$ |
| 1433.3−0126 | 14 33 20.5 −01 26 43 | $0.040 \pm 0.011$ | 324.0 | $+0.34 \pm 0.62$ |
| 1436.9−0239 | 14 36 52.1 −00 39 57 | $0.027 \pm 0.015$ | 342.8 | $+0.41 \pm 0.59$ |
| 1437.5+0216 | 14 37 29.3 +02 16 48 | $0.046 \pm 0.012$ | 341.9 | $+0.60 \pm 0.33$ |
| 1442.7−0039 | 14 42 44.2 −00 39 57 | $0.129 \pm 0.019$ | 352.1 | $+0.25 \pm 0.48$ |
| 1446.3+0153 | 14 46 15.9 +01 53 43 | $0.053 \pm 0.012$ | 356.6 | $-0.03 \pm 0.54$ |
| 1450.7+0055 | 14 50 39.8 +00 55 46 | $0.052 \pm 0.013$ | 300.4 | $+0.81 \pm 0.18$ |
| 1451.9+0201 | 14 51 52.1 +02 01 05 | $0.057 \pm 0.013$ | 359.5 | $-0.18 \pm 0.68$ |

# B Stellar parameters

Various informations about the sources in the studied sample.

Column 1: the ROSAT name of the object.

Column 2: the coordinates, also for equinox 2000.0, of the stellar counterparts of the ROSAT sources.

Column 3: the separation between the X-ray position, as listed in tab. A.1 and the position of the counterpart, in arcseconds.

Column 4: the results from the spectral classification for the sample stars.

Column 5: the distance of the stars from the Sun, in pc, as determined using their spectral classification. Also given is the error, assuming an error for $M_v$ of $\pm 0.3 mag$.

Column 6: the X-ray flux of the X-ray sources, in units of $10^{-12}\ erg\ s^{-1}\ cm^{-2}$, as well as the errors for the flux.

Column 7: the X-ray luminosities of the studied stars, in units of $10^{29}\ erg\ s^{-1}$, as well as the errors, as determined using the errors of the distance and X-ray flux.

Column 8: Catalogue name, if existing.

Column 9: spectral type, from literature (and SIMBAD) or from the first classification obtained from the identification program.

Column 10-14: V magnitude and color indices, from the photometric observations, with exception of the 4 very bright stars that have data from the literature.

Table B.1: Data for the counterparts of the sample sources.

| ROSAT Name RXJ | Counterpart coord. (2000.0) | Diff. (3) | Spect. Type (4) | Dist. (5) | $f_X$ (6) |
|---|---|---|---|---|---|
| 2246.6−3928 | 22 46 33.2 −39 28 45 | 2.5 | G6V | $66^{+04}_{-03}$ | $1.49^{+0.37}_{-0.33}$ |
| 2258.3−4149 | 22 58 16.5 −41 49 36 | 14.0 | G6V+K1V | $136^{+13}_{-08}$ | $1.21^{+0.53}_{-0.68}$ |
| 2305.1−3823 | 23 05 04.5 −38 22 57 | 42.0 | K1/3V | 144±10 | $0.47^{+0.43}_{-0.30}$ |
| 2306.5−3855 | 23 06 34.4 −38 55 36 | 24.7 | K4V | 82±3 | $1.01^{+0.77}_{-0.58}$ |
| 2323.3−3730 | 23 23 14.2 −37 30 54 | 14.3 | K1V | 42±2 | $1.00^{+0.70}_{-0.52}$ |
| 2331.4−4209 | 23 31 25.7 −42 09 34 | 9.6 | F8/9V+F9V+G1V* | $98.4^{+17.9*}_{-13.0}$ | $1.58^{+0.77}_{-0.62}$ |
| 2356.2−3903 | 23 56 10.1 −39 03 05 | 15.0 | K3V | $22.0^{+0.6*}_{-0.4}$ | $0.60^{+0.58}_{-0.40}$ |
| 0005.9−4145 | 00 05 52.2 −41 45 08 | 20.0 | G1V | $40.0^{+2.0*}_{-1.0}$ | $1.50^{+0.51}_{-0.44}$ |
| 0015.0−4036 | 00 14 57.4 −40 35 24 | 49.7 | G4V | $141^{+8}_{-6}$ | $0.42^{+0.38}_{-0.27}$ |
| 0022.2−3943 | 00 22 10.6 −39 43 33 | 9.2 | G3V+G5V | 336±17 | $0.33^{+0.27}_{-0.19}$ |
| 0027.7−4126 | 00 27 42.7 −41 26 18 | 11.5 | K4/5V | $49^{+1}_{-2}$ | $2.11^{+0.43}_{-0.39}$ |
| 0028.8−3930 | 00 28 56.2 −39 30 50 | 67.3 | K3/4V | $92^{+4}_{-3}$ | $0.69^{+0.39}_{-0.31}$ |
| 0032.1−3827 | 00 32 09.9 −38 26 45 | 37.7 | K3/4V | $39^{+2}_{-1}$ | $0.52^{+0.32}_{-0.24}$ |
| 0035.7−2513 | 00 35 43.6 −25 14 03 | 4.2 | G0V+G9V | $119^{+15}_{-08}$ | $1.04^{+0.23}_{-0.29}$ |
| 0038.6−2335 | 00 38 36.2 −23 35 56 | 14.9 | F3/4V | $62.5^{+3.8*}_{-3.5}$ | $0.36^{+0.30}_{-0.21}$ |
| 0041.2−2649 | 00 41 11.5 −26 50 12 | 16.8 | F9V+G8V | $124^{+09}_{-14}$ | $0.53^{+0.35}_{-0.27}$ |
| 0042.7−2956 | 00 42 40.3 −29 56 39 | 10.1 | G3V | $178^{+15}_{-13}$ | $0.43^{+0.23}_{-0.18}$ |
| 0045.0−4014 | 00 45 00.8 −40 14 31 | 6.7 | K4/5V | $125^{+12}_{-11}$ | $0.21^{+0.20}_{-0.13}$ |
| 0045.2−2455 | 00 45 06.4 −24 55 12 | 37.8 | F6V+G2V | $192^{+21}_{-15}$ | $0.25^{+0.23}_{-0.16}$ |
| 0047.3−2245 | 00 47 17.8 −22 45 08 | 6.2 | K4/5V | $71^{+4}_{-3}$ | $1.72^{+0.37}_{-0.33}$ |
| 0050.6−4221 | 00 50 34.4 −42 21 17 | 3.2 | F7/8V+G5V | $202^{+29}_{-20}$ | $0.28^{+0.23}_{-0.16}$ |
| 0052.8−2728 | 00 52 45.6 −27 28 30 | 2.7 | K5V | $180^{+22}_{-20}$ | 1.16±0.35 |
| 0053.0−3021 | 00 52 59.8 −30 21 24 | 12.8 | K2/3V | 14 | $0.27^{+0.19}_{-0.14}$ |
| 0055.5−3731 | 00 55 26.5 −37 31 24 | 31.7 | G6V/IV* | $81.8^{+8.1*}_{-6.7}$ | $0.32^{+0.28}_{-0.20}$ |
| 0100.2−3818 | 01 00 12.3 −38 18 38 | 11.9 | K4V | 54±3 | $1.32^{+0.31}_{-0.28}$ |
| 0105.4−4016 | 01 05 21.7 −40 16 11 | 3.0 | F3V | $54.9^{+2.6*}_{-2.3}$ | $0.25^{+0.22}_{-0.15}$ |
| 0116.8−3932 | 01 16 50.6 −39 32 07 | 14.2 | K1V | 21±1 | $0.27^{+0.17}_{-0.13}$ |
| 0121.2−3729 | 01 21 10.0 −37 29 29 | 1.0 | K5V | $45^{+3}_{-2}$ | $3.27^{+0.47}_{-0.44}$ |

Table B.1 − continued

| $L_X$ (7) | Name (8) | $Sp_0$ (9) | V (10) | U-B (11) | B-V (12) | V-R (13) | V-I (14) |
|---|---|---|---|---|---|---|---|
| $7.74^{+3.07}_{-2.26}$ | | G | 9.45 | 0.18 | 0.71 | 0.40 | 0.77 |
| $26.48^{+23.30}_{-13.46}$ | CD-52 16149 | K3 | 10.60 | 0.03 | 0.73 | 0.45 | 0.85 |
| $11.57^{+14.00}_{-08.00}$ | | K3 | 11.89 | 0.33 | 0.84 | 0.53 | 1.00 |
| $8.19^{+7.37}_{-4.94}$ | | K5 | 11.33 | 0.58 | 1.00 | 0.59 | 1.13 |
| $2.08^{+1.80}_{-1.17}$ | HD 220345 | K2III | 9.35 | 0.54 | 0.87 | 0.47 | 0.89 |
| $18.32^{+19.64*}_{-06.21}$ | HD 221330 | G0V | 8.25 | 0.06 | 0.58 | 0.34 | 0.64 |
| $0.34^{+0.39*}_{-0.22}$ | HD 224228 | K3V | 8.22 | 0.82 | 0.96 | 0.56 | 1.04 |
| $2.91^{+1.33*}_{-0.98}$ | HD 105 | G0V | 7.52 | 0.04 | 0.60 | 0.34 | 0.66 |
| $10.10^{+11.38}_{-06.68}$ | | G5 | 10.74 | 0.14 | 0.65 | 0.36 | 0.70 |
| $44.56^{+44.60}_{-27.51}$ | | K3 | 11.96 | 0.12 | 0.67 | 0.39 | 0.78 |
| $5.97^{+1.56}_{-1.54}$ | | K5Ve | 10.74 | 0.87 | 1.14 | 0.50 | 0.95 |
| $6.94^{+4.97}_{-3.36}$ | | K5V | 10.61 | 0.84 | 1.01 | 0.56 | 1.04 |
| $0.92^{+0.72}_{-0.47}$ | | K5V | 9.74 | 0.75 | 1.01 | 0.53 | 1.03 |
| $17.55^{+11.88}_{-06.60}$ | SAO 166391 | G2V | 9.70 | 0.05 | 0.63 | 0.37 | 0.71 |
| $1.68^{+1.79*}_{-1.06}$ | HD 3581 | F3IV/V | 7.10 | −0.04 | 0.41 | 0.25 | 0.47 |
| $9.83^{+8.94}_{-5.95}$ | HD 3877 | G0V | 9.86 | 0.01 | 0.60 | 0.37 | 0.71 |
| $16.13^{+13.30}_{-08.24}$ | | G5 | 11.18 | 0.04 | 0.64 | 0.34 | 0.69 |
| $3.83^{+5.14}_{-2.72}$ | | dK8e | 12.35 | 0.79 | 1.03 | 0.63 | 1.18 |
| $10.85^{+14.86}_{-07.55}$ | HD 4288 | F3/5V | 9.89 | −0.10 | 0.46 | 0.34 | 0.65 |
| $10.47^{+3.87}_{-2.78}$ | | K8e | 11.27 | 0.79 | 1.06 | 0.64 | 1.23 |
| $13.75^{+18.60}_{-08.98}$ | CD-43 234 | F8 | 10.32 | 0.00 | 0.52 | 0.34 | 0.65 |
| $43.88^{+30.04}_{-19.08}$ | | K8V | 12.34 | 0.82 | 1.10 | 0.70 | 1.38 |
| $0.06^{+0.05}_{-0.03}$ | HD 5133 | K3V+.. | 7.17 | 0.74 | 0.93 | 0.54 | 1.01 |
| $2.57^{+3.22*}_{-1.76}$ | HD 5403 | G5V | 8.67 | 0.22 | 0.71 | 0.41 | 0.77 |
| $4.53^{+1.79}_{-1.28}$ | | K5Ve | 10.58 | 0.77 | 1.04 | 0.61 | 1.15 |
| $0.90^{+0.95*}_{-0.57}$ | HD 6493 | F3V | 7.17 | −0.05 | 0.40 | 0.24 | 0.46 |
| $0.14^{+0.11}_{-0.07}$ | HD 7777 | G8 | 7.97 | 0.46 | 0.89 | 0.47 | 0.90 |
| $7.92^{+2.49}_{-1.67}$ | | K8e | 10.52 | 0.92 | 1.12 | 0.71 | 1.38 |

Table B.1 – continued

| ROSAT Name RXJ | Counterpart coord. (2000.0) | Diff. (3) | Spect. Type (4) | Dist. (5) | $f_X$ (6) |
|---|---|---|---|---|---|
| 0121.5−4058 | 01 21 29.3 −40 58 17 | 3.4 | F6V | $89.6^{+14.1*}_{-10.7}$ | $0.47^{+0.19}_{-0.16}$ |
| 0125.6−4148 | 01 25 33.6 −41 48 36 | 1.5 | G5V+K3V | $130^{+08}_{-11}$ | $0.71^{+0.24}_{-0.21}$ |
| 0126.4−4127 | 01 26 25.3 −41 27 49 | 5.0 | G8V | $91^{+7}_{-8}$ | $0.44^{+0.21}_{-0.17}$ |
| 0135.8−3956 | 01 35 49.3 −39 56 30 | 16.7 | F4V | $37.7^{+1.0*}_{-1.0}$ | $0.48^{+0.36}_{-0.27}$ |
| 0136.8−3811 | 01 36 48.4 −38 11 26 | 11.7 | K2/3V | $137^{+15}_{-10}$ | $0.77^{+0.48}_{-0.36}$ |
| 0141.4−3808 | 01 41 28.6 −38 08 23 | 40.3 | F3V | $41.9^{+1.2*}_{-1.1}$ | $0.78^{+0.24}_{-0.21}$ |
| 0155.4−3846 | 01 55 22.5 −38 46 23 | 11.7 | K5V | 67±4 | $2.71^{+0.57}_{-0.52}$ |
| 0440.3−5856 | 04 40 17.6 −58 56 43 | 12.4 | G5V/IV* | $31.0^{+0.9*}_{-1.0}$ | $0.48^{+0.62}_{-0.14}$ |
| 0450.1−5856 | 04 50 09.7 −58 57 31 | 42.9 | K2V | $205^{+30}_{-20}$ | $8.40^{+5.40}_{-4.08}$ |
| 0454.9−5832 | 04 54 53.1 −58 32 54 | 0.8 | F5V | $30.9^{+0.5*}_{-0.5}$ | $3.81^{+2.01}_{-1.63}$ |
| 0501.5−5930 | 05 01 32.3 −59 30 46 | 6.3 | F9V+G6V | $232^{+21}_{-24}$ | $0.22^{+0.13}_{-0.12}$ |
| 0505.5−5728 | 05 05 31.1 −57 28 25 | 11.5 | F7/8V | $11.6^{+0.1*}_{-0.1}$ | $15.64^{+2.06}_{-1.94}$ |
| 0505.6−5755 | 05 05 36.4 −57 55 36 | 21.4 | K4V | $87^{+5}_{-7}$ | $1.46^{+0.33}_{-0.30}$ |
| 0505.8−6210 | 05 05 47.3 −62 09 58 | 12.1 | K5V | $157^{+21}_{-20}$ | $0.67^{+0.34}_{-0.44}$ |
| 0507.6−5459 | 05 07 34.3 −54 59 21 | 19.1 | F5/6V/IV* | $66.4^{+*}_{-}$ | $0.42^{+0.28}_{-0.22}$ |
| 0508.1−5316 | 05 08 07.0 −53 16 15 | 25.6 | G3V | $150^{+13}_{-11}$ | $0.62^{+0.48}_{-0.34}$ |
| 0510.4−5732 | 05 10 26.8 −57 31 59 | 31.4 | F9V+G5V | $247^{+21}_{-27}$ | $0.29^{+0.21}_{-0.16}$ |
| 0513.2−5507 | 05 13 12.0 −55 07 48 | 5.9 | K5/7V | $95^{+12}_{-14}$ | $0.79^{+0.52}_{-0.39}$ |
| 0516.1−6006 | 05 16 04.7 −60 06 55 | 45.0 | K4/5V | 102±10 | $1.34^{+0.76}_{-0.59}$ |
| 0518.7−5803 | 05 18 42.4 −58 02 48 | 25.0 | K4V | $236^{+31}_{-28}$ | $0.72^{+0.47}_{-0.36}$ |
| 0519.2−5756 | 05 19 16.4 −57 56 53 | 16.2 | G5V+K3V | $466^{+29}_{-56}$ | $0.21^{+0.13}_{-0.11}$ |
| 0523.2−5751 | 05 23 15.3 −57 51 01 | 13.0 | K1/2V | $136^{+13}_{-12}$ | $0.69^{+0.28}_{-0.23}$ |
| 0523.7−6041 | 05 23 43.2 −60 41 25 | 14.5 | K5/7V | $125^{+12}_{-19}$ | $0.51^{+0.28}_{-0.22}$ |
| 0525.8−5451 | 05 25 46.6 −54 51 21 | 12.7 | K3V | $129^{+14}_{-13}$ | $0.13^{+0.10}_{-0.07}$ |
| 0527.6−6024 | 05 27 40.3 −60 24 53 | 8.9 | G9V | $19.6^{+0.2*}_{-0.2}$ | $1.14^{+0.46}_{-0.38}$ |
| 0528.3−6052 | 05 28 21.9 −60 51 59 | 13.0 | F5V | $136^{+13}_{-06}$ | $0.40^{+0.24}_{-0.20}$ |
| 0531.8−5239 | 05 31 51.3 −52 40 00 | 9.3 | K4V | $137^{+17}_{-16}$ | $0.21^{+0.23}_{-0.15}$ |
| 0534.4−6006 | 05 34 26.3 −60 06 15 | 15.6 | F7V | $80.1^{+4.6*}_{-4.1}$ | $0.51^{+0.42}_{-0.29}$ |
| 0535.0−6110 | 05 34 57.6 −61 10 32 | 4.1 | G4/5III* | $106.7^{+6.2*}_{-5.5}$ | $0.55^{+0.32}_{-0.25}$ |

Table B.1 − continued

| $L_X$ (7) | Name (8) | $Sp_0$ (9) | V (10) | U-B (11) | B-V (12) | V-R (13) | V-I (14) |
|---|---|---|---|---|---|---|---|
| $4.49^{+3.98*}_{-2.18}$ | HD 8283 | F3V | 8.58 | −0.06 | 0.48 | 0.29 | 0.55 |
| $14.38^{+7.34}_{-5.91}$ | VW Phe | G2 | 10.48 | 0.15 | 0.72 | 0.47 | 0.89 |
| $4.33^{+3.00}_{-2.11}$ | | K0V | 10.30 | 0.17 | 0.74 | 0.42 | 0.78 |
| $0.81^{+0.69*}_{-0.47}$ | HD 9895 | F3/5V | 6.41 | −0.08 | 0.43 | 0.25 | 0.48 |
| $17.43^{+17.43}_{-09.53}$ | | K0V | 12.12 | 0.48 | 0.91 | 0.54 | 1.03 |
| $1.63^{+0.62*}_{-0.50}$ | HD 10481 | F2V | 6.18 | −0.06 | 0.41 | 0.24 | 0.45 |
| $14.35^{+5.23}_{-3.96}$ | | K5V | 11.15 | 0.81 | 1.07 | 0.70 | 1.36 |
| $0.55^{+0.78*}_{-0.18}$ | HD 30003 | G5V | 6.53 | 0.23 | 0.68 | 0.38 | 0.72 |
| $421.08^{+490.86}_{-244.25}$ | | K2 | 12.91 | 0.42 | 0.89 | 0.50 | 0.99 |
| $4.34^{+2.53*}_{-1.95}$ | HD 31746 | F3V | 6.11 | −0.06 | 0.44 | 0.27 | 0.52 |
| $14.14^{+13.08}_{-09.00}$ | | G2V | 10.85 | −0.00 | 0.58 | 0.35 | 0.67 |
| $2.50^{+0.49*}_{-0.45}$ | HD 33262 | F7V | 4.70 | | 0.52 | 0.31 | 0.60 |
| $13.30^{+5.11}_{-4.27}$ | | K8 | 11.41 | 0.67 | 0.99 | 0.61 | 1.19 |
| $19.66^{+18.40}_{-14.60}$ | | K8 | 13.28 | 0.50 | 1.14 | 0.64 | 1.25 |
| $2.21^{+1.78*}_{-1.23}$ | HD 33514 | F5V | 7.34 | −0.02 | 0.47 | 0.28 | 0.54 |
| $16.65^{+18.05}_{-10.23}$ | | G6V | 10.81 | 0.11 | 0.64 | 0.37 | 0.68 |
| $21.19^{+21.32}_{-13.42}$ | | G2V | 10.93 | 0.05 | 0.57 | 0.34 | 0.67 |
| $8.54^{+9.28}_{-5.40}$ | | K8V | 12.54 | 1.16 | 1.22 | 0.77 | 1.51 |
| $16.76^{+14.74}_{-09.15}$ | | K5 | 12.12 | 0.90 | 1.08 | 0.63 | 1.19 |
| $47.84^{+53.43}_{-29.29}$ | | K5 | 13.66 | 1.36 | 1.01 | 0.62 | 1.10 |
| $54.24^{+44.16}_{-34.50}$ | | G5V | 13.25 | 0.34 | 0.71 | 0.43 | 0.87 |
| $15.14^{+10.30}_{-06.81}$ | | G | 11.81 | 0.42 | 0.85 | 0.52 | 1.02 |
| $9.48^{+8.11}_{-5.54}$ | | K5 | 12.98 | 1.25 | 1.19 | 0.67 | 1.33 |
| $2.58^{+2.93}_{-1.63}$ | | K5 | 12.13 | 0.48 | 0.95 | 0.54 | 1.04 |
| $0.52^{+0.22*}_{-0.18}$ | HD 36435 | G6V | 7.01 | 0.28 | 0.77 | 0.41 | 0.80 |
| $8.75^{+8.11}_{-4.68}$ | HD 36530 | F3V | 9.53 | −0.16 | 0.44 | 0.27 | 0.57 |
| $4.81^{+7.78}_{-3.64}$ | | K8V | 12.52 | 0.82 | 1.02 | 0.59 | 1.13 |
| $3.91^{+4.05*}_{-2.40}$ | HD 37402 | F8 | 8.40 | −0.03 | 0.50 | 0.30 | 0.58 |
| $7.46^{+5.72*}_{-3.78}$ | HD 37501 | G5IV | 6.33 | 0.48 | 0.84 | 0.45 | 0.88 |

Table B.1 − continued

| ROSAT Name RXJ | Counterpart coord. (2000.0) | Diff. (3) | Spect. Type (4) | Dist. (5) | $f_X$ (6) |
|---|---|---|---|---|---|
| 0538.2−5555 | 05 38 08.6 −55 56 02 | 39.3 | K3V | $278^{+37}_{-31}$ | $0.23^{+0.17}_{-0.13}$ |
| 0538.4−5718 | 05 38 24.6 −57 19 08 | 11.0 | F9V | $139^{+10}_{-09}$ | $0.53^{+0.42}_{-0.30}$ |
| 0539.1−5657 | 05 39 05.2 −56 57 58 | 4.3 | K1/2V | $445^{+78}_{-54}$ | $0.28^{+0.24}_{-0.17}$ |
| 0540.0−5343 | 05 39 59.3 −53 43 43 | 18.6 | K0V | $164^{+24}_{-18}$ | $0.49^{+0.34}_{-0.25}$ |
| 0541.1−6151 | 05 41 04.9 −61 51 29 | 7.0 | F3/4V | $204.1^{+44.6*}_{-31.1}$ | $0.74^{+0.52}_{-0.38}$ |
| 0543.9−6005 | 05 43 49.7 −60 05 54 | 15.1 | G7V+K2V | 176±12 | $0.79^{+0.55}_{-0.41}$ |
| 0544.4−5523 | 05 44 20.7 −55 23 30 | 6.9 | K5/7V | $63^{+8}_{-9}$ | $0.37^{+0.22}_{-0.17}$ |
| 0545.3−5543 | 05 45 14.9 −55 43 27 | 5.6 | F5V+G6V | $89.2^{+*}_{-}$ | $0.15^{+0.09}_{-0.07}$ |
| 0545.4−5411 | 05 45 26.8 −54 11 34 | 14.0 | K3V+K4V | $129^{+13}_{-47}$ | $0.45^{+0.32}_{-0.24}$ |
| 0547.3−5450 | 05 47 17.9 −54 50 28 | 7.0 | F6V | $90^{+4}_{-8}$ | $0.21^{+0.20}_{-0.14}$ |
| 0548.0−6241 | 05 48 02.3 −62 41 08 | 10.8 | K0/1V | $170^{+34}_{-22}$ | $0.47^{+0.31}_{-0.23}$ |
| 0549.7−5950 | 05 49 41.1 −59 50 23 | 15.0 | F7V+F7/8V+F7/8V | $141.4^{+38.8*}_{-25.0}$ | $0.67^{+0.37}_{-0.29}$ |
| 1053.9−2423 | 10 53 53.0 −24 23 35 | 27.8 | K4V | $175^{+24}_{-23}$ | $0.34^{+0.22}_{-0.17}$ |
| 1056.1−2653 | 10 56 02.4 −26 52 47 | 40.3 | G5V | $120^{+10}_{-11}$ | $0.41^{+0.32}_{-0.23}$ |
| 1058.2−2926 | 10 58 14.1 −29 26 12 | 36.8 | K0V+K5V | $115^{+20}_{-17}$ | $0.62^{+0.38}_{-0.29}$ |
| 1101.1−3132 | 11 01 10.9 −31 32 49 | 10.3 | K3V | 57±3 | $0.68^{+0.22}_{-0.20}$ |
| 1102.1−2252 | 11 02 06.7 −22 52 33 | 8.0 | K7V | $57^{+8}_{-7}$ | $0.19^{+0.18}_{-0.13}$ |
| 1108.5−3007 | 11 08 34.4 −30 07 39 | 8.0 | F5/6V | 70±3 | $0.17^{+0.13}_{-0.09}$ |
| 1110.5−3027 | 11 10 34.1 −30 27 16 | 21.1 | F3V+F7V | $161^{+16}_{-14}$ | $0.34^{+0.17}_{-0.14}$ |
| 1110.6−2853 | 11 10 38.0 −28 54 01 | 35.9 | F4V | $339^{+33}_{-30}$ | $0.51^{+0.31}_{-0.24}$ |
| 1115.9−2750 | 11 15 55.9 −27 50 15 | 15.1 | K5V | 50±3 | $0.43^{+0.29}_{-0.22}$ |
| 1118.3−3234 | 11 18 23.1 −32 34 23 | 26.5 | K2/3V | $449^{+78}_{-52}$ | $0.37^{+0.28}_{-0.22}$ |
| 1119.5−2351 | 11 19 30.1 −23 52 02 | 16.2 | K1V | $145^{+18}_{-15}$ | $0.29^{+0.18}_{-0.14}$ |
| 1121.5−3131 | 11 21 35.4 −31 31 16 | 26.1 | F7/8V | $59.4^{+3.4*}_{-3.0}$ | $0.45^{+0.34}_{-0.25}$ |
| 1121.8−2411 | 11 21 49.8 −24 11 23 | 11.9 | G3V | $48.0^{+2.3*}_{-2.0}$ | $0.57^{+0.32}_{-0.25}$ |
| 1122.0−2446 | 11 22 05.4 −24 46 38 | 11.6 | K4/5V+... | $46.7^{+7.1*}_{-5.5}$ | $8.19^{+0.99}_{-0.94}$ |
| 1122.9−2545 | 11 22 56.0 −25 45 53 | 14.1 | K4/5V | $64^{+5}_{-4}$ | $0.40^{+0.28}_{-0.21}$ |
| 1123.3−2342 | 11 23 18.4 −23 42 25 | 4.6 | G8III | $170.9^{+25.2*}_{-19.4}$ | $0.31^{+0.26}_{-0.19}$ |
| 1124.0−2404 | 11 24 00.4 −24 04 44 | 30.4 | F8V+G4V | $705^{+50}_{-56}$ | $0.68^{+0.41}_{-0.32}$ |

Table B.1 − continued

| $L_X$ (7) | Name (8) | $Sp_0$ (9) | V (10) | U-B (11) | B-V (12) | V-R (13) | V-I (14) |
|---|---|---|---|---|---|---|---|
| $21.39^{+26.06}_{-14.08}$ | | K7V | 13.79 | 0.86 | 0.95 | 0.49 | 1.06 |
| $12.13^{+12.73}_{-07.50}$ | | G | 10.06 | 0.03 | 0.55 | 0.33 | 0.63 |
| $66.93^{+102.89}_{-045.62}$ | | K2V | 14.49 | 0.59 | 0.87 | 0.52 | 0.97 |
| $15.71^{+19.30}_{-09.60}$ | | G2V | 11.97 | 0.18 | 0.80 | 0.44 | 0.86 |
| $36.77^{+56.27*}_{-23.93}$ | HD 38372 | F0V | 9.62 | 0.02 | 0.38 | 0.27 | 0.50 |
| $29.12^{+27.18}_{-17.04}$ | | G6 | 11.31 | 0.12 | 0.74 | 0.44 | 0.91 |
| $1.76^{+1.81}_{-1.08}$ | | K5 | 11.70 | 1.26 | 1.23 | 0.68 | 1.26 |
| $1.42^{+1.29*}_{-0.77}$ | HD 38829 | F5V | 8.22 | 0.03 | 0.49 | 0.29 | 0.54 |
| $9.01^{+9.56}_{-7.26}$ | | K5+K8 | 11.51 | 0.64 | 0.98 | 0.61 | 1.12 |
| $2.02^{+2.30}_{-1.44}$ | HD 39139 | F6V | 8.77 | −0.04 | 0.49 | 0.28 | 0.57 |
| $16.05^{+22.59}_{-09.98}$ | | G6V | 12.00 | 0.30 | 0.79 | 0.47 | 0.92 |
| $15.94^{+24.36*}_{-09.80}$ | HD 39579 | F7V | 8.86 | 0.03 | 0.53 | 0.29 | 0.55 |
| $12.37^{+14.09}_{-07.59}$ | | K2/5V | 13.17 | 0.87 | 1.05 | 0.60 | 1.16 |
| $6.94^{+7.59}_{-4.51}$ | | G8V+K8V | 10.48 | 0.20 | 0.67 | 0.38 | 0.74 |
| $9.83^{+11.92}_{-06.04}$ | | G5V | 10.98 | 0.23 | 0.82 | 0.50 | 1.02 |
| $2.60^{+1.20}_{-0.92}$ | | K7V | 10.30 | 0.55 | 0.94 | 0.55 | 1.10 |
| $0.74^{+1.16}_{-0.54}$ | 1E 1059.6-2236 | K5Ve | 11.77 | 1.05 | 1.28 | 0.80 | 1.55 |
| $0.99^{+0.92}_{-0.59}$ | HD 96803 | F5V | 7.94 | −0.03 | 0.46 | 0.29 | 0.58 |
| $10.68^{+8.65}_{-5.47}$ | HD 97131 | F2V | 8.81 | −0.01 | 0.41 | 0.26 | 0.53 |
| $69.74^{+65.94}_{-39.13}$ | | F2V | 11.05 | 0.08 | 0.42 | 0.26 | 0.51 |
| $1.27^{+1.12}_{-0.71}$ | | K5V | 10.92 | 0.78 | 1.17 | 0.64 | 1.22 |
| $88.36^{+126.37}_{-060.07}$ | | K0V | 14.56 | −0.14 | 0.88 | 0.59 | 1.03 |
| $7.36^{+7.69}_{-4.27}$ | | G4V | 12.00 | 0.24 | 0.86 | 0.46 | 0.92 |
| $1.89^{+1.82*}_{-1.13}$ | HD 98753 | F6V | 7.74 | −0.03 | 0.51 | 0.30 | 0.60 |
| $1.57^{+1-12*}_{-0.69}$ | HD 98764 | G5 | 8.12 | 0.13 | 0.64 | 0.37 | 0.74 |
| $21.36^{+10.20*}_{-06.62}$ | HD 98800 | K5V + ?? | 8.94 | 1.14 | 1.26 | 0.80 | 1.59 |
| $1.92^{+1.89}_{-1.12}$ | | K8Ve | 11.24 | 0.99 | 1.11 | 0.63 | 1.16 |
| $10.86^{+15.21*}_{-07.58}$ | HD 98975 | K0 | 7.17 | 0.67 | 0.94 | 0.50 | 0.97 |
| $402.43^{+340.96}_{-219.96}$ | | F8V | 13.03 | −0.03 | 0.54 | 0.34 | 0.66 |

Table B.1 − continued

| ROSAT Name RXJ | Counterpart coord. (2000.0) | Diff. (3) | Spect. Type (4) | Dist. (5) | $f_X$ (6) |
|---|---|---|---|---|---|
| 1132.9−3151 | 11 33 00.4 −31 51 10 | 44.2 | G8III | $39.6^{+1.4*}_{-1.2}$ | $3.97^{+0.90}_{-0.81}$ |
| 1345.2−0043 | 13 45 10.3 −00 43 58 | 19.0 | F8V | $312^{+30}_{-27}$ | $0.37^{+0.27}_{-0.20}$ |
| 1354.2−0157 | 13 54 07.3 −01 57 56 | 58.8 | F8V | $71.3^{+5.6*}_{-4.9}$ | $0.31^{+0.26}_{-0.19}$ |
| 1354.9−0222 | 13 54 51.9 −02 22 50 | 3.3 | F9V+G5V | $119.0^{+19.9*}_{-14.8}$ | $0.21^{+0.19}_{-0.13}$ |
| 1355.5+0015 | 13 55 27.8 +00 15 23 | 5.4 | K5/7V | $62^{+9}_{-5}$ | $0.24^{+0.20}_{-0.14}$ |
| 1358.4−0139 | 13 58 24.8 −01 39 38 | 7.1 | G0V+G5V | $125.9^{+29.4*}_{-20.0}$ | $1.74^{+0.35}_{-0.32}$ |
| 1358.9+0058 | 13 58 52.2 +00 58 00 | 1.5 | G9V+G9V | $125^{+09}_{-16}$ | $0.39^{+0.25}_{-0.19}$ |
| 1401.9+0025 | 14 01 52.1 +00 25 20 | 20.4 | F8V | $64.1^{+5.9*}_{-5.0}$ | $0.60^{+0.33}_{-0.26}$ |
| 1404.0−0021 | 14 04 02.2 −00 21 45 | 5.8 | F8IV+G3IV+G3IV* | $232.0^{+88.5*}_{-50.2}$ | $1.09^{+0.31}_{-0.27}$ |
| 1411.5+0121 | 14 11 31.2 +01 21 44 | 16.8 | F6V | $45.9^{+1.9*}_{-1.7}$ | $0.43^{+0.26}_{-0.21}$ |
| 1413.7−0050 | 14 13 40.6 −00 05 40 | 5.2 | F6V | $55.7^{+2.7*}_{-2.4}$ | $1.01^{+0.30}_{-0.26}$ |
| 1428.2−0213 | 14 28 12.1 −02 13 36 | 5.0 | G2III/IV+K0V* | $41.4^{+1.8*}_{-1.6}$ | $12.49^{+0.73}_{-1.12}$ |
| 1429.4−0049 | 14 29 26.2 −00 49 46 | 12.1 | K0V | 87±6 | $1.26^{+0.34}_{-0.30}$ |
| 1432.1−0114 | 14 32 07.4 −01 14 47 | 5.2 | K3/4V | $91^{+9}_{-8}$ | $0.35^{+0.29}_{-0.20}$ |
| 1433.3−0126 | 14 33 20.5 −01 25 44 | 1.0 | K0/1V | $506^{+116}_{-075}$ | $0.40^{+0.30}_{-0.21}$ |
| 1436.9−0239 | 14 36 54.2 −02 44 32 | 34.0 | K4/5V | 111±12 | $0.28^{+0.19}_{-0.14}$ |
| 1437.5+0216 | 14 37 29.3 +02 16 40 | 8.0 | F9V | $26^{+1}_{-2}$ | $0.53^{+0.23}_{-0.19}$ |
| 1442.7−0039 | 14 42 44.3 −00 39 54 | 3.3 | G5V+K1V | $118^{+08}_{-10}$ | $1.24^{+0.56}_{-0.46}$ |
| 1446.3+0153 | 14 46 14.7 +01 53 13 | 26.9 | A0V | $39.4^{+1.4*}_{-1.3}$ | $0.43^{+0.28}_{-0.21}$ |
| 1450.7+0055 | 14 50 38.2 +00 55 53 | 25.0 | F6V | $375^{+36}_{-33}$ | $0.65^{+0.23}_{-0.20}$ |
| 1451.9+0201 | 14 51 53.3 +02 00 51 | 22.8 | G5/6V | $38.9^{+2.1*}_{-1.8}$ | $0.42^{+0.34}_{-0.25}$ |

Table B.1 − continued

| $L_X$ (7) | Name (8) | $Sp_0$ (9) | V (10) | U-B (11) | B-V (12) | V-R (13) | V-I (14) |
|---|---|---|---|---|---|---|---|
| $7.43^{+2.29*}_{-1.88}$ | HD 100407 | G7III | 3.54 | | 0.94 | 0.33 | 0.68 |
| $43.43^{+46.58}_{-26.66}$ | | F8V | 11.67 | 0.04 | 0.39 | 0.32 | 0.62 |
| $1.89^{+2.13*}_{-1.26}$ | HD 121218 | F8 | 8.32 | 0.01 | 0.54 | 0.31 | 0.62 |
| $3.55^{+5.62*}_{-2.51}$ | HD 121322 | F8V | 8.89 | 0.03 | 0.56 | 0.34 | 0.67 |
| $1.10^{+1.52}_{-0.71}$ | | K8 | 11.95 | 1.11 | 1.28 | 0.73 | 1.40 |
| $32.87^{+27.45*}_{-13.96}$ | HD 121909 | G0 | 9.61 | 0.05 | 0.61 | 0.35 | 0.71 |
| $7.24^{+6.38}_{-4.40}$ | BD+01 2868 | G5V | 10.38 | 0.28 | 0.76 | 0.43 | 0.84 |
| $2.95^{+2.50*}_{-1.53}$ | HD 122444 | F8V | 8.30 | 0.02 | 0.54 | 0.30 | 0.58 |
| $70.10^{+101.47*}_{-037.73}$ | HD 122798 | F8V | 8.50 | 0.07 | 0.58 | 0.34 | 0.67 |
| $1.08^{+0.80*}_{-0.57}$ | HD 124115 | F7V | 6.41 | 0.02 | 0.48 | 0.28 | 0.55 |
| $3.74^{+1.58*}_{-1.21}$ | HD 124425 | F7V | 5.90 | −0.00 | 0.47 | 0.28 | 0.55 |
| $25.64^{+4.02*}_{-4.10}$ | HD 126868 | G2IV+G4V | 4.82 | | 0.74 | 0.39 | 0.75 |
| $11.50^{+5.26}_{-3.88}$ | BD-00 2832 | G5V | 10.66 | 0.26 | 0.81 | 0.47 | 0.82 |
| $3.40^{+4.08}_{-2.24}$ | CM Vir | G2/5V | 11.62 | 0.01 | 1.02 | 0.56 | 1.04 |
| $122.72^{+191.96}_{-079.43}$ | | K5 | 14.32 | 1.08 | 0.78 | 0.50 | 0.92 |
| $4.07^{+4.41}_{-2.49}$ | | K5 | 12.32 | 0.47 | 1.09 | 0.61 | 1.19 |
| $0.42^{+0.24}_{-0.19}$ | HD 128563 | F8 | 6.45 | 0.11 | 0.56 | 0.32 | 0.62 |
| $20.66^{+13.78}_{-09.89}$ | | K5 | 10.12 | 0.20 | 0.70 | 0.41 | 0.82 |
| $0.80^{+0.60*}_{-0.42}$ | HD 130109 | A0V | 3.72 | −0.02 | −0.01 | | |
| $109.05^{+67.79}_{-46.49}$ | | F | 11.67 | −0.01 | 0.48 | 0.29 | 0.58 |
| $0.76^{+0.76*}_{-0.48}$ | HD 131179 | G5V | 8.34 | 0.17 | 0.70 | 0.39 | 0.75 |

# C Spectroscopic Data

Here we list the results of the spectroscopic observations of the southern hemisphere sample stars.

Column 1: ROSAT name.

Column 2: Spectral type.

Column 3: $(B-V)$ colour index. For the single stars the observed index is listed, for the multiple system components the index taken from the tables of Cutispoto et al. (1996).

Column 4: Effective temperature.

Column 5: gravitational acceleration.

Column 6: Radial velocity, in km/s.

Column 7: Projected rotational velocity, in km/s. Values marked with an $*$ are literature values

Column 8: Lihtium abundance.

Column 9: Radius fo the star, in units of the solar radius.

Table C.1: Velocities, Li abundances for the southern hemisphere sample.

| ROSAT Name RXJ | Spectral type | $(B-V)$ (3) | $T_{eff}$ (4) | log(g) (5) | $V_{rad}$ (6) | $v \cdot sini$ (7) | N(Li) (8) | Radius (9) |
|---|---|---|---|---|---|---|---|---|
| 2246.6−3928 | G6V | 0.71 | 5461 | 4.48 | −5.43 | 12.40 | 2.75 | 0.868 |
| 2258.3−4149a | G6V | 0.71 | 5461 | 4.48 | 54.38 | 59.80 | 0.00 | 0.864 |
| b | K1V | 0.86 | 5017 | 4.55 | −71.64 | 34.40 | 0.00 | 0.738 |
| 2305.1−3823 | K1/3V | 0.84 | 5072 | 4.57 | −14.87 | 16.70 | 0.70 | 0.746 |
| 2306.5−3855 | K4V | 1.00 | 4662 | 4.60 | 22.42 | 76.40 | 2.30 | 0.717 |
| 2323.3−3730 | K1V | 0.87 | 4990 | 4.55 | −117.05 | 84.30 | 1.00 | 0.72 |
| 2331.4−4209a | F8/9V | 0.55 | 6027 | 4.40 | −51.20 | 25.00 | 2.80 | 1.069 |
| b | F9V | 0.56 | 5988 | 4.41 | 48.70 | 26.50 | 2.50 | 0.900 |
| c | G1V | 0.62 | 5765 | 4.44 | −7.40 | 3.80 | 2.50 | 1.251 |
| 2356.2−3903 | K3V | 0.96 | 4759 | 4.58 | 12.79 | 4.00 | 1.49 | 0.718 |
| 0005.9−4145 | G1V | 0.60 | 5838 | 4.44 | 1.61 | 13.50 | 3.01 | 1.001 |
| 0015.0−4036 | G4V | 0.65 | 5660 | 4.46 | 1.34 | 3.50 | 1.95 | 0.940 |
| 0022.2−3943a | G3V | 0.65 | 5660 | 4.46 | −5.55 | 9.90 | | 0.936 |
| b | G5V | 0.68 | 5559 | 4.46 | 6.55 | 10.60 | | 0.902 |
| 0027.7−4126 | K4/5V | 1.14 | 4353 | 4.60 | 23.54 | 12.20 | 1.10 | 0.697 |
| 0028.8−3930 | K3/4V | 1.01 | 4639 | 4.59 | 38.42 | 3.50 | 0.44 | 0.712 |
| 0032.1−3827 | K3/4V | 1.01 | 4639 | 4.59 | −1.66 | 3.50 | 0.59 | 0.712 |
| 0035.7−2513a | G0V | 0.60 | 5838 | 4.42 | 27.83 | 15.40 | 2.80 | 0.997 |
| b | G9V | 0.76 | 5305 | 4.52 | 4.92 | 12.80 | 2.00 | 0.820 |
| 0038.6−2335 | F3/4V | 0.41 | 6625 | 4.30 | 13.05 | 38.00 | 2.30 | 1.427 |
| 0041.2−2649 | F9V | 0.56 | 5988 | 4.41 | 10.22 | 3.50 | 2.00 | 1.083 |
| b | G8V | 0.74 | 5366 | 4.50 | 19.02 | 14.00 | 1.80 | 0.847 |
| 0042.7−2956 | G3V | 0.64 | 5695 | 4.46 | 23.56 | 8.20 | 1.23 | 0.955 |
| 0045.0−4014 | K4/5V | 1.03 | 4593 | 4.60 | 52.71 | 19.60 | 0.50 | 0.713 |
| 0045.2−2455a | F6V | 0.48 | 6312 | 4.35 | 45.11 | 5.20 | 1.00 | 1.261 |
| b | G2V | 0.63 | 5730 | 4.45 | 67.22 | 8.40 | 2.00 | 0.956 |
| 0047.3−2245 | K4/5V | 1.06 | 4525 | 4.60 | 13.20 | 51.10 | 1.50 | 0.704 |
| 0050.6−4221a | F7/8V | 0.52 | 6146 | 4.38 | −1.32 | 36.80 | 2.80 | 1.174 |
| b | G5V | 0.68 | 5559 | 4.46 | 66.06 | 24.80 | 2.50 | 0.902 |
| 0052.8−2728 | K5V | 1.10 | 4438 | 4.60 | 33.34 | 32.70 | 0.50 | 0.699 |
| 0053.0−3021 | K2/3V | 0.93 | 4833 | 4.58 | −13.65 | 3.50 | −0.50 | 0.715 |
| 0055.5−3731 | G6V/IV | 0.71 | 5461 | 4.48 | −43.95 | 4.90 | −0.50 | 0.868 |
| 0100.2−3818 | K4V | 1.04 | 4570 | 4.60 | 32.75 | 9.60 | 0.66 | 0.713 |
| 0105.4−4016 | F3V | 0.40 | 6673 | 4.29 | 13.14 | 68.30 | 2.00 | 1.474 |
| 0116.8−3932 | K1V | 0.89 | 4937 | 4.55 | −19.97 | 3.80 | 0.42 | 0.711 |
| 0121.2−3729 | K5V | 1.12 | 4395 | 4.60 | 6.83 | 17.70 | 0.95 | 0.690 |
| 0121.5−4058 | F6V | 0.48 | 6312 | 4.35 | 16.95 | 15.10 | 1.41 | 1.261 |

Table C.1 − continued

| ROSAT Name RXJ | Spectral type | $(B-V)$ (3) | $T_{eff}$ (4) | log(g) (5) | $V_{rad}$ (6) | $v \cdot sini$ (7) | N(Li) (8) | Radius (9) |
|---|---|---|---|---|---|---|---|---|
| 0125.6−4148a | G5V | 0.68 | 5559 | 4.46 | 65.48 | 46.10 | 2.00 | 0.902 |
| b | K3V | 0.95 | 4783 | 4.58 | −42.50 | 11.00 | 2.00 | 0.737 |
| 0126.4−4127 | G8V | 0.74 | 5366 | 4.50 | 16.10 | 20.80 | 1.30 | 0.847 |
| 0135.8−3956 | F4V | 0.43 | 6533 | 4.31 | 15.65 | 33.00 | 2.00 | 1.402 |
| 0136.8−3811 | K2/3V | 0.91 | 4885 | 4.58 | 34.15 | 22.40 | 0.50 | 0.717 |
| 0141.4−3808 | F3V | 0.41 | 6625 | 4.29 | 10.16 | 40.30 | 2.00 | 1.495 |
| 0155.4−3846 | K5V | 1.07 | 4503 | 4.60 | 38.05 | 30.30 | 0.50 | 0.705 |
| 0440.3−5856 | G5V/IV | 0.68 | 5559 | 4.46 | 10.85 | 3.50 | 0.64 | 0.906 |
| 0450.1−5856 | K2V | 0.89 | 4937 | 4.57 | −16.65 | 14.40 | 1.29 | 0.711 |
| 0454.9−5832 | F5V | 0.44 | 6488 | 4.32 | 21.09 | 9.80 | 2.80 | 1.297 |
| 0501.5−5930a | F9V | 0.56 | 5988 | 4.41 | 50.22 | 4.60 | 2.30 | 1.083 |
| b | G6V | 0.71 | 5461 | 4.48 | 77.96 | 15.40 | 2.00 | 0.864 |
| 0505.5−5728 | F7/8V | 0.52 | 6146 | 4.38 | −1.86 | 13.70 | 2.82 | 1.142 |
| 0505.6−5755 | K4V | 0.99 | 4686 | 4.60 | 17.32 | 62.00 | 2.10 | 0.720 |
| 0505.8−6210 | K5V | 1.14 | 4353 | 4.60 | 23.69 | 13.60 | 0.00 | 0.697 |
| 0507.6−5459 | F5/6V/IV | 0.47 | 6355 | 4.34 | 15.89 | 8.10 | 2.00 | 1.244 |
| 0508.1−5316 | G3V | 0.64 | 5695 | 4.46 | 43.50 | 8.90 | 2.04 | 0.955 |
| 0510.4−5732a | F9V | 0.56 | 5988 | 4.41 | 19.00 | 9.20 |  | 1.083 |
| b | G5V | 0.68 | 5559 | 4.46 | 42.66 | 23.10 |  | 0.902 |
| 0513.2−5507 | K5/7V | 1.22 | 4194 | 4.60 | 8.67 | 18.00 | 0.50 | 0.682 |
| 0516.1−6006 | K4/5V | 1.08 | 4481 | 4.60 | 43.48 | 13.80 | 0.34 | 0.702 |
| 0518.7−5803 | K4V | 1.01 | 4639 | 4.60 | 20.71 | 11.10 | 0.00 | 0.712 |
| 0519.2−5756a | G5V | 0.68 | 5559 | 4.46 | 19.27 | 7.80 | 1.50 | 0.902 |
| b | K3V | 0.95 | 4783 | 4.58 | 23.59 | 4.00 | 1.50 | 0.737 |
| 0523.2−5751 | K1/2V | 0.85 | 5045 | 4.56 | 48.53 | 61.60 | 0.50 | 0.740 |
| 0523.7−6041 | K5/7V | 1.19 | 4253 | 4.60 | 2.16 | 22.70 | 0.30 | 0.691 |
| 0525.8−5451 | K3V | 0.95 | 4783 | 4.58 | −0.49 | 12.40 | 0.80 | 0.717 |
| 0527.6−6024 | G9V | 0.77 | 5274 | 4.52 | 13.36 | 4.50 | 1.30 | 0.845 |
| 0528.3−6052 | F5V | 0.44 | 6488 | 4.32 | 6.50 | 33.00 | 2.50 | 1.297 |
| 0531.8−5239 | K4V | 1.02 | 4616 | 4.60 | 78.09 | 12.30 | 0.00 | 0.712 |
| 0534.4−6006 | F7V | 0.50 | 6228 | 4.37 | 16.66 | 19.00 | 3.13 | 1.187 |
| 0535.0−6110 | G4/5III | 0.84 | 5072 | 3.30 | 7.08 | 3.50 | −0.06 | 2.969 |
| 0538.2−5555 | K3V | 0.95 | 4783 | 4.58 | 8.34 | 11.50 | 0.50 | 0.717 |
| 0538.4−5718 | F9V | 0.55 | 6027 | 4.41 | −25.96 | 34.30 | 2.80 | 1.089 |
| 0539.1−5657 | K1/2V | 0.87 | 4990 | 4.56 | 60.18 | 11.80 | 1.00 | 0.722 |
| 0540.0−5343 | K0V | 0.80 | 5186 | 4.53 | 50.32 | 32.40 | 1.70 | 0.768 |
| 0541.1−6151 | F3/4V | 0.38 | 6769 | 4.30 | 11.06 | 65.20 | 3.20 | 1.425 |

Table C.1 − continued

| ROSAT Name RXJ | Spectral type | $(B-V)$ (3) | $T_{eff}$ (4) | log(g) (5) | $V_{rad}$ (6) | $v \cdot sini$ (7) | N(Li) (8) | Radius (9) |
|---|---|---|---|---|---|---|---|---|
| 0543.9−6005a | G7V | 0.73 | 5397 | 4.48 | 43.83 | 33.70 | 2.80 | 0.852 |
| b | K2V | 0.91 | 4885 | 4.57 | −19.93 | 32.10 | 2.80 | 0.720 |
| 0544.4−5523 | K5/7V | 1.23 | 4175 | 4.60 | 43.76 | 24.20 | 0.22 | 0.676 |
| 0545.3−5543a | F5V | 0.45 | 6443 | 4.32 | −9.62 | 13.40 | 1.00 | 1.321 |
| b | G6V | 0.71 | 5461 | 4.48 | −23.04 | 6.70 | 1.00 | 0.868 |
| c | G9V | 0.76 | 5305 | 4.52 | 11.93 | 6.90 | 1.00 | 0.812 |
| 0545.4−5411a | K3V | 0.95 | 4783 | 4.58 | 33.36 | 4.20 | 0.50 | 0.737 |
| b | K4V | 1.03 | 4593 | 4.60 | 32.47 | 20.10 | 0.50 | 0.733 |
| 0547.3−5450 | F6V | 0.49 | 6270 | 4.35 | 23.02 | 16.30 | 2.96 | 1.226 |
| 0548.0−6241 | K0/1V | 0.79 | 5215 | 4.54 | 17.14 | 16.90 | 1.50 | 0.777 |
| 0549.7−5950a | F7V | 0.50 | 6228 | 4.38 | −49.82 | 11.00 | 2.80 | 1.133 |
| b | F7/8V | 0.53 | 6106 | 4.38 | 8.40 | 11.70 | 2.50 | 1.184 |
| c | F7/8V | 0.53 | 6106 | 4.38 | 61.72 | 13.10 | 2.80 | 1.184 |
| 1053.9−2423 | K4V | 1.05 | 4547 | 4.60 | −22.49 | 16.40 | 0.50 | 0.707 |
| 1056.1−2653 | G5V | 0.67 | 5592 | 4.46 | 28.49 | 3.60 | 1.85 | 0.920 |
| 1058.2−2926a | K0V | 0.81 | 5157 | 4.53 | −1.46 | 40.20 | 1.00 | 0.693 |
| b | K5V | 1.15 | 4333 | 4.60 | 13.42 | 49.50 | 1.00 | 0.435 |
| 1101.1−3132 | K3V | 0.94 | 4808 | 4.58 | 22.88 | 61.20 | 0.70 | 0.720 |
| 1102.1−2252 | K7V | 1.28 | 4082 | 4.59 | 16.62 | 13.20 | 0.38 | 0.642 |
| 1108.5−3007 | F5/6V | 0.46 | 6399 | 4.34 | −9.37 | 16.60 | 1.12 | 1.279 |
| 1110.5−3027a | F3V | 0.40 | 6673 | 4.29 | −26.31 | 14.80 | 2.80 | 1.467 |
| b | F7V | 0.50 | 6228 | 4.37 | 16.41 | 16.40 | 2.50 | 1.187 |
| 1110.6−2853 | F4V | 0.42 | 6579 | 4.31 | −10.67 | 9.20 | 2.85 | 1.383 |
| 1115.9−2750 | K5V | 1.17 | 4292 | 4.60 | 50.34 | 20.40 | 0.30 | 0.691 |
| 1118.3−3234 | K2/3V | 0.88 | 4963 | 4.58 | 7.05 | 12.20 | 1.00 | 0.727 |
| 1119.5−2351 | K1V | 0.86 | 5017 | 4.55 | 26.53 | 10.00 | 0.50 | 0.735 |
| 1121.5−3131 | F7/8V | 0.51 | 6187 | 4.38 | 4.60 | 9.20 | 2.58 | 1.154 |
| 1121.8−2411 | G3V | 0.64 | 5695 | 4.46 | 6.60 | 3.60 | 2.61 | 0.955 |
| 1122.0−2446a | K4/5V | 1.17 | 4292 | 4.60 | | 6.30∗ | 3.20∗ | 0.543 |
| b | K7V | 1.37 | 3924 | 4.59 | | 6.50∗ | 2.20∗ | 0.409 |
| c | M1V | 1.41 | 3858 | 4.59 | | | 2.00∗ | 0.336 |
| d | ?? | | | | | | | |
| 1122.9−2545 | K4/5V | 1.11 | 4416 | 4.60 | 71.38 | 10.50 | −0.50 | 0.696 |
| 1123.3−2342 | G8III | 0.94 | 4808 | 2.90 | 16.22 | 3.50 | 0.93 | 10.02 |
| 1124.0−2404a | F8V | 0.53 | 6106 | 4.39 | 13.18 | 3.80 | 2.00 | 1.136 |
| b | G4V | 0.66 | 5626 | 4.46 | 16.48 | 3.50 | 2.00 | 0.930 |
| 1132.9−3151 | G8III | 0.94 | 4808 | 2.90 | 1.43 | 3.50 | 1.00 | 10.02 |
| 1345.2−0043 | F8V | 0.49 | 6270 | 4.39 | −23.01 | 10.60 | 0.70 | 1.068 |

Table C.1 − continued

| ROSAT Name RXJ | Spectral type | $(B-V)$ (3) | $T_{eff}$ (4) | log(g) (5) | $V_{rad}$ (6) | $v \cdot sini$ (7) | N(Li) (8) | Radius (9) |
|---|---|---|---|---|---|---|---|---|
| 1354.2−0157 | F8V | 0.54 | 6066 | 4.39 | −9.75 | 12.00 | 2.68 | 1.100 |
| 1354.9−0222a | F9V | 0.56 | 5988 | 4.41 | 66.71 | 5.10 | 2.70 | 1.083 |
| b | G5V | 0.68 | 5559 | 4.46 | −60.32 | 4.00 | 3.00 | 0.902 |
| 1355.5+0015 | K5/7V | 1.28 | 4082 | 4.60 | 58.80 | 21.90 | 0.20 | 0.642 |
| 1358.4−0139a | G0V | 0.60 | 5838 | 4.42 | 52.09 | 77.30 | 2.00 | 0.997 |
| b | G5V | 0.68 | 5559 | 4.46 | −105.39 | 54.40 | 2.00 | 0.902 |
| 1358.9+0058a | G9V | 0.76 | 5305 | 4.52 | 45.71 | 30.90 | 1.80 | 0.820 |
| b | G9V | 0.76 | 5305 | 4.52 | −77.96 | 8.90 | 1.80 | 0.820 |
| 1401.9+0025 | F8V | 0.54 | 6066 | 4.39 | −2.73 | 3.50 | 2.64 | 1.100 |
| 1404.0−0021a | F8IV | 0.53 | 6105 | 3.50 | 25.66 | 55.50 | | 2.173 |
| b | G3IV | 0.66 | 5626 | 3.50 | 45.44 | 60.70 | | 2.213 |
| c | G3IV | 0.66 | 5626 | * | 87.77 | 60.00 | | 2.213 |
| 1411.5+0121 | F6V | 0.48 | 6312 | 4.35 | −17.14 | 28.40 | 2.00 | 1.261 |
| 1413.7−0050 | F6V | 0.47 | 6355 | 4.35 | 0.57 | 23.80 | 2.50 | 2.359 |
| 1428.2−0213a | G2III/IV | 0.70 | 5366 | 3.45 | −5.49 | 12.70 | 2.31 | 5.000 |
| b | K0V | 0.81 | 5157 | 4.53 | | | | 0.693 |
| 1429.4−0049 | K0V | 0.81 | 5157 | 4.53 | 10.74 | 3.50 | 0.80 | 0.762 |
| 1432.1−0114 | K3/4V | 1.02 | 4616 | 4.59 | 51.45 | 17.20 | 0.30 | 0.712 |
| 1433.3−0126 | K0/1V | 0.78 | 5245 | 4.54 | −79.96 | 12.00 | 1.00 | 0.783 |
| 1436.9−0239 | K4/5V | 1.09 | 4459 | 4.60 | −42.88 | 16.90 | 0.80 | 0.706 |
| 1437.5+0216a | F9V | 0.56 | 5988 | 4.41 | −0.03 | 25.80 | 2.00 | 1.083 |
| b | K1V | 0.86 | 5017 | 4.55 | 27.87 | 8.10 | 1.50 | 0.738 |
| 1442.7−0039a | G5V | 0.68 | 5559 | 4.46 | 87.71 | 13.00 | 1.00 | 0.902 |
| b | K1V | 0.86 | 5017 | 4.55 | 65.20 | 13.00 | 1.50 | 0.738 |
| 1446.3+0153 | A0V | −0.01 | 9409 | 4.27 | | 340.0 | | 2.366 |
| 1450.7+0055 | F6V | 0.48 | 6312 | 4.35 | 15.95 | 26.70 | 2.60 | 1.261 |
| 1451.9+0201 | G5/6V | 0.70 | 5493 | 4.47 | −3.11 | 3.50 | 2.08 | 0.878 |

# D Standards

The standards used for the data analysis.

Table D.1: The photometric standards from the E-regions used in the photometry for the southern sample. Data from Vogt et al. (1981)

| Name | Spectr. type | V | U-B | B-V | V-R | V-I | Coordinates (2000.0) |
|---|---|---|---|---|---|---|---|
| E101 | A0V | 7.704 | 0.091 | 0.087 | 0.038 | 0.084 | 01 27 34 -46 09 05 |
| E102 | A3III/IV | 8.444 | 0.112 | 0.206 | 0.126 | 0.274 | 01 22 10 -46 13 18 |
| E106 | F3V | 7.864 | -0.026 | 0.396 | 0.235 | 0.472 | 01 31 29 -44 39 19 |
| E107 | F5V | 8.613 | -0.038 | 0.440 | 0.253 | 0.516 | 01 18 22 -44 11 49 |
| E124 | K0III | 8.928 | 0.933 | 1.082 | 0.555 | 1.063 | 01 18 54 -44 56 12 |
| E126 | K0/1V | 7.831 | 0.477 | 0.829 | 0.456 | 0.860 | 01 33 25 -43 54 08 |
| E130 | K2III | 6.580 | 1.268 | 1.204 | 0.614 | 1.154 | 01 16 12 -42 00 53 |
| E131 | K2IIICNIa/ | 6.975 | 1.265 | 1.164 | 0.571 | 1.064 | 01 38 03 -46 05 03 |
| E135 | K3III | 9.464 | 1.710 | 1.428 | 0.770 | 1.506 | 01 22 02 -44 25 31 |
| E141 | K1II | 6.265 | 1.079 | 1.144 | 0.575 | 1.092 | 01 24 41 -44 31 41 |
| E142 | F0V | 6.665 | -0.007 | 0.330 | 0.196 | 0.397 | 01 38 30 -42 55 39 |
| E146 | B9III/Iv | 7.857 | -0.370 | -0.086 | -0.042 | -0.091 | 01 17 00 -42 31 56 |
| E164 | A3V | 6.640 | 0.123 | 0.129 | 0.068 | 0.143 | 01 41 41 -50 02 19 |
| E168 | K1/2III | 8.567 | 1.202 | 1.177 | 0.595 | 1.122 | 01 36 41 -44 48 20 |
| E176 | K2III | 8.946 | 1.410 | 1.302 | 0.680 | 1.302 | 01 18 01 -45 21 01 |
| E301 | B8V | 8.059 | -0.290 | -0.085 | -0.046 | -0.095 | 06 37 24 -44 58 33 |
| E304 | A0V | 7.689 | -0.024 | -0.014 | -0.014 | -0.030 | 06 37 42 -44 29 44 |
| E326 | F3/5IV | 9.530 | 0.133 | 0.463 | 0.264 | 0.520 | 06 42 31 -45 21 21 |
| E331 | G8III | 8.044 | 0.686 | 0.956 | 0.489 | 0.945 | 06 52 40 -46 48 33 |
| E335 | G8III | 6.689 | 0.737 | 1.000 | 0.513 | 0.992 | 06 31 04 -43 43 03 |
| E338 | K3III | 7.978 | 1.764 | 1.487 | 0.786 | 1.503 | 06 46 46 -44 58 26 |
| E346 | B8V | 7.341 | -0.388 | -0.111 | -0.050 | -0.112 | 06 48 43 -43 48 06 |
| E348 | F5II/III | 6.519 | 0.142 | 0.412 | 0.238 | 0.464 | 06 52 39 -42 30 15 |
| E351 | A0IV | 6.829 | -0.223 | -0.065 | -0.019 | -0.050 | 06 58 00 -46 05 45 |
| E352 | A0V | 6.219 | -0.061 | -0.003 | -0.005 | -0.014 | 06 58 41 -45 46 03 |
| E389 | B2III | 7.215 | -0.740 | -0.156 | -0.062 | -0.142 | 06 45 10 -47 13 22 |
| E502 | B8/9V | 8.061 | -0.238 | -0.032 | -0.014 | -0.031 | 12 08 43 -44 55 33 |
| E507 | A5V | 8.830 | 0.178 | 0.178 | 0.098 | 0.206 | 11 57 47 -46 47 11 |
| E523 | G3V | 8.378 | 0.180 | 0.652 | 0.350 | 0.680 | 12 00 04 -46 46 57 |
| E584 | K1/2III | 7.431 | 1.316 | 1.280 | 0.660 | 1.248 | 11 54 50 -43 36 39 |

Table D.1 − continued

| Name | Spectr. type | V | U-B | B-V | V-R | V-I | Coordinates (2000.0) |
|---|---|---|---|---|---|---|---|
| E633 | K2III | 6.834 | 1.208 | 1.176 | 0.602 | 1.134 | 14 38 13 -45 52 16 |
| E682 | B9V | 6.890 | -0.125 | -0.017 | 0.005 | 0.012 | 14 35 10 -46 27 42 |
| E703 | B3III | 8.110 | -0.564 | -0.004 | 0.014 | 0.027 | 17 36 40 -44 33 51 |
| E722 | F3/5V | 7.254 | -0.026 | 0.430 | 0.254 | 0.504 | 17 27 32 -43 32 30 |
| E723 | F0III | 7.213 | 0.544 | 0.624 | 0.415 | 0.844 | 17 18 41 -46 47 56 |
| E732 | G8IIICNII | 7.645 | 1.148 | 1.248 | 0.625 | 1.194 | 17 25 40 -44 46 45 |
| E739 | K4III | 7.383 | 1.701 | 1.432 | 0.764 | 1.434 | 17 36 41 -44 52 43 |
| E740 | K3III | 7.931 | 1.707 | 1.518 | 0.816 | 1.552 | 17 38 30 -44 52 32 |
| E746 | A0V | 7.252 | 0.069 | 0.088 | 0.029 | 0.071 | 17 20 50 -45 25 11 |
| E748 | F3V | 6.656 | -0.012 | 0.382 | 0.223 | 0.443 | 17 24 43 -45 00 30 |
| E749 | A0V | 5.789 | -0.034 | -0.011 | 0.005 | 0.012 | 17 41 16 -46 55 18 |
| E750 | ApSi | 7.549 | -0.351 | -0.056 | 0.007 | -0.010 | 17 29 52 -44 44 28 |
| E765 | G2/3V | 7.165 | 0.164 | 0.648 | 0.356 | 0.692 | 17 37 53 -42 33 44 |
| E766 | G5V | 7.245 | 0.250 | 0.722 | 0.393 | 0.764 | 17 39 00 -43 08 34 |
| E780 | B9V | 5.759 | -0.132 | -0.048 | -0.018 | -0.040 | 17 18 47 -44 07 46 |
| E782 | B0.5Ib | 6.458 | -0.684 | 0.256 | 0.173 | 0.355 | 17 17 05 -44 46 42 |
| E789 | B8/9V | 6.091 | -0.250 | -0.057 | -0.017 | -0.038 | 17 38 08 -42 52 47 |
| E790 | B9IV/V | 6.918 | -0.153 | -0.026 | -0.006 | -0.012 | 17 43 37 -45 58 15 |
| E801 | ApEuCr | 7.788 | -0.036 | -0.015 | 0.014 | 0.014 | 20 13 34 -45 35 25 |
| E802 | ApSi | 7.915 | -0.251 | -0.042 | -0.014 | -0.046 | 20 02 10 -44 27 58 |
| E803 | A0V | 8.744 | 0.017 | 0.030 | 0.002 | 0.010 | 20 00 53 -45 41 57 |
| E809 | A9IV | 7.821 | 0.072 | 0.296 | 0.171 | 0.343 | 20 04 29 -44 56 48 |
| E816 | F5V | 8.476 | -0.034 | 0.448 | 0.260 | 0.518 | 20 08 01 -44 11 31 |
| E826 | G5/6III | 6.542 | 0.568 | 0.885 | 0.460 | 0.887 | 20 11 15 -43 39 43 |
| E828 | K1III | 6.567 | 1.222 | 1.224 | 0.633 | 1.208 | 20 02 36 -43 11 46 |
| E830 | K3/4III | 6.954 | 1.854 | 1.509 | 0.803 | 1.546 | 20 05 07 -46 05 48 |
| E834 | K1III | 7.846 | 1.232 | 1.188 | 0.602 | 1.132 | 20 09 26 -43 55 00 |
| E840 | K3/4III | 8.104 | 1.640 | 1.416 | 0.756 | 1.431 | 20 06 55 -44 18 11 |
| E846 | G8IV | 9.978 | 0.504 | 0.885 | 0.486 | 0.940 | 20 08 50 -44 24 55 |
| E870 | B8/9V | 7.166 | -0.216 | -0.072 | -0.024 | -0.052 | 19 56 05 -44 00 44 |
| E872 | A9III/IV | 6.727 | 0.078 | 0.274 | 0.148 | 0.284 | 20 26 04 -46 39 35 |
| E876 | K3/4III | 8.880 | 1.900 | 1.526 | 0.822 | 1.598 | 20 01 04 -44 23 06 |

| Name | Coordinates (2000.0) | Source |
|---|---|---|
| NGC 7790 | 23 58 40.30 +61 13 00.0 | 1,2 |
| NGC 2419 | 07 38 08.45 +38 52 54.9 | 1 |
| NGC 7006 | 21 01 29.34 +16 11 14.2 | 1,2 |

Table D.2: The open clusters used for standard stars in the photometry for the northern sample. The standards from the clusters and their colors are taken from: 1: Christian et al. (1985), 2: Odewahn et al. (1992).

| Name | Spectr. type | V | $v_{\rm rad}$ | Coordinates (2000.0) | Source |
|---|---|---|---|---|---|
| HD 4813 | F8V | 5.19 | 8.16 | 00 50 08.30 −10 38 28.3 | 1 |
| HD 18455 | G5 | 7.35 | 50.63 | 02 57 14.40 −24 58 07.6 | 1 |
| HD 22879 | F9V | 6.74 | 120.31 | 03 40 19.70 −03 12 51.1 | 1 |
| HD 30495 | dG1 | 5.50 | 21.63 | 04 47 35.80 −16 56 12.5 | 1 |
| HD 36079 | G5II | 2.84 | -13.50 | 05 28 14.69 −20 45 29.8 | 2 |
| HD 73752 | | 5.05 | 44.60 | 08 39 08.82 −22 40 04.2 | 2 |
| HD 109379 | G5II | 2.65 | -7.00 | 12 34 23.16 −23 23 45.2 | 2 |
| HD 150798 | K2IIb/IIIa | 1.92 | -3.70 | 16 48 39.60 −69 01 38.0 | 2 |
| HD 158614 | G9IV/V | 5.31 | -80.62 | 17 30 24.14 −01 03 36.7 | 1 |
| HD 168454 | K2.5IIIa | 2.70 | -20.00 | 18 20 59.40 −29 49 40.0 | 2 |
| HD 184985 | F7V | 5.47 | -15.36 | 19 37 34.66 −14 17 59.2 | 1 |
| HD 188512 | G8IV | 3.71 | -40.71 | 19 55 18.54 +06 24 48.3 | 1 |

Table D.3: The radial velocity standards used for the southern sample. The standards were taken from 1: Duquennoy and Mayor (1991) 2: The Astronomical Almanach (1996)

| Name | Spectr. type | V | $v \sin i$ | Coordinates (2000.0) | Comments | Source |
|---|---|---|---|---|---|---|
| HD 1835 | G2V | 6.38 | 7.0 | 00 22 50.30 −12 12 37.3 | Hyades group | 1 |
| HD 3196 | F8V | 5.20 | 30.0 | 00 35 13.40 −03 35 33.0 | | 4 |
| HD 4813 | F8V | 5.19 | 3.5 | 00 50 08.30 −10 38 28.3 | CV? | 1 |
| HD 17206 | F6V | 4.50 | 36.0 | 02 45 04.90 −18 34 23.0 | | 4 |
| HD 27290 | F2V | 4.20 | 50.0 | 04 16 01.00 −51 29 21.3 | | 2 |
| HD 31993 | K2III | 8.30 | 29.0 | 05 00 08.10 +03 17 12.7 | | 3 |
| HD 36705 | K1IV | 6.83 | 85.0 | 05 28 44.50 −65 27 02.2 | single | 3 |
| HD 37824 | K2III | 7.10 | 13.0 | 05 41 26.60 +03 46 40.3 | SB1 | 3 |
| HD 84117 | F9IV | 4.94 | 5.0 | 09 42 15.80 −23 55 09.0 | | 4 |
| HD 94388 | F6V | 5.24 | 8.3 | 10 53 29.20 −20 08 07.0 | | 4 |
| HD 101309 | K1IV | 8.50 | 20.0 | 11 39 22.50 −39 23 04.0 | | 3 |
| HD 101379 | G5IIIp | 5.17 | 14.0 | 11 39 29.80 −65 23 52.0 | | 3 |
| HD 102634 | F7V | 6.15 | 6.5 | 11 49 01.86 −00 19 06.9 | | 4 |
| HD 102870 | F8V | 4.00 | 4.0 | 11 50 39.20 +01 46 07.0 | | 1 |
| HD 105211 | F0IV | 4.20 | 50.0 | 12 06 52.60 −64 36 47.0 | | 2 |
| HD 119756 | F2IV | 4.23 | 65.0 | 13 45 43.00 −33 02 30.0 | | 2 |
| HD 125451 | F3IV | 5.40 | 39.0 | 14 19 15.80 +13 00 17.0 | | 4 |
| HD 126053 | G2V | 6.30 | 1.0 | 14 23 14.46 +01 14 53.8 | | 1 |
| HD 136905 | K1III | 7.40 | 35.0 | 15 23 25.90 −06 36 31.0 | | 3 |
| HD 141004 | G0V | 4.43 | 2.4 | 15 46 27.30 +07 21 15.0 | | 1 |
| HD 146233 | G2V | 5.50 | 2.4 | 16 15 36.38 −08 21 45.3 | | 1 |
| HD 147449 | F0V | 4.80 | 70.0 | 16 22 04.78 +01 01 42.1 | | 4 |
| HD 154417 | F8.5IV/V | 6.01 | 5.5 | 17 05 11.82 +00 42 25.7 | variable | 1,4 |
| HD 165141 | G8III+wd | 6.80 | 16.0 | 18 07 00.12 −48 14 48.7 | SB1 | 3 |
| HD 174429 | K5V+Ps | 7.80 | 70.0 | 18 53 05.64 −50 10 45.1 | single | 3 |
| HD 182640 | F0IV | 3.40 | 80.0 | 19 25 28.95 +03 06 49.0 | variable | 2 |
| HD 182776 | K2/3III | 8.20 | 12.0 | 19 28 05.32 −40 50 03.9 | SB1 | 3 |
| HD 185510 | K0III/IV | 8.00 | 17.0 | 19 39 38.62 −06 03 48.0 | SB1 | 3 |
| HD 190540 | K0III | 8.30 | 19.0 | 20 06 02.60 −18 42 16.2 | SB1 | 3 |
| HD 204121 | F3V | 6.13 | 18.5 | 21 26 27.60 +01 06 20.0 | | 4 |
| HD 205249 | K1III | 7.90 | 9.0 | 21 34 16.42 −13 29 01.9 | SB1 | 3 |
| HD 208450 | F0IV | 4.40 | 110.0 | 21 57 54.71 −54 59 33.6 | double/multiple | 2 |
| HD 212697 | | 6.57 | 7.5 | 22 26 33.20 −16 44 29.0 | | 3 |

Table D.4: The $v \sin i$ standards used for the southern sample. The standards were taken from 1: Soderblom (1982), 2: Sletteback et al. (1975), 3: Randich et al. (1993), 4: Soderblom et al. (1989)

| Name | Spectr. type | V | $v_{\rm rad}$ | Coordinates (2000.0) |
|---|---|---|---|---|
| HD 5294 | G5 | 7.38 | -8.56 | 00 54 59.8 +24 06 10 |
| HD 6582 | G5Vb | 5.12 | -98.74 | 01 07 56.1 +54 56 35 |
| HD 12235 | G2IV | 5.90 | -18.47 | 02 00 08.3 +03 06 02 |
| HD 19373 | G0V | 4.05 | 49.51 | 03 08 57.4 +49 36 52 |
| HD 22879 | F9V | 6.74 | 120.31 | 03 40 19.7 −03 12 51 |

Table D.5: The radial velocity standards used for the northern sample.The standards were taken from Duquennoy and Mayor (1991).

| Name | Spectr. type | V | $v \sin i$ | Coordinates (2000.0) | Source |
|---|---|---|---|---|---|
| HD 17094 | F0IV | 4.20 | 40.0 | 02 44 55.5 +10 06 52 | 2 |
| HD 25680 | G5V | 5.90 | 3.0 | 04 05 19.6 +22 00 38 | 1 |
| HD 27859 | G2V | 7.80 | 8.0 | 04 24 27.9 +16 53 11 | 1 |
| HD 30652 | F6V | 3.19 | 10.0 | 04 49 48.8 +06 57 40 | 2 |
| HD 31738 | G5 | 7.10 | 30.0 | 04 58 17.4 +00 27 16 | 3 |
| HD 32923 | G4V | 5.01 | 1.6 | 05 07 25.1 +18 38 41 | 1 |
| HD 37824 | G5 | 7.10 | 13.0 | 05 41 26.6 +03 46 40 | 3 |
| HD 39587 | G0V | 4.41 | 9.4 | 05 54 23.5 +20 16 38 | 1 |

Table D.6: The $v \sin i$ standards used for the northern sample.The standards were taken from 1: Soderblom (1982), 2: Sletteback et al. (1975), 3: Randich et al. (1993).

| Name | Spectr. type | V | Coordinates (2000.0) |
|---|---|---|---|
| HD 2834 | A0V | 4.77 | 00 31 24.2 −48 48 14 |
| HD 13709 | B9V | 5.29 | 02 12 54.4 −30 43 27 |
| HD 40200 | B3V | 6.10 | 05 54 41.2 −49 37 38 |
| HD 160461 | A1V | 7.47 | 17 41 30.6 −34 04 25 |
| HD 169398 | B5IV | 6.30 | 18 25 54.5 −33 56 43 |
| HD 170770 | B5IV | 7.76 | 18 32 15.6 −27 13 16 |
| HD 174996 | B3IV | 7.20 | 18 54 22.7 −24 46 08 |
| HD 175544 | B2V | 7.35 | 18 55 46.5 +00 15 54 |
| HD 181074 | B3 | 9.00 | 19 19 00.9 +00 31 07 |

Table D.7: A- and B-type stars used in the Ca II H & K and He I $D_3$ observations.

# *E Northern Sample*

Description of the sources in the northern hemisphere sub-sample.

Column 1: ROSAT name.

Column 2: coordinates of the ROSAT X-ray source.

Column 3: the countrate for the X-ray source, in counts per second.

Column 4: the total exposure time for the X-ray source.

Column 5: the hardness ratio 1 of the X-ray source.

Column 6: spectral type, from SIMBAD or from the low-resolution spectra.

Column 7: catalogue name.

Column 8: visual magnitude.

Column 9: Johnson $(B/V)$ index.

Column 10: Separation in R.A. between the X-ray source and the counterpart, in arcsec.

Column 11: Separation in Dec. between the X-ray source and the counterpart, in arcsec.

Table E.1: The northern sample stars.

| ROSAT Name RXJ | ROSAT coordinates (2000.0) | Countrate (3) | $t_{exp}$ (4) | HR 1 (5) |
|---|---|---|---|---|
| 0328.2+0409 | 03 28 14.6 +04 09 48 | $0.824 \pm 0.040$ | 534.3 | $-0.07 \pm 0.05$ |
| 0330.7+0305 | 03 30 43.7 +03 05 55 | $0.082 \pm 0.014$ | 542.5 | $+0.96 \pm 0.16$ |
| 0331.1+0713 | 03 31 08.3 +07 13 21 | $0.274 \pm 0.030$ | 390.5 | $-0.26 \pm 0.10$ |
| 0334.8+0624 | 03 34 50.0 +06 24 45 | $0.093 \pm 0.018$ | 356.1 | $+0.77 \pm 0.16$ |
| 0336.5+0726 | 03 36 35.0 +07 26 20 | $0.087 \pm 0.017$ | 382.5 | $-0.15 \pm 0.19$ |
| 0336.7+0035 | 03 36 47.2 +00 35 10 | $14.000 \pm 0.185$ | 443.4 | $-0.08 \pm 0.01$ |
| 0338.7+0136 | 03 38 44.5 +01 36 57 | $0.061 \pm 0.015$ | 368.2 | $-0.29 \pm 0.20$ |
| 0338.7+0243 | 03 38 42.9 +02 43 27 | $0.048 \pm 0.013$ | 385.3 | $+0.26 \pm 0.27$ |
| 0338.8+0216 | 03 38 48.7 +02 16 29 | $0.231 \pm 0.026$ | 382.7 | $-0.10 \pm 0.11$ |
| 0339.9+0314 | 03 39 59.1 +03 14 12 | $0.037 \pm 0.012$ | 373.3 | $-0.12 \pm 0.34$ |
| 0341.4−0013 | 03 41 24.5 −00 13 11 | $0.160 \pm 0.022$ | 392.3 | $+0.61 \pm 0.13$ |
| 0343.9+0327 | 03 43 55.7 +03 27 04 | $0.039 \pm 0.012$ | 367.0 | $-1.11 \pm 0.46$ |
| 0344.4−0123 | 03 44 25.9 −01 23 28 | $0.407 \pm 0.034$ | 393.8 | $-0.24 \pm 0.08$ |
| 0344.8+0359 | 03 44 53.6 +03 59 37 | $0.047 \pm 0.013$ | 378.7 | $+0.85 \pm 0.15$ |
| 0344.9+0819 | 03 44 59.0 +08 19 30 | $0.128 \pm 0.022$ | 340.7 | $+0.46 \pm 0.17$ |
| 0345.0+0237 | 03 45 03.5 +02 37 14 | $0.084 \pm 0.017$ | 353.4 | $-0.17 \pm 0.19$ |
| 0347.1−0052 | 03 47 09.9 −00 52 02 | $0.032 \pm 0.011$ | 371.3 | $+0.72 \pm 0.29$ |
| 0347.4−0217 | 03 47 25.7 −02 17 47 | $0.080 \pm 0.017$ | 389.9 | $+0.03 \pm 0.20$ |
| 0348.5+0831 | 03 48 32.5 +08 31 33 | $0.051 \pm 0.014$ | 357.0 | $+0.84 \pm 0.23$ |
| 0348.9+0110 | 03 48 59.0 +01 10 51 | $0.090 \pm 0.018$ | 344.9 | $-0.03 \pm 0.19$ |
| 0349.6−0219 | 03 49 38.3 −02 19 45 | $0.119 \pm 0.021$ | 380.1 | $-0.05 \pm 0.16$ |
| 0350.2−0131 | 03 50 15.5 −01 31 14 | $0.119 \pm 0.020$ | 370.1 | $-0.04 \pm 0.16$ |
| 0350.6+0133 | 03 50 41.0 +01 33 46 | $0.073 \pm 0.016$ | 359.6 | $-0.16 \pm 0.22$ |
| 0353.1−0149 | 03 53 07.5 −01 49 42 | $0.062 \pm 0.016$ | 367.1 | $+0.10 \pm 0.24$ |
| 0354.2−0257 | 03 54 17.1 −02 57 20 | $0.203 \pm 0.025$ | 357.0 | $+0.13 \pm 0.12$ |
| | | | | |
| 0354.3+0535 | 03 54 21.3 +05 35 27 | $0.042 \pm 0.012$ | 362.7 | $+0.76 \pm 0.28$ |
| 0355.2+0329 | 03 55 14.8 +03 29 20 | $0.049 \pm 0.014$ | 349.5 | $-0.06 \pm 0.28$ |
| 0355.3−0143 | 03 55 20.2 −01 43 44 | $0.414 \pm 0.037$ | 343.3 | $-0.03 \pm 0.09$ |
| 0356.8−0034 | 03 56 53.7 −00 34 41 | $0.044 \pm 0.014$ | 330.3 | $-0.12 \pm 0.29$ |
| 0357.4−0109 | 03 57 28.7 −01 09 20 | $0.436 \pm 0.037$ | 335.4 | $-0.35 \pm 0.08$ |
| | | | | |
| 0358.1−0121 | 03 58 10.1 −01 21 36 | $0.041 \pm 0.013$ | 331.9 | $+0.04 \pm 0.36$ |
| 0358.9−0017 | 03 58 55.1 −00 17 53 | $0.032 \pm 0.012$ | 331.8 | $-0.34 \pm 0.33$ |
| 0400.1+0818 | 04 00 09.8 +08 18 24 | $0.347 \pm 0.033$ | 334.1 | $+0.26 \pm 0.09$ |

Table E.1 − continued

| Spect. type (6) | Catal. Name (7) | $m_v$ (8) | $(B/V)$ (9) | $\Delta\alpha$ (10) | $\Delta\delta$ (11) | observed Li | Ca | He | Ph. |
|---|---|---|---|---|---|---|---|---|---|
| K0 | SAO 111210 | 10.93 | +0.77 | −3 | −2 | no | no | no | no |
| K1 | | 13.49 | | +6 | +4 | no | no | no | no |
| K4e | | 12.60 | +0.89 | −2 | −4 | no | no | no | no |
| F7 | HD 22211 | 6.49 | +0.63 | +13 | −24 | yes | no | yes | no |
| K0 | | 10.59 | +0.75 | +9 | +1 | no | no | no | no |
| K2 | HR 1099 | 5.71 | +0.92 | −6 | −19 | no | no | no | no |
| K5e | | 13.82 | +1.01 | +0 | +7 | no | no | no | no |
| A2V | HD 26653 | 8.00 | +0.50 | +5 | −10 | yes | no | yes | no |
| K4 | SAO 111315 | 8.80 | +1.40 | +2 | −2 | yes | yes | no | no |
| K2 | | 12.48 | +0.96 | +2 | −20 | no | no | no | no |
| K3 | | | | +26 | +14 | no | no | no | no |
| K1 | HD 23261 | 8.44 | +1.05 | +26 | +21 | no | no | no | no |
| G9 | BD-01 524 | 11.16 | +1.04 | −2 | +3 | no | yes | no | no |
| K1e | | 12.86 | +0.79 | +8 | +7 | no | no | no | no |
| F6 | HD 23376 | 8.49 | +0.68 | +2 | +18 | yes | yes | no | no |
| F5 | HD 23412 | 6.71 | +1.69 | +9 | −8 | yes | no | yes | no |
| K3 | | 13.15 | +0.81 | = 20 | −17 | no | no | no | no |
| K7e | | | | −14 | +36 | no | no | no | no |
| G4 | | 10.90 | +0.75 | +18 | −4 | no | no | no | no |
| K3e | | 11.23 | | +5 | −8 | no | no | no | no |
| G0V | HD 24031 | 7.00 | +0.70 | −9 | −4 | yes | yes | no | no |
| F4 | HD 24098 | 8.72 | −1.12 | −5 | +5 | yes | no | yes | no |
| F5 | HD 24133 | 10.86 | | −14 | −5 | yes | no | yes | no |
| F7 | HD 24435 | 8.94 | +0.41 | −14 | +29 | no | yes | yes | no |
| G8III | HR 1212 | | | | | no | no | no | no |
| A2V | HR 1211 | | | | | no | no | no | no |
| G1 | | 9.80 | +0.58 | +0 | −14 | no | no | no | no |
| K3e | | 11.60 | +0.73 | +8 | +10 | no | no | no | no |
| G5 | HD 24681 | 11.24 | +0.92 | −3 | −2 | no | no | no | no |
| K4e | | 12.61 | +0.92 | +12 | +1 | no | no | no | no |
| K5 | GJ 157A | 8.00 | +1.13 | −11 | +3 | yes | yes | no | no |
| M3e | GJ 157B | 12.62 | +0.92 | | | no | no | no | no |
| K4 | | 11.52 | +1.11 | +0 | +8 | no | no | no | no |
| K3 | | 10.95 | +0.92 | +27 | −14 | no | no | no | no |
| G5 | BD+07 582 | 9.90 | | +4 | +7 | no | no | no | no |
| G5 | BD+07 582B | 9.80 | | | | no | no | no | no |

Table E.1 − continued

| ROSAT Name RXJ | ROSAT coordinates (2000.0) | Countrate (3) | $t_{exp}$ (4) | HR 1 (5) |
|---|---|---|---|---|
| 0402.2−0137 | 04 02 15.3 −01 37 40 | $0.034 \pm 0.012$ | 323.7 | $-0.62 \pm 0.27$ |
| 0402.5+0551 | 04 02 34.5 +05 51 51 | $0.040 \pm 0.012$ | 315.5 | $+0.64 \pm 0.28$ |
| 0402.6−0016 | 04 02 36.7 −00 16 05 | $1.550 \pm 0.070$ | 320.8 | $-0.07 \pm 0.05$ |
| 0403.8+0846 | 04 03 49.1 +08 46 14 | $0.074 \pm 0.017$ | 314.9 | $-0.27 \pm 0.22$ |
| 0403.9+0811 | 04 03 56.7 +08 11 48 | $0.155 \pm 0.024$ | 313.2 | $-0.24 \pm 0.14$ |
| 0404.1+0249 | 04 04 09.6 +02 49 44 | $0.235 \pm 0.030$ | 325.6 | $+0.26 \pm 0.12$ |
| 0404.4+0518 | 04 04 28.1 +05 18 49 | $0.046 \pm 0.013$ | 315.6 | $+5.48 \pm 4.27$ |
| 0405.5+0323 | 04 05 30.1 +03 23 57 | $0.074 \pm 0.017$ | 317.2 | $+2.90 \pm 0.95$ |
| 0405.6+0341 | 04 05 40.5 +03 41 52 | $0.075 \pm 0.017$ | 319.0 | $-0.12 \pm 0.23$ |
| 0406.6+0140 | 04 06 41.1 +01 40 54 | $0.101 \pm 0.020$ | 321.4 | $-0.33 \pm 0.17$ |
| 0406.8+0053 | 04 06 49.6 +00 53 19 | $0.049 \pm 0.015$ | 325.7 | $-0.25 \pm 0.27$ |
| 0407.1−0206 | 04 07 09.2 −02 06 20 | $0.046 \pm 0.015$ | 331.8 | $+1.00 \pm 0.28$ |
| | | | | |
| 0412.1+0044 | 04 12 09.1 +00 44 06 | $0.108 \pm 0.020$ | 325.0 | $+0.45 \pm 0.18$ |
| | | | | |
| 0413.5+0742 | 04 13 32.3 +07 42 52 | $0.112 \pm 0.024$ | 260.9 | $-0.60 \pm 0.15$ |
| 0415.0+0724 | 04 15 02.7 +07 24 51 | $0.042 \pm 0.014$ | 278.4 | $+0.69 \pm 0.27$ |
| 0415.4+0611 | 04 15 27.2 +06 11 30 | $0.499 \pm 0.043$ | 274.5 | $-0.42 \pm 0.08$ |
| | | | | |
| 0416.2+0709 | 04 16 16.9 +07 09 21 | $0.049 \pm 0.015$ | 292.6 | $-1.15 \pm 0.35$ |
| 0416.5+0247 | 04 16 35.1 +02 47 16 | $0.076 \pm 0.019$ | 268.3 | $+0.94 \pm 0.19$ |
| 0638.9+6409 | 06 38 58.5 +64 09 02 | $0.032 \pm 0.011$ | 360.7 | $+0.27 \pm 0.35$ |
| 0642.7+6405 | 06 42 46.3 +64 05 34 | $0.044 \pm 0.013$ | 374.3 | $+0.13 \pm 0.28$ |
| 0648.5+6639 | 06 48 35.6 +66 39 06 | $0.043 \pm 0.012$ | 403.9 | $+0.44 \pm 0.35$ |
| 0701.0+6541 | 07 01 01.2 +65 41 50 | $0.052 \pm 0.014$ | 371.3 | $+0.24 \pm 0.26$ |
| 0701.3+6827 | 07 01 23.4 +68 27 43 | $0.052 \pm 0.013$ | 407.4 | $+0.01 \pm 0.25$ |
| 0704.0+6214 | 07 04 05.0 +62 14 40 | $0.040 \pm 0.013$ | 365.4 | $+0.23 \pm 0.35$ |
| | | | | |
| 0707.0+5752 | 07 07 00.5 +57 52 01 | $0.076 \pm 0.017$ | 373.6 | $-0.06 \pm 0.21$ |
| 0708.0+5815 | 07 08 01.2 +58 15 42 | $0.041 \pm 0.013$ | 361.8 | $-0.27 \pm 0.29$ |
| 0711.9+5730 | 07 11 56.7 +57 30 07 | $0.045 \pm 0.012$ | 389.5 | $+0.18 \pm 0.27$ |
| | | | | |
| 0714.8+6208 | 07 14 52.3 +62 08 02 | $0.046 \pm 0.013$ | 348.0 | $-0.03 \pm 0.27$ |
| 0717.4+6603 | 07 17 28.8 +66 03 34 | $0.072 \pm 0.014$ | 430.4 | $-0.11 \pm 0.19$ |
| 0720.6+6139 | 07 20 39.8 +61 39 47 | $0.036 \pm 0.012$ | 366.7 | $-0.05 \pm 0.32$ |

Table E.1 − continued

| Spect. type (7) | Catal. Name (8) | $m_v$ (9) | $(B/V)$ (10) | $\Delta\alpha$ (11) | $\Delta\delta$ (12) | observed Li | Ca | He | Ph. |
|---|---|---|---|---|---|---|---|---|---|
| F6 | HD 25414 | 8.23 | +0.75 | −26 | +13 | no | no | no | no |
| G4 | | 12.57 | +0.86 | −16 | +17 | no | no | no | no |
| F5 | HR 1249 | 5.38 | +0.50 | +0 | +3 | yes | no | yes | no |
| K9e | | 13.44 | +1.14 | +0 | −6 | no | no | no | no |
| F2V | HR 1254 | 5.50 | +0.33 | +5 | −2 | yes | no | yes | no |
| F6V | HR 1257 | 5.36 | +0.50 | +5 | +1 | yes | no | yes | no |
| G7 | | 12.44 | +0.84 | −5 | +6 | no | no | no | no |
| G4e | | 11.28 | +0.90 | −2 | +5 | no | no | no | no |
| G0 | SAO 111600 | 11.19 | +0.38 | −3 | +5 | no | no | no | no |
| F7 | HD 25953 | 8.86 | +0.87 | −3 | −10 | yes | no | yes | no |
| K8e | | 12.93 | +1.22 | −6 | −4 | no | no | no | no |
| F5 | | | | | | no | no | no | no |
| G5 | | | | | | no | no | no | no |
| G5 | HD 26573 | 6.62 | | | | yes | yes | no | no |
| G0 | BD+00 710B | | | | | no | no | no | no |
| F2V | HR 1309 | 5.29 | +0.36 | −10 | −3 | yes | no | yes | no |
| G0 | HD 26861 | 10.54 | +0.83 | −6 | −2 | yes | no | yes | no |
| G5IV | HR 1321 | 6.93 | | | | yes | yes | no | no |
| G0 | HR 1322 | 6.30 | | | | yes | yes | no | no |
| G0 | HD 26990 | 9.98 | | +0 | −18 | yes | yes | no | no |
| A5 | HD 27039 | 7.99 | | −6 | −12 | yes | no | yes | no |
| K2 | HD 46606 | 7.90 | +1.00 | +9 | −23 | yes | yes | no | no |
| G5 | HD 47373 | 7.80 | +1.10 | +1 | −13 | yes | yes | no | no |
| G5 | | 10.91 | | −1 | −5 | no | no | no | no |
| K2e | | 12.25 | +1.04 | −6 | +0 | no | no | no | no |
| F5 | HD 51069 | 8.80 | +0.10 | −9 | −12 | no | no | yes | no |
| K7e | | 12.85 | +1.16 | −6 | −21 | no | no | no | no |
| K9 | | | | | | no | no | no | no |
| K7e | | 12.68 | +1.33 | −11 | −35 | no | no | no | no |
| K7 | | 10.90 | | −7 | −43 | no | no | no | no |
| F5 | AG+57 634 | 8.00 | | | | yes | no | yes | no |
| G5 | BD+57 1045B | 10.30 | | | | no | no | no | no |
| G0 | HD 54943 | 7.80 | +0.70 | −12 | −12 | yes | yes | no | no |
| K3e | | 12.09 | +1.17 | −2 | −5 | no | no | no | no |
| F7 | | 10.40 | +0.74 | −35 | +23 | no | no | no | no |

Table E.1 − continued

| ROSAT Name RXJ | ROSAT coordinates (2000.0) | Countrate (3) | Exp. time (4) | HR 1 (5) |
|---|---|---|---|---|
| 0721.1+6739 | 07 21 06.7 +67 39 37 | $0.069 \pm 0.014$ | 430.4 | $-0.45 \pm 0.20$ |
| 0724.3+5857 | 07 24 21.3 +58 57 13 | $0.040 \pm 0.013$ | 314.8 | $+0.68 \pm 0.30$ |
| 0725.9+6840 | 07 25 56.9 +68 40 44 | $0.046 \pm 0.011$ | 420.5 | $+0.49 \pm 0.21$ |
| 0731.1+6118 | 07 31 07.7 +61 18 15 | $0.043 \pm 0.017$ | 204.6 | $+0.34 \pm 0.34$ |
| 0732.3+6441 | 07 32 20.9 +64 41 22 | $0.069 \pm 0.016$ | 345.5 | $+0.64 \pm 0.30$ |
| 0735.1+6540 | 07 35 08.8 +65 40 31 | $0.069 \pm 0.016$ | 345.5 | $-0.03 \pm 0.23$ |
| 0741.3+6241 | 07 41 19.6 +62 41 59 | $0.038 \pm 0.014$ | 254.6 | $-0.71 \pm 0.33$ |
| 0742.8+6109 | 07 42 49.8 +61 09 24 | $0.436 \pm 0.034$ | 384.3 | $+0.63 \pm 0.06$ |
| 0752.5+5732 | 07 52 30.3 +57 32 11 | $0.044 \pm 0.012$ | 422.9 | $+0.37 \pm 0.25$ |
| 0752.8+6304 | 07 52 48.3 +63 04 54 | $0.038 \pm 0.011$ | 443.4 | $-0.03 \pm 0.29$ |
| 0755.1+5819 | 07 55 11.5 +58 19 22 | $0.047 \pm 0.013$ | 416.6 | $-0.06 \pm 0.26$ |
| 0755.8+6509 | 07 55 52.4 +65 09 04 | $0.055 \pm 0.013$ | 485.5 | $+1.33 \pm 0.21$ |
| 0759.2+5722 | 07 59 15.2 +57 22 44 | $0.061 \pm 0.014$ | 495.2 | $+0.06 \pm 0.23$ |
| 0801.3+5902 | 08 01 20.9 +59 02 53 | $0.102 \pm 0.018$ | 442.3 | $+0.23 \pm 0.17$ |
| 0801.4+6845 | 08 01 27.8 +68 45 35 | $0.043 \pm 0.012$ | 375.0 | $+0.20 \pm 0.27$ |
| 0802.5+5716 | 08 02 35.0 +57 16 29 | $1.330 \pm 0.055$ | 447.6 | $+0.03 \pm 0.04$ |
| 0803.2+6141 | 08 03 17.9 +61 41 06 | $0.048 \pm 0.013$ | 406.8 | $+0.03 \pm 0.25$ |
| 0809.2+6639 | 08 09 17.0 +66 39 13 | $0.049 \pm 0.012$ | 414.8 | $+0.54 \pm 0.23$ |
| 0811.9+5730 | 08 11 54.5 +57 30 56 | $0.040 \pm 0.012$ | 434.2 | $+0.32 \pm 0.30$ |
| 0814.5+6256 | 08 14 35.9 +62 56 05 | $0.046 \pm 0.012$ | 441.4 | $-0.26 \pm 0.23$ |
| 0818.3+5923 | 08 18 18.6 +59 23 03 | $0.031 \pm 0.010$ | 406.5 | $+0.90 \pm 0.19$ |
| 0818.8+6029 | 08 18 53.0 +60 29 49 | $0.040 \pm 0.012$ | 404.7 | $-0.38 \pm 0.26$ |
| 0819.1+6842 | 08 19 09.6 +68 42 18 | $0.048 \pm 0.012$ | 437.3 | $-0.28 \pm 0.22$ |
| 0819.3+6230 | 08 19 18.9 +62 30 35 | $0.038 \pm 0.012$ | 422.0 | $-0.40 \pm 0.25$ |
| 0820.4+5744 | 08 20 25.7 +57 44 44 | $0.110 \pm 0.019$ | 413.3 | $-0.21 \pm 0.16$ |
| 0821.0+6526 | 08 21 04.9 +65 26 33 | $0.077 \pm 0.016$ | 423.9 | $-0.26 \pm 0.18$ |
| 0823.2+6127 | 08 23 15.0 +61 27 46 | $0.197 \pm 0.025$ | 405.6 | $+0.07 \pm 0.12$ |
| 0824.5+6453 | 08 24 32.3 +64 53 28 | $0.295 \pm 0.027$ | 436.2 | $-0.11 \pm 0.09$ |
| 0825.2+6442 | 08 25 17.5 +64 42 26 | $0.036 \pm 0.011$ | 433.9 | $-0.82 \pm 0.20$ |
| 0826.5+6835 | 08 26 33.9 +68 35 49 | $0.036 \pm 0.011$ | 433.7 | $-0.27 \pm 0.27$ |
| 0827.5+5735 | 08 27 34.3 +57 35 02 | $0.032 \pm 0.010$ | 450.2 | $-0.35 \pm 0.28$ |
| 0830.2+6043 | 08 30 15.8 +60 43 00 | $0.093 \pm 0.017$ | 426.1 | $-0.38 \pm 0.16$ |

Table E.1 − continued.

| Spect. type (6) | Catal. Name (7) | $m_v$ (8) | $(B/V)$ (9) | $\Delta\alpha$ (10) | $\Delta\delta$ (11) | observed Li | Ca | He | Ph. |
|---|---|---|---|---|---|---|---|---|---|
| K0 | HD 56168 | 8.50 | +0.70 | −3 | −2 | yes | yes | no | no |
| G8 | | 15.06 | +0.63 | −18 | +9 | no | no | no | no |
| K6 | | 12.21 | +0.82 | −7 | −13 | no | no | no | no |
| K0 | | | | −12 | +7 | no | no | no | no |
| K9 | | | | | | no | no | no | no |
| K5e | | 13.76 | +1.07 | +28 | +25 | no | no | no | no |
| F5 | HD 59581 | 8.60 | +0.10 | −6 | +1 | yes | yes | no | no |
| K7 | | 18.69 | +1.02 | +15 | +23 | no | no | no | no |
| K0 | HD 61396 | 7.90 | +1.20 | −5 | −3 | yes | yes | no | no |
| G1 | | 11.84 | +0.60 | −5 | +2 | no | no | no | no |
| M4 | | | | | | no | no | no | no |
| F5 | HD 63408 | 8.50 | +0.60 | −16 | −5 | yes | no | yes | no |
| G2 | | 11.69 | +0.50 | −2 | −10 | no | no | no | no |
| G5 | BD+65 601 | 9.90 | +1.00 | −12 | −8 | no | no | no | no |
| G5 | 2E0755.1+5731 | 13.48 | +0.48 | −5 | −12 | no | no | no | no |
| F2V | HD 65301 | 5.70 | +0.46 | +2 | +4 | yes | no | yes | no |
| F8 | | 12.43 | +0.92 | −4 | −4 | no | no | no | no |
| F8V | HD 65626 | 6.49 | +0.62 | −7 | +1 | yes | yes | no | no |
| F8 | SAO 14417 | 9.10 | +0.70 | −26 | −35 | no | no | no | no |
| G5 | | 8.16 | +1.40 | −7 | −11 | no | no | no | no |
| F8 | | 13.08 | +0.67 | +1 | −5 | no | no | no | no |
| G7 | SAO 14468 | 9.20 | +0.70 | −27 | −8 | no | no | no | no |
| K0e | | 13.94 | +1.01 | −15 | −6 | no | no | no | no |
| F0 | HD 69135 | 8.50 | +0.20 | −10 | +13 | no | no | yes | no |
| K0e | | 13.67 | +1.02 | +3 | −22 | no | no | no | no |
| G8III | HD 69148 | 5.70 | +0.90 | +11 | +9 | no | no | no | no |
| F4V | HD 69548 | 5.90 | +0.38 | +0 | +9 | yes | no | yes | no |
| G0 | HD 69433 | 8.03 | +0.73 | +8 | +0 | no | no | no | no |
| G5 | HD 70050 | 8.50 | +0.60 | −8 | +9 | yes | yes | no | no |
| K5e | SAO 14532 | 8.60 | +0.60 | +37 | +1 | yes | yes | no | no |
| F5 | HD 70312 | 7.50 | +0.40 | +15 | −25 | no | no | no | no |
| F5 | HD 70399 | 9.00 | −0.20 | +28 | +0 | no | no | yes | no |
| G1 | | 12.73 | +0.69 | +27 | +27 | no | no | no | no |
| G3 | HD 71369 | 3.40 | +0.80 | −7 | −10 | no | no | no | no |
| | BD+61 1054B | 15.20 | | | | no | no | no | no |

Table E.1 − continued.

| ROSAT Name RXJ | ROSAT coordinates (2000.0) | Countrate (3) | $t_{exp}$ (4) | HR 1 (5) |
|---|---|---|---|---|
| 1016.4−0520 | 10 16 28.7 −05 20 26 | $3.980 \pm 0.108$ | 358.7 | $-1.00 \pm 0.00$ |
| 1017.5−0808 | 10 17 31.0 −08 08 58 | $0.080 \pm 0.014$ | 501.7 | $+0.66 \pm 0.18$ |
| 1018.1+0043 | 10 18 07.7 +00 43 00 | $0.051 \pm 0.012$ | 447.8 | $+0.38 \pm 0.24$ |
| 1019.5−0506 | 10 19 33.4 −05 06 06 | $0.118 \pm 0.018$ | 471.0 | $+0.21 \pm 0.15$ |
| 1019.5−0513 | 10 19 34.7 −05 13 44 | $0.036 \pm 0.011$ | 470.7 | $-0.15 \pm 0.27$ |
| 1020.0−0754 | 10 20 00.6 −07 54 01 | $0.052 \pm 0.013$ | 452.8 | $+0.30 \pm 0.22$ |
| 1022.3+0128 | 10 22 23.4 +01 28 03 | $0.038 \pm 0.013$ | 376.9 | $+0.41 \pm 0.32$ |
| 1027.0+0048 | 10 27 03.4 +00 48 39 | $0.031 \pm 0.012$ | 356.1 | $-0.23 \pm 0.34$ |
| 1027.4−0351 | 10 27 29.9 −03 51 03 | $0.065 \pm 0.015$ | 395.3 | $-0.42 \pm 0.21$ |
| 1028.0−0117 | 10 28 01.7 −01 17 34 | $0.032 \pm 0.010$ | 454.3 | $+0.84 \pm 0.32$ |
| 1028.6−0127 | 10 28 38.4 −01 27 45 | $0.059 \pm 0.013$ | 465.1 | $+0.27 \pm 0.24$ |
| 1029.2−0159 | 10 29 13.8 −01 59 54 | $0.043 \pm 0.013$ | 448.0 | $-0.30 \pm 0.24$ |
| 1029.7+0129 | 10 29 42.1 +01 29 32 | $0.363 \pm 0.032$ | 416.4 | $-0.12 \pm 0.13$ |
| 1032.6−0653 | 10 32 39.5 −06 53 25 | $0.226 \pm 0.025$ | 411.4 | $+0.50 \pm 0.10$ |
| 1036.9−0850 | 10 36 59.9 −08 50 26 | $0.135 \pm 0.021$ | 431.5 | $-0.27 \pm 0.14$ |
| 1038.1−0615 | 10 38 06.8 −06 15 51 | $0.039 \pm 0.012$ | 429.5 | $+0.81 \pm 0.25$ |
| 1041.3−0144 | 10 41 23.6 −01 44 26 | $0.152 \pm 0.022$ | 390.0 | $-0.38 \pm 0.13$ |
| 1047.8−0113 | 10 47 51.2 −01 13 15 | $0.168 \pm 0.022$ | 433.7 | $+0.32 \pm 0.12$ |
| 1049.2−0401 | 10 49 16.3 −04 01 18 | $0.042 \pm 0.012$ | 437.7 | $-0.16 \pm 0.25$ |
| 1051.2−0553 | 10 51 12.6 −05 53 21 | $0.046 \pm 0.013$ | 446.2 | $-0.13 \pm 0.26$ |
| 1051.3−0734 | 10 51 23.8 −07 34 01 | $0.048 \pm 0.013$ | 436.9 | $+0.20 \pm 0.29$ |
| 1051.8−0547 | 10 51 52.2 −05 47 14 | $0.036 \pm 0.011$ | 449.3 | $-0.05 \pm 0.29$ |
| 1051.8+0235 | 10 51 53.0 +02 35 34 | $0.036 \pm 0.011$ | 423.8 | $-1.61 \pm 0.40$ |
| 1055.6+0044 | 10 55 41.6 +00 44 19 | $0.058 \pm 0.014$ | 434.4 | $-0.35 \pm 0.21$ |
| 1056.1−0540 | 10 56 09.2 −05 40 27 | $0.046 \pm 0.013$ | 439.9 | $-0.41 \pm 0.23$ |
| 1057.1−0101 | 10 57 06.3 −01 01 11 | $0.120 \pm 0.019$ | 438.9 | $-0.91 \pm 0.08$ |
| 1059.7−0522 | 10 59 45.8 −05 22 10 | $0.068 \pm 0.015$ | 445.1 | $+0.23 \pm 0.20$ |
| 1100.0−0657 | 11 00 02.7 −06 57 35 | $0.038 \pm 0.011$ | 435.5 | $+0.56 \pm 0.24$ |
| 1102.5−0634 | 11 02 31.6 −06 34 27 | $0.035 \pm 0.011$ | 446.7 | $+0.43 \pm 0.28$ |
| 1103.2−0654 | 11 03 15.8 −06 54 11 | $0.039 \pm 0.012$ | 438.3 | $+0.38 \pm 0.32$ |
| 1103.6−0442 | 11 03 38.5 −04 42 19 | $0.063 \pm 0.014$ | 434.4 | $-0.34 \pm 0.19$ |
| 1103.8−0741 | 11 03 51.4 −07 41 51 | $0.053 \pm 0.013$ | 411.9 | $+0.11 \pm 0.25$ |
| 1105.3−0735 | 11 05 21.1 −07 35 32 | $0.067 \pm 0.016$ | 406.5 | $-0.16 \pm 0.21$ |

Table E.1 − continued.

| Spect. type (6) | Catal. Name (7) | $m_v$ (8) | $(B/V)$ (9) | $\Delta\alpha$ (10) | $\Delta\delta$ (11) | observed Li | Ca | He | Ph. |
|---|---|---|---|---|---|---|---|---|---|
| K9 | | 11.69 | | +3 | +8 | no | no | no | no |
| G8 | BD-07 3000 | 9.40 | | +3 | +8 | no | no | no | no |
| F8 | BD+01 2420 | 9.80 | +0.60 | −9 | +1 | no | no | no | no |
| K0 | HD 89490 | 6.37 | +0.90 | +8 | +12 | no | no | no | no |
| F2 | HD 89507 | 7.60 | +0.30 | −17 | −7 | no | no | no | no |
| K2 | | 10.87 | | −4 | +0 | no | no | no | no |
| F2 | HD 89895 | 8.60 | +0.80 | −36 | −1 | no | no | no | no |
| G0 | SAO 118308 | 9.10 | +0.70 | −9 | +8 | no | no | no | no |
| K7e | | 12.47 | | −2 | −2 | no | no | no | no |
| K1 | | 11.98 | +0.93 | −3 | +3 | no | no | no | no |
| K3 | | | | | | no | no | no | no |
| K5e | | | | | | no | no | no | no |
| G4 | | | | | | no | no | no | no |
| K4e | G162-61 | 11.58 | +1.18 | +2 | +3 | no | no | no | no |
| F5 | HD 90905 | 6.85 | +0.45 | +0 | +4 | no | no | no | no |
| G0 | HD 91351 | 9.60 | +0.90 | −3 | +10 | no | no | no | no |
| F9 | HD 91962 | 7.03 | +0.62 | −6 | −5 | no | no | no | no |
| F7 | | 11.14 | | −6 | −7 | no | no | no | no |
| K1 | HR 4182 | 6.26 | +0.88 | −15 | −3 | no | no | no | no |
| K0 | BD-00 2375 | 9.20 | +1.20 | −6 | +15 | no | no | no | no |
| A2 | HR 4229 | 6.61 | +0.22 | −16 | +10 | no | no | no | no |
| F8 | HD 94044 | 8.80 | +0.60 | +6 | +15 | no | no | no | no |
| K2 | PPM 193867 | 9.50 | | −5 | +2 | no | no | no | no |
| G0 | HD 94137 | 9.10 | +0.70 | +12 | +5 | no | no | no | no |
| K8e | | 13.93 | +1.25 | −50 | −19 | no | no | no | no |
| F2 | HD 94672 | 5.91 | +0.42 | −6 | +6 | no | no | no | no |
| K7e | | 12.79 | | −5 | −6 | no | no | no | no |
| K5 | | | | | | no | no | no | no |
| G3 | | | | | | no | no | no | no |
| K1 | | 10.21 | | +3 | +1 | no | no | no | no |
| | BD-6 3282 | 9.40 | +0.59 | −16 | −6 | no | no | no | no |
| K6 | | 15.24 | | +43 | +18 | no | no | no | no |
| | | 14.55 | +0.75 | −13 | +6 | no | no | no | no |
| G0 | | 15.64 | | −15 | +14 | no | no | no | no |
| K0 | HD 95900 | 7.30 | +1.20 | +21 | −37 | no | no | no | no |
| K5e | | 11.44 | | −13 | +27 | no | no | no | no |

Table E.1 − continued.

| ROSAT Name RXJ | ROSAT coordinates (2000.0) | Countrate (3) | Exp. time (4) | HR 1 (5) |
|---|---|---|---|---|
| 1201.6+3602 | 12 01 38.0 +36 02 38 | $0.039 \pm 0.012$ | 484.2 | $-0.53 \pm 0.23$ |
| 1202.7+3520 | 12 02 42.7 +35 20 13 | $0.083 \pm 0.016$ | 493.2 | $-0.29 \pm 0.17$ |
| 1205.2+3336 | 12 05 12.3 +33 36 58 | $0.033 \pm 0.011$ | 488.4 | $+0.02 \pm 0.32$ |
| 1208.0+3110 | 12 08 02.6 +31 10 45 | $0.067 \pm 0.014$ | 501.5 | $-0.22 \pm 0.30$ |
| 1209.5+3356 | 12 09 34.8 +33 56 35 | $0.034 \pm 0.010$ | 509.4 | $+0.08 \pm 0.28$ |
| 1210.6+3732 | 12 10 38.1 +37 32 43 | $0.033 \pm 0.010$ | 497.3 | $+0.53 \pm 0.31$ |
| 1220.6+2703 | 12 20 40.2 +27 03 35 | $0.041 \pm 0.012$ | 491.0 | $-0.32 \pm 0.26$ |
| 1224.9+3602 | 12 24 56.2 +36 02 10 | $0.031 \pm 0.010$ | 537.2 | $-0.11 \pm 0.27$ |
| 1225.9+3346 | 12 25 56.6 +33 46 46 | $0.040 \pm 0.011$ | 517.2 | $-0.08 \pm 0.27$ |
| | | | | |
| 1619.5+7022 | 16 19 32.2 +70 22 08 | $0.085 \pm 0.008$ | 1669.9 | $-0.22 \pm 0.09$ |
| 1620.8+7014 | 16 20 49.1 +70 14 60 | $0.025 \pm 0.005$ | 1720.2 | $+0.46 \pm 0.18$ |
| 1625.3+7455 | 16 25 21.2 +75 55 43 | $0.010 \pm 0.004$ | 1358.9 | $+4.39 \pm 5.09$ |
| 1625.5+7123 | 16 25 30.3 +71 23 06 | $0.171 \pm 0.011$ | 1728.5 | $-0.23 \pm 0.09$ |
| 1627.8+7042 | 16 27 48.0 +70 42 12 | $0.017 \pm 0.004$ | 1740.7 | $-0.03 \pm 0.25$ |
| 1627.8+7258 | 16 27 51.4 +72 58 16 | $0.010 \pm 0.003$ | 1868.8 | $+0.21 \pm 0.32$ |
| 1628.4+7401 | 16 28 24.1 +74 01 01 | $0.063 \pm 0.007$ | 1633.6 | $+0.09 \pm 0.11$ |
| 1629.0+7318 | 16 29 00.0 +73 18 25 | $0.019 \pm 0.004$ | 1895.6 | $+0.15 \pm 0.21$ |
| 1636.6+6947 | 16 36 41.3 +69 47 47 | $0.042 \pm 0.005$ | 2142.4 | $+0.29 \pm 0.12$ |
| 1637.6+6919 | 16 37 41.3 +69 19 09 | $0.014 \pm 0.003$ | 2430.1 | $-0.44 \pm 0.38$ |
| 1637.8+7239 | 16 37 48.2 +72 39 30 | $0.031 \pm 0.005$ | 2001.1 | $+0.10 \pm 0.15$ |
| 1648.0+7157 | 16 48 04.4 +71 57 52 | $0.011 \pm 0.003$ | 2189.6 | $+0.33 \pm 0.28$ |
| 1653.2+7015 | 16 53 15.7 +70 15 58 | $0.086 \pm 0.007$ | 2284.9 | $+0.42 \pm 0.08$ |
| 1653.5+7344 | 16 53 34.2 +73 44 17 | $0.068 \pm 0.008$ | 1611.6 | $+0.05 \pm 0.11$ |
| 1656.4+7407 | 16 56 24.7 +74 07 05 | $0.014 \pm 0.004$ | 1573.5 | $+0.49 \pm 0.31$ |
| 1705.4+7436 | 17 05 25.2 +74 36 03 | $0.053 \pm 0.007$ | 1685.4 | $+0.33 \pm 0.13$ |
| 1706.3+7329 | 17 06 22.9 +73 29 31 | $0.070 \pm 0.008$ | 1756.7 | $-0.10 \pm 0.10$ |
| 1709.4+7056 | 17 09 26.3 +70 56 27 | $0.012 \pm 0.003$ | 2703.9 | $+0.09 \pm 0.22$ |
| 1711.2+6930 | 17 11 16.5 +69 30 13 | $0.030 \pm 0.004$ | 3084.9 | $+0.54 \pm 0.14$ |
| 1712.5+7107 | 17 12 35.0 +71 07 34 | $0.019 \pm 0.004$ | 2694.6 | $+0.04 \pm 0.18$ |
| 1716.1+7147 | 17 16 11.6 +71 47 39 | $0.103 \pm 0.007$ | 2390.2 | $+0.31 \pm 0.07$ |
| 1721.1+6947 | 17 21 11.1 +69 47 58 | $0.012 \pm 0.002$ | 3463.4 | $+0.00 \pm 0.20$ |
| 1722.6+7316 | 17 22 40.7 +73 16 39 | $0.035 \pm 0.005$ | 2189.8 | $-0.11 \pm 0.12$ |
| 1723.3+7347 | 17 23 18.2 +73 47 46 | $0.012 \pm 0.003$ | 2165.3 | $+0.75 \pm 0.34$ |
| 1724.0+6940 | 17 24 00.5 +69 40 23 | $0.048 \pm 0.004$ | 3655.6 | $+0.43 \pm 0.09$ |
| 1724.0+7354 | 17 24 05.6 +73 54 44 | $0.013 \pm 0.003$ | 2168.3 | $+0.34 \pm 0.23$ |

Table E.1 − continued.

| Spect. type (6) | Catal. Name (7) | $m_v$ (8) | $(B/V)$ (9) | $\Delta\alpha$ (10) | $\Delta\delta$ (11) | observed Li | Ca | He | Ph. |
|---|---|---|---|---|---|---|---|---|---|
| G2 | | | | −22 | +0 | no | no | no | no |
| K7 | | 13.80 | +0.94 | −20 | +2 | no | no | no | no |
| G4 | | 14.44 | +0.65 | −11 | +23 | no | no | no | no |
| K4 | | 11.24 | +1.01 | +3 | −19 | no | no | no | no |
| F2 | | 12.69 | +0.62 | +8 | −4 | no | no | no | no |
| K0 | | 13.35 | +0.64 | +7 | +3 | no | no | no | no |
| F3 | HR 4698 | 7.13 | +0.36 | −15 | +12 | no | no | no | no |
| K0 | | 13.74 | +0.44 | +15 | −10 | no | no | no | no |
| G0 | | | | | | no | no | no | no |
| M2e | | | | | | no | no | no | no |
| F8 | HD 8004 | 7.40 | +1.00 | +0 | +2 | no | no | no | no |
| K1e | | 11.80 | +0.92 | +3 | +8 | no | no | no | no |
| F8 | SAO 8518 | 9.60 | +0.80 | −9 | +4 | no | no | no | no |
| F8 | HD 148941 | 7.10 | +1.20 | +6 | −2 | no | no | no | no |
| G1 | | | | | | no | no | no | no |
| K7e | | 12.15 | +1.20 | +9 | +0 | no | no | no | no |
| K0 | SAO 8533 | 9.20 | +1.30 | +10 | +8 | no | no | no | no |
| F7 | | 7.95 | +0.87 | +7 | −8 | no | no | no | no |
| F5 | HD 150631 | | | +12 | +12 | no | no | no | no |
| K3 | SAO 17172 | | | +32 | −8 | no | no | no | no |
| K0 | | 10.47 | +1.11 | +9 | −11 | no | no | no | no |
| F8 | HD 152628 | 9.11 | | +18 | −9 | no | no | no | no |
| K1 | | 10.07 | +0.88 | +7 | −1 | no | no | no | no |
| K0 | SAO 8653 | 8.44 | +0.91 | −10 | +1 | no | no | no | no |
| K3e | | 17.34 | +0.98 | −10 | −16 | no | no | no | no |
| K0 | | 9.43 | +0.85 | +4 | −5 | no | no | no | no |
| K7 | | 9.94 | +1.70 | −9 | −4 | no | no | no | no |
| K0 | | 10.86 | +0.86 | +17 | −3 | no | no | no | no |
| F8 | SAO 17386 | 9.20 | +0.70 | −2 | +3 | no | no | no | no |
| F2 | SAO 8737 | 9.50 | +0.50 | −3 | −4 | no | no | no | no |
| K2 | HD 15370 | 7.61 | +1.20 | −6 | +7 | no | no | no | no |
| F8 | HD 158063 | 7.40 | +0.90 | +4 | −5 | no | no | no | no |
| K1e | | 11.57 | +0.89 | +1 | +9 | no | no | no | no |
| K1 | | 12.69 | +0.96 | +7 | +3 | no | no | no | no |
| G4 | | 10.62 | +0.69 | +1 | −7 | no | no | no | no |
| K1 | | 11.11 | +1.21 | −3 | +7 | no | no | no | no |

Table E.1 − continued.

| ROSAT Name RXJ | ROSAT coordinates (2000.0) | Countrate (3) | Exp. time (4) | HR 1 (5) |
|---|---|---|---|---|
| 1726.7+6937 | 17 26 47.0 +69 37 40 | $0.012 \pm 0.002$ | 3805.5 | $+1.19 \pm 0.29$ |
| 1728.1+7239 | 17 28 11.5 +72 39 27 | $0.066 \pm 0.006$ | 2424.6 | $+0.32 \pm 0.09$ |
| 1730.3+6955 | 17 30 20.4 +69 55 20 | $0.039 \pm 0.004$ | 3735.7 | $+0.25 \pm 0.10$ |
| 1732.6+7413 | 17 32 41.4 +74 13 46 | $1.240 \pm 0.023$ | 2472.3 | $+0.13 \pm 0.02$ |
| 1734.6+7300 | 17 34 41.6 +73 00 28 | $0.013 \pm 0.003$ | 2756.1 | $+0.71 \pm 0.26$ |
| 1736.9+7420 | 17 36 54.1 +74 20 47 | $0.029 \pm 0.004$ | 2653.8 | $-0.25 \pm 0.13$ |
| 2152.0+1436 | 21 52 04.9 +14 36 20 | $0.036 \pm 0.012$ | 329.7 | $+0.74 \pm 0.26$ |
| 2154.7+1433 | 21 54 44.3 +14 33 28 | $0.095 \pm 0.019$ | 320.8 | $+0.75 \pm 0.15$ |
| 2156.4+0516 | 21 56 27.0 +05 16 01 | $0.375 \pm 0.036$ | 340.3 | $-0.08 \pm 0.09$ |
| 2159.9+0302 | 21 59 59.1 +03 02 32 | $0.147 \pm 0.023$ | 331.2 | $+0.74 \pm 0.12$ |
| 2202.3+0353 | 22 02 20.8 +03 53 06 | $0.105 \pm 0.021$ | 310.7 | $-0.38 \pm 0.18$ |
| 2204.9+0749 | 22 04 58.9 +04 49 43 | $0.081 \pm 0.018$ | 306.0 | $+0.65 \pm 0.20$ |
| 2206.1+1005 | 22 06 10.8 +10 05 14 | $0.208 \pm 0.034$ | 225.3 | $+0.19 \pm 0.15$ |
| 2209.7+1032 | 22 09 45.3 +10 32 00 | $0.043 \pm 0.014$ | 296.1 | $+0.59 \pm 0.27$ |
| 2212.2+1329 | 22 12 13.8 +13 29 14 | $0.051 \pm 0.016$ | 294.7 | $-0.22 \pm 0.27$ |
| 2214.1+0546 | 22 14 06.1 +05 46 23 | $0.061 \pm 0.020$ | 203.5 | $-1.45 \pm 0.47$ |
| 2214.1+0810 | 22 14 10.8 +08 10 18 | $0.063 \pm 0.016$ | 310.2 | $+0.56 \pm 0.21$ |
| 2217.4+0606 | 22 17 27.5 +06 06 03 | $0.034 \pm 0.012$ | 303.9 | $+1.04 \pm 0.27$ |
| 2217.4+1037 | 22 17 28.3 +10 37 28 | $0.033 \pm 0.012$ | 273.3 | $-1.63 \pm 0.98$ |
| 2224.4+0821 | 22 24 28.4 +08 21 45 | $0.036 \pm 0.014$ | 251.6 | $+0.27 \pm 0.40$ |
| 2225.2+0826 | 22 25 13.3 +08 26 13 | $0.038 \pm 0.015$ | 243.3 | $+0.40 \pm 0.43$ |
| 2226.3+0351 | 22 26 18.2 +03 51 44 | $0.101 \pm 0.020$ | 270.6 | $+1.92 \pm 0.36$ |
| 2228.6+0305 | 22 28 36.7 +03 05 08 | $0.031 \pm 0.012$ | 241.2 | $+0.70 \pm 0.29$ |
| 2232.9+1040 | 22 32 57.8 +10 40 35 | $0.046 \pm 0.013$ | 422.1 | $-0.15 \pm 0.24$ |
| 2233.6+0506 | 22 33 40.0 +05 06 22 | $0.037 \pm 0.014$ | 248.5 | $+2.67 \pm .98$ |
| 2233.7+1230 | 22 33 44.4 +12 30 16 | $0.041 \pm 0.012$ | 447.7 | $+0.82 \pm 0.29$ |
| 2236.2+0601 | 22 36 16.5 +06 01 06 | $0.038 \pm 0.012$ | 380.0 | $+0.52 \pm 0.29$ |
| 2237.0+0416 | 22 37 02.4 +04 16 54 | $0.053 \pm 0.016$ | 294.5 | $+0.98 \pm 0.36$ |
| 2239.3+0325 | 22 39 18.1 +03 25 21 | $0.054 \pm 0.016$ | 297.5 | $+0.33 \pm 0.31$ |
| 2240.7+1326 | 22 40 46.2 +13 26 12 | $0.097 \pm 0.016$ | 430.3 | $+0.71 \pm 0.15$ |
| 2240.8+1433 | 22 40 52.3 +14 33 07 | $0.039 \pm 0.011$ | 445.0 | $-0.72 \pm 0.21$ |
| 2241.9+1431 | 22 41 58.2 +14 31 04 | $0.083 \pm 0.015$ | 439.4 | $+0.10 \pm 0.18$ |
| 2242.0+0946 | 22 42 01.1 +09 46 00 | $0.098 \pm 0.017$ | 416.0 | $-0.18 \pm 0.17$ |

Table E.1 − continued.

| Spect. type (6) | Catal. Name (7) | $m_v$ (8) | $(B/V)$ (9) | $\Delta\alpha$ (10) | $\Delta\delta$ (11) | observed Li | Ca | He | Ph. |
|---|---|---|---|---|---|---|---|---|---|
| F5 | | 9.27 | +0.65 | +8 | −13 | no | no | no | no |
| K4e | | 11.50 | | −5 | +6 | no | no | no | no |
| F0 | | 8.77 | +1.16 | +3 | −7 | no | no | no | no |
| K0 | HD 160538 | 6.55 | +1.05 | +4 | +9 | no | no | no | no |
| F0 | | 9.03 | +0.72 | −22 | −23 | no | no | no | no |
| K0 | | 7.75 | +0.96 | −2 | +24 | no | no | no | no |
| K0 | HD 207902 | 8.20 | +1.20 | +44 | +9 | no | no | no | no |
| F5 | SAO 107496 | 9.05 | | +13 | −1 | no | no | no | no |
| K2 | | 11.05 | +0.94 | −3 | +5 | no | no | no | no |
| G8 | SAO 127215 | 9.70 | +0.90 | −10 | +7 | no | no | no | no |
| K7e | | 14.30 | +1.05 | +10 | −2 | no | no | no | no |
| K5e | | 13.45 | +1.01 | −21 | −4 | no | no | no | no |
| G8 | SAO 127298 | 10.00 | +0.10 | −15 | −16 | no | no | no | no |
| G8 | | 11.10 | +0.80 | +13 | +8 | no | no | no | no |
| G5 | HD 210750 | 8.70 | +0.66 | +7 | −7 | no | no | no | no |
| F8 | HD 210985 | 8.20 | +0.20 | +51 | −10 | no | no | no | no |
| G0 | | 14.99 | +0.81 | +19 | −20 | no | no | no | no |
| K1e | | 13.52 | +0.80 | −8 | −2 | no | no | no | no |
| G5 | | 13.77 | +0.74 | +25 | +27 | no | no | no | no |
| K5 | | 13.69 | +1.02 | −13 | +15 | no | no | no | no |
| G3 | | | | | | no | no | no | no |
| K1 | | 10.58 | +0.81 | −5 | −4 | no | no | no | no |
| G5 | | 10.89 | | +8 | +3 | no | no | no | no |
| K2 | | 11.89 | +1.03 | +8 | −18 | no | no | no | no |
| K2 | | 11.10 | +0.99 | −37 | +0 | no | no | no | no |
| F8 | | 10.01 | +0.80 | +11 | +2 | no | no | no | no |
| M1 | | 16.90 | | −19 | +18 | no | no | no | no |
| K2e | | 13.30 | | −9 | +2 | no | no | no | no |
| G8 | | 10.70 | +0.76 | +16 | +14 | no | no | no | no |
| K8 | | 17.15 | +1.38 | +17 | +30 | no | no | no | no |
| F9 | | 12.87 | +0.46 | +11 | +8 | no | no | no | no |
| G8 | | 13.80 | +0.60 | −4 | +0 | no | no | no | no |
| G4 | HD 214850 | 5.71 | +0.72 | +9 | +17 | no | no | no | no |
| K0 | HD 214995 | 5.90 | +1.11 | +18 | +4 | no | no | no | no |
| K8e | | 12.56 | +1.38 | −7 | −9 | no | no | no | no |

## Aknowldegements

I would like now to thank all the persons that have helped me realize this thesis work.

∗ Dr. Joachim Krautter, for supplying me with such an interesting research subject, for his help with the project, and for leaving me enough free room to develop the work my own way.

∗ Dr. Reiner Wehrse for accepting to be second corrector for my thesis.

∗ Prof. Dr. Immo Appenzeller, for accepting me among the astronomers at the *Landessternwarte Heidelberg*, and for the most pleasant work atmosphere reigning in the institute.

∗ Dr. Luca Pasquini, my "second advisor", for the many discussions we had, for all hte helpful tips and for advising me on the observations. Many thanks also for accepting to be my supervisor during my studentship at ESO.

∗ Dr. Giuseppe Cutispoto, for his help with the analysis of the photometric data, and for his interest in my research.

∗ Dr. Sofia Randich, for supplying the line list that helped calculate the synthetic spectra.

∗ Dr. Thomas Fleming, for his help, and for his EMSS data.

∗ Dr. Matthew Shetrone, for many a disussion, for teaching me how to use IRAF.

∗ Dipl.-Phys. Holger Bock, for his patience in accepting to listen to one music CD 100 times in a row, for all the discussions about Life, the Universe and Everything Else, though we didn't discover the question to the answer "42", and in general for having been such a pleasant office and terminal sharer.

∗ Dr. Thomas Seifert, for touring me around Santiago de Chile and the La Silla observatory during my first observing run.

∗ Dr. Andreas Kaufer and Dr. Otmar Stahl for observing one of my stars during their last run at the ESO 50 cm, and for giving me the reduced data. Dr. Rainer Wichman for observing some stars for me during his CTIO run 1996.

∗ Dipl.-Phys. H. Bock, Dr. M. Shetrone, Dr. T. Szeifert and Dr. A. Kaufer again, for accepting to work their way through, comment and criticize my thesis work.

∗ All the astronomers, and employees of the *Landessternwarte Heidelberg*, simply for being there, and making life all the more pleasant during my thesis.

∗ The students at ESO, Stephane Brillant, David Le Mignant, Isabel Perez, Patrice Corporon, Paul Breeswijk, for making life in Santiago and La Sila much nicer, and especially for making up for mussing entertainement during work schedules at La Silla with long discussions and the telling of anecdotes about their respective telescopes and teams.

∗ And last, but not least by far, my parents and my husband Juan Molina, whose support allowed me to work on this thesis.